19

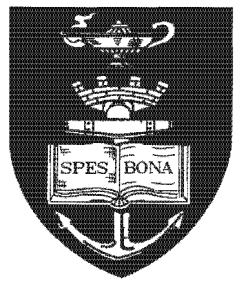

The geochemistry and amelioration of a sulphur-contaminated environment near Somerset West, South Africa

Stephen Mc Keown
BSc (Hons) Geology (UCT)

Submitted in partial fulfilment of the requirements of the degree of

Master of Science

in the Department of Geological Sciences
Faculty of Science
University of Cape Town

January 2000

PREFACE

The analytical work required for the compilation of this thesis was conducted at the Department of Geological Sciences at the University of Cape Town (UCT) from August to November 1999, under the supervision of Associate Professors M.V. Fey and J.P. Willis. Facilities from the Departments of Physics and Chemical Engineering at UCT were also utilised, where appropriate, and certain analyses were out-sourced to ARC-Infruitec and the CSIR in Stellenbosch.

This study represents original research by the author, and no part of this work has been submitted for a degree at any other University. Where use was made of the research of other authors, it has been acknowledged in the text.

Signed by candidate

R.S. Mc Keown

ACKNOWLEDGEMENTS

My sincere appreciation and acknowledgement is extended to the following people and organisations for their contributions to this study:

Firstly, it is both a duty and a pleasure to acknowledge my Professors, Martin Fey and James Willis for their dedication to their work and the students whom they supervise. I believe that I can embark on a career in environmental geochemistry in the sound knowledge that I have been expertly tutored and professionally treated by my supervisors. Martin, your enthusiasm, consideration and sense of humour is remarkable and is a credit. The appreciation for geochemistry that I have acquired this year can largely be attributed the advice, assistance and constructive criticism that you have given me on various occasions this year. James, for your careful appraisal of the analytical techniques in this department, and the data they produce, I am grateful, and also secure in the knowledge that the quality of my data is of an exceptionally high standard.

Vusi Gubevu, Bernadette Azzie, Peter Abanda and Leslie Petrik for all the assistance with the laboratory work this year.

Patrick Sieas and Andreas Spath for assistance with the IC and the ICP-MS, respectively.

Mervin Traut and Cyril Matthys for openly allowing me to take samples at AECI, and to Ted Mills for providing valuable assistance at the site. I would also like to thank Mervin Traut for the generous offer of financial assistance that covered most of the analytical work for this project.

Fran Pocock and Ernest Stout for assisting with XRFS preparation and analysis.

Neville Buchanan for assistance with copying and binding, especially before urgent deadlines.

Mike Louw and staff at CSIR for promptly attending to the DOC samples.

ARC-Infruitec for textural and organic carbon analyses.

Hartwig Frimmel for assisting with optical microscopy.

Dane Gernecke and Miranda Waldron at the electron microscope unit for patiently assisting with the SEM.

Shireen at the Department of Chemical Engineering for promptly attending to the FAAS analyses.

Lisa and Stewart for assistance and encouragement at various times this year.

My classmates, Sarah, Richard, Senzo, Gerry, Mandla, Anja and Marietta, for providing the *mélange* of different personalities and perspectives that always kept the class interesting and exciting. We were a good team and are a credit to one another.

My friends and family for their encouragement and support at various times this year.

Most importantly, to my wife, Tamsin, without whose love, support and encouragement, none of this would have been possible. This thesis opens a new chapter in our lives together, and I dedicate it to you, Tamsin.

ABSTRACT

The accidental burning and decomposition of a sulphur stockpile at an industrial site near Somerset West has caused severe contamination of the soil on which it was stored. The obvious environmental effect of this was the acidification of the soil caused by the oxidation of S to H_2SO_3. In addition to this, the mere presence of the S stockpile prior to the fire was also likely to have generated acidity as a result of the bacterial activity of *Thiobacillus thiooxidans*. Recent literature with respect to acid mine drainage (AMD) confirms the similarity between the processes controlling the geochemistry at this site and those from AMD environments. The key objectives of this study are, firstly, to determine the extent and effects of the S contamination and, secondly, to determine an effective means of ameliorating the site.

The most marked response of the S oxidation is that the pH of the soil and surface water has decreased to abnormally low concentrations (ranging from pH 1.2 to 3.8). This acidification is accompanied by correspondingly high concentrations of SO_4^{2-} (10 – 60 g/L) in solution, as well as acid metal cations, particularly Al, Fe and Mn. The dominant basic cation in solution is Mg^{2+}. A further symptom of the S contamination is the EC level of the waters and soils, which often exceed 40 mS/cm (10 times the accepted cut-off limit of saline environments).

The activities of ions and saturation indices of salient mineral phases were calculated using PHREEQC for all waters and soil solutions from this study. The Al^{3+} activity of the water samples suggests that they may be in equilibrium with typical acid sulphate minerals such as jurbanite and alunite. The solutions become supersaturated with respect to both these phases at pH > 3, and are close to being in equilibrium with quartz and gypsum over the full acidic pH range. A p*e* window of between 10 and 12 was estimated for this system based on ferrous Fe determinations made on the water samples from the site. Ferrous Fe activity data suggest equilibrium with goethite or an amorphous $Fe(OH)_3$ phase, and the saturation index data for Fe minerals (p*e* = 12) show that the solutions become supersaturated with respect to goethite and jarosite above pH 1 and 2, respectively.

The soil at the site was ameliorated using dolomitic limestone which was found to be have a $CaCO_3$ equivalence (CCE) of 58%. An incubation experiment was set up using composite samples of contaminated topsoil and subsoil treated with progressive increments of the same commercial limestone, which was finely crushed for experimental purposes. The lime requirement of the topsoil and subsoil was estimated from their exchangeable acidity, which was

determined to be 342 and 136 $mmol_c/kg$, respectively. From the CCE value, the lime requirement was thus estimated at 29.3 and 11.6 g lime/kg soil for the topsoil and subsoil composites, respectively. The limed samples were incubated in a controlled environment at 25°C for periods of two and four weeks.

Liming experiments were successful in increasing the pH of the topsoil and subsoil to neutral values and decreasing the EC of the topsoil from >100 mS/cm to <40 mS/cm. The EC of the subsoil decreased from >30 mS/cm to <20 mS/cm. The topsoil also showed marked decreases in SO_4^{2-} from >1000 $mmol_c/L$ to <400 $mmol_c/L$. The SO_4^{2-} concentrations of the subsoil decreased from >250 $mmol_c/L$ to <150 $mmol_c/L$. Sulphate may be precipitating as gypsum and acid sulphate mineral phases, or it may be adsorbed to Fe and Al oxyhydroxide surfaces.

The Mg^{2+} concentration increases with liming in the topsoil and decreases in the subsoil solution, while soluble Ca^{2+} decreases slightly in the topsoil and remains constant in the subsoil. The mobility of cations in solution may be partly controlled by the precipitation of mineral phases such as gypsum, jarosite and jurbanite. It is also possible that cations in solution may be participating in exchange reactions on the surfaces of clay minerals and oxides within the soil, since the dominant clay mineral in these soils is smectite, which has an exceptionally high cation exchange capacity (CEC). The concentration of Al, Fe and most other trace metals in solution expectedly decreases with progressive liming of soils.

The activities of ions and saturation indices of the limed solutions show that the system is supersaturated with respect to alunite and jurbanite above pH 3. These solutions are, once again, approximately in equilibrium with quartz and gypsum. Saturation index data for Fe show that at a pe of 12, the solutions are supersaturated with respect to goethite and jarosite, which is consistent with the fact that jarosite precipitates have been identified at the site. It is interesting to note that the saturation index data for the topsoil and subsoil solutions follow the same trend for each mineral when compared to pH. This suggests that the solid phases controlling the concentrations of dissolved Al and Fe in these soils appear to dominate the soil solution, regardless of the mineralogy of each soil horizon.

The results of this study demonstrate that soil acidity can effectively be neutralised with the use of commercial limestone. However the environment has developed into a highly saline brine, and the accumulation of salts will need to be leached from the site before it can be restored to a condition fit for development or habitation.

Table of contents

PREFACE i
ACKNOWLEDGEMENTS ii
ABSTRACT iv
Table of contents vi
List of illustrations x
List of tables xiii

1 Introduction 1
1.1 The study area 1
1.1.1 Geological setting 1
1.1.2 Climate 4
1.1.3 Ecology 4
1.2 Historical background of sulphur stockpile 4
1.3 Research objectives 5

2 The origin and treatment of acid sulphate environments – a review 6
2.1 Introduction 6
2.2 Classes of acid sulphate environments and their impact 6
2.2.1 Soils, sediments and other sulphur-containing materials 6
2.2.1.1 Sulphidic oxidation and the generation of acidity 8
2.2.1.2 Mineralogy of acid sulphate environments 10
2.2.1.3 Metal mobility in acidic soils 12
2.2.2 Mine spoils 13
2.3 Remediation of acid sulphate environments 14
2.3.1 Neutralising agents and techniques 14
2.3.1.1 Cement waste 15
2.3.1.2 Passive treatment with anoxic limestone drains 15
2.3.1.3 Barium carbonate 16
2.3.1.4 Liming of sulphides 17
2.3.1.5 Organic amendment 17
2.3.1.6 Electrochemical methods 18

2.4 Conclusions 18

3 Geochemical investigation of soil and water 21

3.1 Introduction 21
3.2 Sample collection 21
3.2.1 Water sampling 23
3.2.2 Soil sampling 23
3.3 Sample analysis 24
3.3.1 Water and soil solution analysis 24
3.3.1.1 pH and electrical conductivity (EC) 24
3.3.1.2 Alkalinity and acidity 25
3.3.1.3 Major ions 25
3.3.1.4 Trace elements 26
3.3.1.5 Ferrous and ferric iron 26
3.3.1.6 Dissolved organic carbon (DOC) 26
3.3.2 Soil analysis 26
3.3.2.1 Soil composition 26
3.3.2.2 Soil texture 27
3.3.2.3 Organic carbon 27
3.3.2.4 Exchangeable acidity and basicity 27
3.3.2.5 Mineralogy of clay fraction 27
3.3.2.6 Saturated paste extraction 28
3.3.2.7 Micro-analysis of acid precipitates 28
3.4 Results and discussion 29
3.4.1 Historical results 29
3.4.2 Surface and groundwater geochemistry 30
3.4.2.1 Chemical composition 30
3.4.2.2 Chemical speciation and saturation indices 34
3.4.3 Soil geochemistry 42
3.4.3.1 Chemical composition 42
3.4.3.2 Soil solution chemistry 42
3.4.3.3 Soil acidity 44
3.4.3.4 Mineralogy of the clay fraction 46
3.4.3.5 Micro-analysis of acid precipitates 51
3.5 Comparison between water and soil chemistry 55

3.6 Potential processes involved in soil acidification 57
3.6.1 Sulphur content of soil 57
3.6.2 Sulphur oxidising bacteria 58
3.6.3 Sulphur melting experiments 58
3.7 Summary and conclusions 61

4 Amelioration of the site 63
4.1 Introduction 63
4.2 Liming of acidic soils 63
4.2.1 Liming agent used in this study 63
4.2.2 Lime requirement of soil 65
4.3 Limed soil incubation experiments 66
4.3.1 Method of preparation and analysis 66
4.3.1.1 Liming of soils 66
4.3.1.2 Plant growth experiments 67
4.3.2 Results and discussion 67
4.3.2.1 pH, exchangeable acidity and EC_e 67
4.3.2.2 Major ions in solution 71
4.3.2.3 Other trace metals in solution 75
4.3.2.4 Dissolved organic carbon (DOC) 77
4.3.2.5 Alkalinity 79
4.3.2.6 Chemical speciation and saturation indices 80
4.3.3 Plant growth experiments 86
4.4 Water quality 89
4.5 Summary and conclusions 91

5 General discussion and conclusions 93

6 References 100

Appendix A: Soil profile and water descriptions 105
A1. Soil profile descriptions 105
A2. Water descriptions 108

Appendix B: Analytical methods 109
B1. Water and soil solution methods 109
B1.1. pH measurement 109
B1.2. Electrical conductivity (EC) 110
B1.3. Alkalinity 110
B1.4. Exchangeable acidity 111
B1.5. Ion analysis by High Performance Ion Chromatography (HPIC) 112
B1.6. Trace metal analysis by Inductively Coupled Plasma – Mass Spectrometry (ICP-MS) 114
B1.7. Iron colorimetry 115
B2. Soil analysis 117
B2.1. Soil composition by X-ray Fluorescence Spectrometry (XRFS) 117
B2.2. Mineralogical characterisation by X-ray Diffractometry (XRD) 121
B2.3. Soil solution analysis by saturated paste extraction 122
B2.4. Precipitate analysis by Scanning Electron Microscopy with Energy Dispersive X-ray Spectrometer (SEM-EDS) 123
B3. Limestone analysis 124
B3.1. Limestone neutralising value 124
B3.2. Lime requirement of soil 124
B3.3. Description of limed incubation samples 126
Appendix C: Geochemical data 127
C1. Water data 127
C1.1. Water activities and saturation indices 129
C1.2. Equilibrium reactions and log*K* values of selected minerals at 25°C 130
C2. Soil data 131
C2.1. Soil texture and organic carbon 131
C2.2. Extractable acidity 132
C2.2.1. KCl extractable acidity of all soil samples 132
C2.2.2. KCl extractable acidity of sulphur melting experiments 133
C2.3. Incubation results – major ions in solution 134
C2.4. Incubation results – trace elements in solution 135
C2.5. Incubation results – activities and saturation indices 136

List of illustrations

Figure 1. Map of southern Africa with the enlarged map of the greater Cape Town area showing the location of the industrial complex near Somerset West, on which the sulphur stockpile site is located (after Doel, 1997).....2
Figure 2. Industrial complex near Somerset West showing the sulphur stockpile site (the photograph depicted in Figure 2B is a magnification of the block shown in Figure2A). 3
Figure 3. Sulphide accumulation and acid sulphate generation on a coastal margin (after McBride, 1994).....7
Figure 4. Maximum pH for growth of *T. ferrooxidans* (after Bloomfield, 1972).....9
Figure 5. Ferric iron activity as a function of pH for mine drainage waters (after Bigham *et al.*, 1996b).....10
Figure 6. Relative abundances of mineral precipitates normalised to 100% (after data by Bigham *et al.*, 1996a).....11
Figure 7. Effect of pH on metal adsorption by hematite and goethite (after Schwertmann and Taylor, 1989).....12
Figure 8. Total acidity as a function of pH in AMD environments (after Kelly, 1988).....13
Figure 9. Sampling locations for all water and soil samples.....22
Figure 10. Sampling locations of waters taken for Fe^{2+} determination.....23
Figure 11. Characteristic acidic red-brown water occurring in close proximity to limed water with Fe oxyhydroxide precipitates.....32
Figure 12. Water samples plotted on a Piper diagram using AQUACHEM, showing the distinctive geochemical facies of the samples from this environment.....34
Figure 13. The activity of Al^{3+} as a function of pH for all water samples containing measurable concentrations of Al.....36
Figure 14. Saturation indices of Al-sulphate mineral phases as a function of pH for all water samples containing measurable concentrations of Al.....36
Figure 15. Saturation indices of gypsum and quartz as a function of pH for all water samples. 36
Figure 16. The proportion of Fe^{2+} in solution as a function of *pe* for water sample AWC as calculated by PHREEQC.....39
Figure 17. A comparison of *pe* and pH for all water samples in which Fe^{2+} was determined..39
Figure 18. Activity of ferrous Fe as a function of pH for all water samples at *pe* values of 4 and 12 (presented in blue and magenta, respectively).....41
Figure 19. Saturation indices of goethite and jarosite as a function of pH for all water samples (assuming a *pe* of 12).....41
Figure 20. Acid saturation as a function of pH for all soil samples, with bounding lines based on data of Thomas and Hargrove (1984) for natural soils.....46
Figure 21. X-ray diffractogram of the clay fraction from the acidic subsoil composite sample (ASSC) showing expansion of smectite by glycerol solvation (K = kaolinite; 7.2 Å).48
Figure 22. X-ray diffractograms comparing the acidic topsoil and subsoil composite samples (ATSC and ASSC respectively) with uncontaminated samples taken from a test pit adjacent to the site (*d*-spacings of major peaks in Å).....48
Figure 23. X-ray diffractograms comparing the hardened horizons of two soil profiles (A3 and B4) with the horizons above in each case being A2 and B2, respectively (*d*-spacings of major peaks in Å).....49
Figure 24. X-ray diffractogram of pale yellow precipitate from the surface of a hardened soil sample showing characteristic jarosite peaks at *d*-spacings of 3.08, 3.11, 5.09 and 5.93Å.....49
Figure 25. SEM image of Fe oxide precipitates and gypsum formed at the soil surface.....52

Figure 26. SEM images showing different morphologies of acid precipitates adhering to larger grains. 52
Figure 27. SEM images of gypsum crystals growing from the surface of a lime grain coated with an Fe oxide precipitate. 52
Figure 28. SEM-EDS spectra of ochreous precipitate from the site shown in Figure 25. 53
Figure 29. SEM-EDS spectra of acid sulphate crystals (possibly jarosite) shown in Figure 26. 53
Figure 30. SEM-EDS spectra of Fe oxide coating of a lime particle from the site (Figure 27A). 53
Figure 31. A comparison of the major ions in solution between water and soil samples. 56
Figure 32. A comparison of the Al and Fe concentrations between selected water and soil samples. 56
Figure 33. A comparison of trace elements in solution between selected water and soil samples. 56
Figure 34. Proportions of different S species in selected soil samples. 58
Figure 35. X-ray diffractogram of rhombic S from the site showing the distinctive S reflections at *d*-spacing values of 3.85, 3.21 and 3.45Å. 59
Figure 36. The effects of molten S on soil pH. 60
Figure 37. X-ray diffractogram of dolomitic limestone used to neutralise the acidity of the soil at the site (*d*-spacings of major dolomite peaks are shown in Å; Q = quartz). 64
Figure 38. pH_{KCl} of limed topsoil and subsoil samples for short and long-term incubation as a function of the amount of limestone added. 68
Figure 39. Acid saturation of limed topsoil and subsoil samples for short and long-term incubation as a function of the amount of limestone added. 68
Figure 40. Al concentration of limed topsoil and subsoil saturated paste extracts for short and long-term incubation as a function of the amount of limestone added. 70
Figure 41. EC_e of limed topsoil and subsoil saturated paste extracts for short and long-term incubation as a function of the amount of limestone added. 70
Figure 42. SO_4 concentration of limed topsoil and subsoil saturated paste extracts for short and long-term incubation as a function of the amount of limestone added. 71
Figure 43. Ca and Mg concentration of limed topsoil saturated paste extracts for short and long-term incubation as a function of limestone added. 73
Figure 44. Ca and Mg concentration of limed subsoil saturated paste extracts for short and long-term incubation as a function of the amount of limestone added. 73
Figure 45. Dissolved organic carbon (DOC) of topsoil saturated paste extracts after incubation with limestone (No's 1-4 refer to equivalent solutions in Figure 46). 78
Figure 46. Saturated paste extracts of topsoil samples after incubation with limestone, showing changes in solution colour with variation in DOC (values in brackets represent amount of limestone added to sample per kg of soil with DOC concentrations plotted in Figure 45). 78
Figure 47. Alkalinity as a function of pH for all the saturated paste extracts of the limed incubation samples with pH > 4.5 (short and long-term samples shown as closed and open shapes, respectively). 80
Figure 48. Al^{3+} activity as a function of pH for all saturated paste extracts containing soluble Al (the solubility line for gibbsite is shown in black and the solubility windows for jurbanite and alunite are shown in blue and orange, respectively, based on minimum and maximum activity data from this study). 82
Figure 49. Fe^{2+} activity as a function of pH for all saturated paste extracts containing Fe at *pe* = 12 (estimated maximum and minimum (*pe*+pH) windows for $Fe(OH)_3$ and goethite are shown in blue and orange, respectively). 82
Figure 50. Saturation indices of selected aluminium mineral phases as a function of pH. 84

Figure 51. Saturation indices of selected silicate and carbonate mineral phases as a function of pH. 84
Figure 52. Saturation indices of Fe^{3+} mineral phases as a function of pH under various p*e* conditions. 85
Figure 53. Dried maize biomass of limed topsoil and subsoil samples as a function of the amount of limestone added. 86
Figure 54. Plant growth experiments using sweetcorn in residual saturated paste soil samples from the limed incubation study. 87

Figure B1. EC of all water samples as a function of the sum of anions and cations, respectively. 113
Figure B2. Fe calibration curve used for calculating the concentration of ferrous and total Fe in solution. 116
Figure B3. Calibration curve for S speciation using various proportions of S to SO_4. 119
Figure B4. Sulphur K_β peaks for WDXRFS powder briquette soil samples from this study. 119

List of tables

Table 1. Geochemistry of surface and groundwater from the site and vicinity. 31
Table 2. The iron composition and speciation of surface waters....38
Table 3. Composition of selected soil samples by XRFS. 42
Table 4. Geochemical data from composite topsoil and subsoil samples. 43
Table 5. Particle size distribution of the limestone used at the site. 64
Table 6. Trace element data for the saturated paste extracts of limed samples from the incubation study. 76
Table 7. Water quality regulation data compared with data from this study. 90

Table A1. Character of all surface and groundwater samples 108
Table B1. Duplicate pH measurements for the soil horizon samples. 109
Table B2. Duplicate EC analyses for selected water samples. 110
Table B3. Analytical parameters of the *Dionex* HPIC system. 112
Table B4. Duplicate HPIC analyses for selected soil solution samples. 113
Table B5. ICP-MS analyses of NIST water standards compared with published results. 114
Table B6. ICP-MS duplicate results for soil solution (TS0) and water samples (LWE). 115
Table B7. A comparison of the total soluble Fe concentrations of selected samples. 116
Table B8. Analytical conditions for determination of major elements using a Philips PW1480 WDXRF spectrometer (after Willis, 1999). 117
Table B9. Sulphur speciation determined by WDXRFS for selected soil samples. 120
Table B10. Description of limed incubation samples. 126
Table C1. Geochemical data for all surface and groundwater samples. 127
Table C2. Activities of selected species at p*e* = 4. 129
Table C3. Saturation indices of selected minerals at p*e* = 4. 129
Table C4. Saturation indices of goethite and jarosite at p*e* = 12. 129
Table C5. Texture and organic carbon content of all soil profile and composite samples. 131
Table C6. KCl extractable acidity of all soil profile, composite and limed incubation samples 132
Table C7. KCl extractable acidity of soil/sulphur melting experiments. 133
Table C8. pH_{KCl} of soil/sulphur melting experiments. 133
Table C9. Major ions in solution for limed incubation samples. 134
Table C10. Trace elements in solution for limed incubation samples. 135
Table C11. Selected activities of limed soil solutions below pH 5. 136
Table C12. Saturation indices of selected Al phases of limed soil solutions. 136
Table C13. Saturation indices of selected silicate and carbonate phases of limed soil solutions 137
Table C14. Saturation indices of selected Fe (III) phases of limed soil solutions. 137

1 Introduction

The study site for this investigation is about 40km SE of the Cape Town CBD along the main coastal arterial road (N2) stretching along the southern coast of South Africa. The site forms part of a larger industrial complex adjacent to the False Bay coastline, the location of which is depicted in Figures 1 and 2. Industry at this site was mainly confined to the manufacture of chemicals for use in the fertiliser and explosive industries.

The purpose of this work was to assess the geochemical character of a site of severely acidified soil at this industrial complex near Somerset West. The site had been designated as a storage area for a stockpile of elemental sulphur. In late 1995, the S dump was set alight by a nearby veld fire causing the S to melt and volatilising toxic concentrations of SO_2 gas. Apart from the obvious implications of SO_2 to the atmospheric environment, the soil and water at the site have suffered severe acidification. Strong parallels can be drawn between the S-induced contamination at this site and the processes involved in the formation of acid mine drainage (AMD). In both cases, the oxidation of sulphidic materials releases a great deal of acidity into the environment.

1.1 The study area

The site on which the S was stored comprises approximately 3 hectares of ground in a low tract of land adjacent to a natural wetland area to the south (Figure 2). In the rainy season, the site is poorly drained with large pools of standing water frequently forming across the surface. The topsoil has been physically disturbed and chemically altered to form a heterogeneous cover on the area.

1.1.1 Geological setting

The regional geology consists of Malmesbury group shales and sandstones with hornfels forming in places from contact metamorphism with surrounding granites of the Cape Granite Suite. The surrounding mountains comprise rocks of the Table Mountain Group (TMG) and Cape Granite Suite (CGS). To the south east of the site, the Hottentots Holland mountain range of TMG rocks runs in a north-south direction forming part of the eastern margin of False Bay. The Kuils River-Helderberg pluton lies to the north of the site and further north are the TMG sandstones of the Helderberg and Stellenbosch mountain ranges.

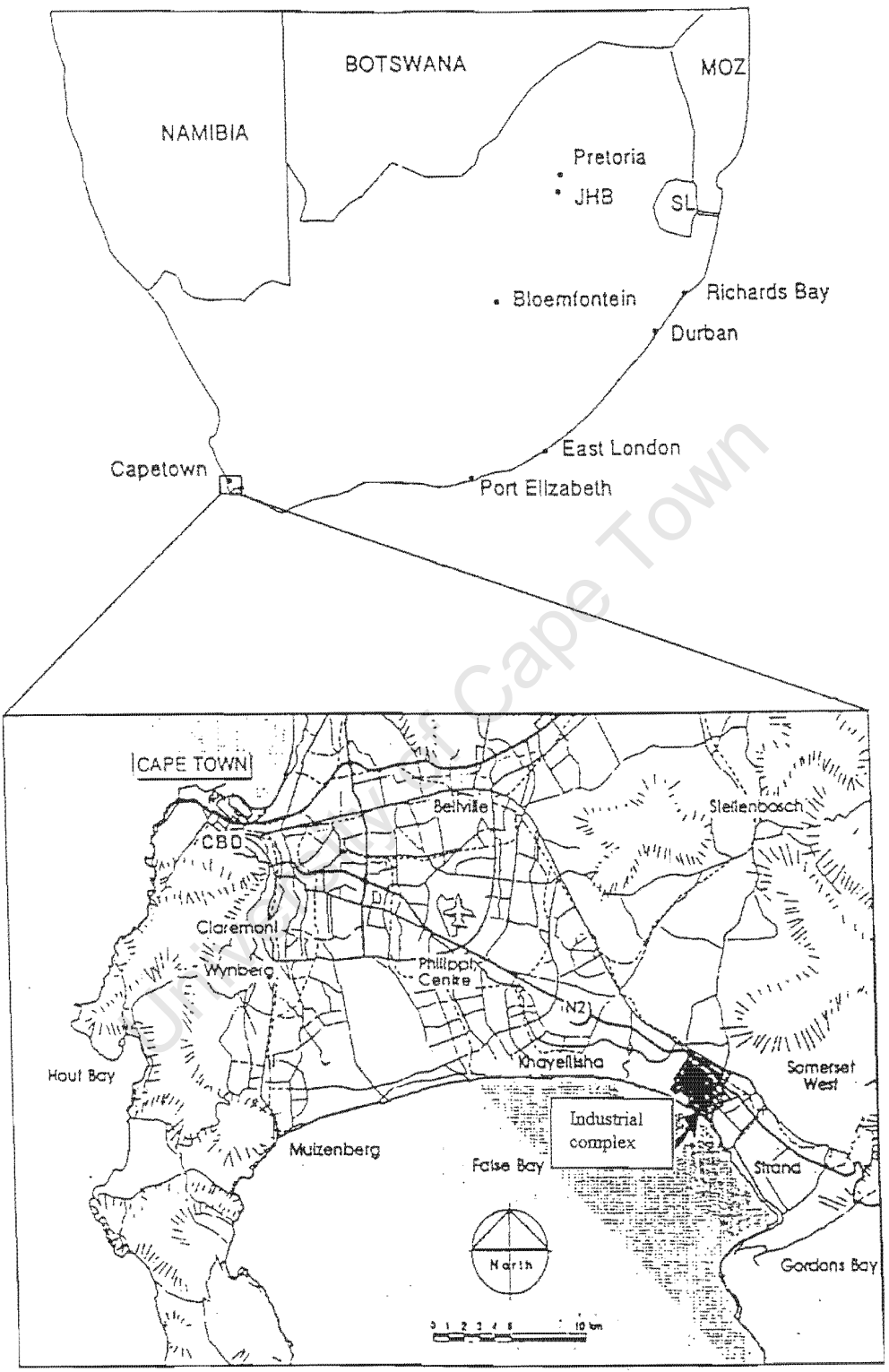

Figure 1. Map of southern Africa with the enlarged map of the greater Cape Town area showing the location of the industrial complex near Somerset West, on which the sulphur stockpile site is located (after Doel, 1997).

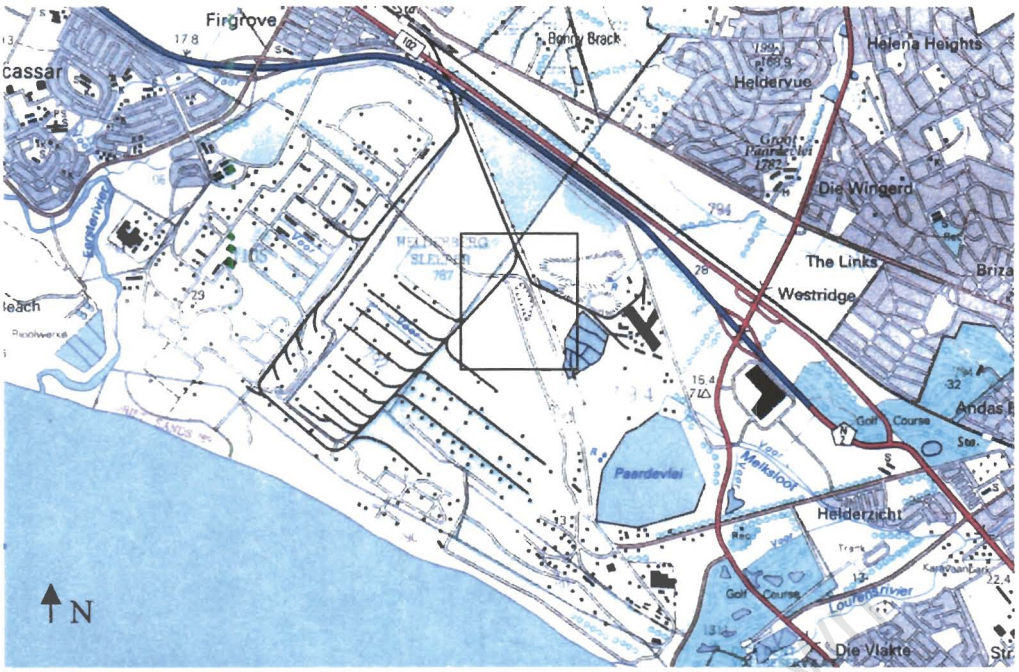

A. Topographic map of the industrial complex (Scale 1:50 000).

B. Aerial photograph (January 1996) of sulphur stockpile.

Figure 2. Industrial complex near Somerset West showing the sulphur stockpile site (the photograph depicted in Figure 2B is a magnification of the block shown in Figure2A).

A large portion of the land at the site and in the vicinity is situated within the Coastal Plain and Coastal Dune Belt of Quaternary sands that stretch along the coast of False Bay with the Malmesbury shales forming the basement bedrock at the site.

1.1.2 Climate

The site forms part of the winter rainfall region of the southern Cape with a rainfall of 570mm per annum. The mean average temperatures vary from 15 to 25°C in summer, and 9 to 20°C in winter. The wind is predominantly south-easterly in summer and north-westerly in winter.

1.1.3 Ecology

The area has been highly disturbed by human activity and the site thus encompasses a number of anthropogenic zones of vegetation. Indigenous flora is limited to a number of annuals occurring towards the north of the industrial complex, and the bulbous species *Spiloxene aquatica*, which is found in a number of seasonal pools along the margins of the cultivated areas. The annuals include species of *Dimorphotheca, Scenecio* and *Manulea* (Doel, 1997). There are fields, which are grazed by cattle on a rotational basis, and *Eucalyptus* plantations located sporadically across the site.

Most bird species known to the Cape have been spotted on the site including birds of prey such as fish eagles, hawks and black sparrow hawks (Doel, 1997). A large colony of Egyptian geese have also made their home at this site. Other fauna include steenbok, springbok, duiker, bontebok, mongoose, otter and the dune mole rat, with the latter three occurring naturally and the antelope having being introduced into the area.

1.2 Historical background of sulphur stockpile

Elemental sulphur was stored at this site for a number of years prior to the fire in 1995, forming a strategic stockpile to be used in the fertilizer and explosive industries. The stockpile was stored in an uncovered state on an unlined area of land, as elemental sulphur was considered to be relatively inert, posing little threat to the surrounding environment. The events of the fire in 1995 led to re-evaluation of the site and it was decided to dispose of the sulphur in due course. The last of the sulphur was thus removed in 1997 and since then, the site has been left barren and is devoid of any sign of life.

1.3 Research objectives

The objectives of this study are to assess the site in terms of its general geochemistry to gain a better understanding of the processes controlling the chemistry of the environment, and to quantitatively establish the environmental impacts that this land may have on its surroundings. In addition to this, an attempt will be made at establishing practical and cost-effective means of ameliorating the site in terms of its acidity. The strategies employed to carry out this project are briefly summarised as follows:

- A review of literature pertaining to acid sulphate environments and the oxidation of sulphidic materials will be made, to obtain a better understanding of the findings of other authors. This may be beneficial in approaching the environmental concerns at this site, as strategies for dealing with sulphide oxidation and subsequent acidification of the environment are well documented, in light of the commonly encountered problem of acid rock drainage environments.
- A comprehensive geochemical investigation will be undertaken of the water and soil at the site as well as the precipitates forming at the soil surface. In this way, an understanding of the chemical processes controlling this system can be obtained and rehabilitation strategies can be attempted.
- An attempt will be made to ameliorate the soils at the site in terms of their acidity by conducting laboratory liming experiments with commercial limestone. This will hopefully provide a benchmark for management strategies pertaining to the rehabilitation of this area of highly contaminated land.

To meet these objectives, detailed analyses will be conducted using standard methods of water and soil chemistry and, where necessary, experiments will be conducted to establish the response of the environment to inputs of neutralising agents and to monitor any trends in the data that might appear.

2 The origin and treatment of acid sulphate environments – a review

2.1 Introduction

The accidental burning and decomposition of a sulphur stockpile at an industrial site near Somerset West has caused severe contamination of the soil on which it was stored (Doel, 1997). The obvious implication of this is the acidification of the soil caused by the oxidation of S to H_2SO_4. The elevated levels of SO_4^{2-} in the soil, as well as anomalously high levels of heavy metals in solution, such as Al, Fe, Mn and As, result from this acidification as can be seen in the data reported by Doel (1997). The key questions arising from this site are thus the effects of S oxidation on soil acidity and toxicity, including practical and cost effective ways of restoring the site to its original condition. A further geochemical question is to determine whether the long-term S contamination may have led to the formation of a cemented soil horizon within the profile, as was noted on an earlier inspection of the site. This will be done by conducting a full geochemical assessment of the soil profile prior to the addition of neutralising agents.

To restore the soil and groundwater at this site to an acceptable level in terms of toxicity to plants and animals, certain rehabilitation strategies need to be applied in line with the liming experiments conducted by Fey and Abanda (1998) on soil samples taken from this site. The literature reviewed in this work thus concentrates on the problem of sulphur/sulphide oxidation as well as possible and practical strategies for restoring the environment to its pristine state. The problems associated with sulphide oxidation and H_2SO_4 formation are well documented in literature dealing with acid mine drainage (AMD) as the sulphide spoils of certain mining activities often pose a huge problem in terms of S contamination to the environment.

2.2 Classes of acid sulphate environments and their impact

2.2.1 Soils, sediments and other sulphur-containing materials

Submerged soils commonly contain iron sulphides (pyrites), which oxidise readily on exposure to air by means of fluctuating water tables or drainage. Soils and sediments rich in sulphides are commonly found on the coastal margins of oceans, as a result of the diffusion of SO_4^{2-} from sulphate-rich oceanic waters and the subsequent reduction of sulphate to sulphide. Soils showing evidence of acidifying weathering reactions associated with sulphide oxidation and the precipitation of sulphate minerals, such as gypsum and jarosite, are called 'acid sulphate soils'

(McBride, 1994). The process of sulphide accumulation and acid sulphate generation is illustrated in Figure 3.

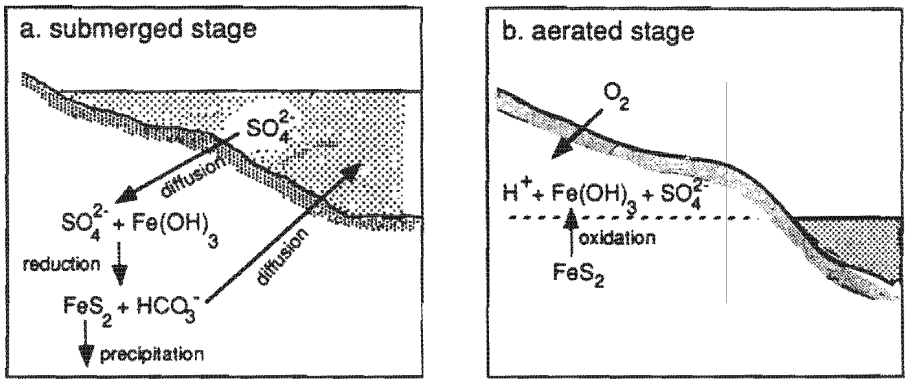

Figure 3. Sulphide accumulation and acid sulphate generation on a coastal margin (after McBride, 1994).

In semi-arid climates, sulphate deposits in the soil are sometimes reduced under conditions of poor drainage leading to the opposite effect of the acidifying process above. The conditions for reduction are created in natural basins on sodic soils where water accumulates due to the low permeability of the soil. In this case, the reduction reaction proceeds as follows:

$$Na_2SO_4 + 2H_2O + 2(C) \rightarrow 2NaHCO_3 + H_2S(g) \qquad (1)$$

where (C) represents organic carbon. In this reaction, H_2S is released to the atmosphere, and the alkalinity of the soil is increased by the production of $NaHCO_3$ (McBride, 1994).

Organic S is the dominant form of S in most soil and freshwater aquatic environments. Only in low organic matter, calcareous soils typical in arid and semi-arid environments will concentrations of inorganic S be greater than that of organic S. The amount of organic S in soil and aquatic environments differs considerably and is primarily dependent on the amount of organic matter present in the soil. S-containing amino acids are the most prevalent form of organic S in soils, making up 10-30% of the total S in various soils (Pierzynski *et al.*, 1994). Other substances that are important sources of organic S are sewage sludges and manures which can be applied to nutrient deficient soils.

2.2.1.1 Sulphidic oxidation and the generation of acidity

Acid sulphate soils result from the release of H_2SO_4 into soil through the oxidation of sulphidic material. Although the oxidation of S is primarily a biochemically-driven process, chemical oxidation of sulphides does also occur in nature, but at a much slower rate. The oxidation of reduced S is also an acidifying process, which is a major source of concern. An example of S oxidation that results in the formation of acidity is as follows (Pierzynski *et al.*, 1994):

$$2S + 3O_2 + 2H_2O \rightarrow 2H_2SO_4 \rightarrow 4H^+ + 2SO_4^{2-} \quad (2)$$

Microorganisms capable of oxidizing S include bacteria of the *Thiobacillus* genus, some of which are capable of surviving over a broad range of soil and environmental conditions, encompassing a pH range from 1.5 to 9 (Pierzynski *et al.*, 1994). It can be seen from Reaction 2 above that each mole of S oxidised produces 2 moles of acidity (H^+), emphasizing the severity of the acidifying process. The increase in acidity and subsequent lowering of pH also leads to the mobilization of potentially toxic metals, such as Al, Cu, Fe, Mn, Ni, Zn and As.

AMD is a common phenomenon caused by the oxidation of sulphides from mining activities, releasing SO_4^{2-} into the soil by the following reaction sequence (Singer and Stumm, 1970):

$$2FeS_2(s) + 7O_2(aq) + 2H_2O \rightarrow 2Fe^{2+} + 4SO_4^{2-} + 4H^+ \quad (3)$$

$$Fe^{2+} + O_2(aq) \rightarrow Fe^{3+} \quad (4)$$

$$14Fe^{3+} + FeS_2(s) + 8H_2O \rightarrow 15Fe^{2+} + 2SO_4^{2-} + 16H^+ \quad (5)$$

In these reactions, pyrite is oxidized to release Fe^{2+} which then oxidizes to Fe^{3+} after which the Fe^{3+} is again reduced to Fe^{2+} by reacting with a pyrite molecule and generating acidity. Reaction 4 proceeds much slower than Reaction 3 and, because the oxidation of pyrite in Reaction 5 is controlled only by the presence of ferric iron, the rate-determining reaction is the oxidation of Fe^{2+} (Reaction 4). Microorganisms such as *Thiobacillus ferrooxidans* catalyse the oxidation of Fe^{2+} and pyrite and can speed up the reaction by a factor of more than 10^6 (Singer and Stumm, 1970). The oxidation of Fe^{2+} at pH values of 3, 3.5 and 4.0 is illustrated in Figure 4, showing that the maximum pH at which *T. ferrooxidans* can grow lies between 3.5 and 4.0 (Bloomfield, 1972). This bacterium is most active from pH 1 to 3.5. It acquires C by fixation of CO_2 and obtains energy via the oxidation of Fe^{2+} to Fe^{3+} (Bigham *et al.*, 1996a). Although the oxidation

of pyrite plays no role at the S-contaminated site near Somerset West, the low pH has caused the mobilization of metals including Fe. It is thus likely that Fe plays an equally significant role at this site as it does in the case of acid mine drainage. This is confirmed by the reddish-brown colour of the highly acidic water at this site. What is also important to note is that the balanced equivalent of Reaction 4 consumes acidity and produces water as follows (Blowes *et al.*, 1991):

$$Fe^{2+} + {}^{1}/_{4}O_2 + H^{+} \rightarrow Fe^{3+} + {}^{1}/_{2}H_2O \qquad (6)$$

Elevated levels of Fe^{2+} may thus help to buffer increases in acidity, although Reactions 3 and 5 generate acidity and the net effect will thus be for the system to become more acidic.

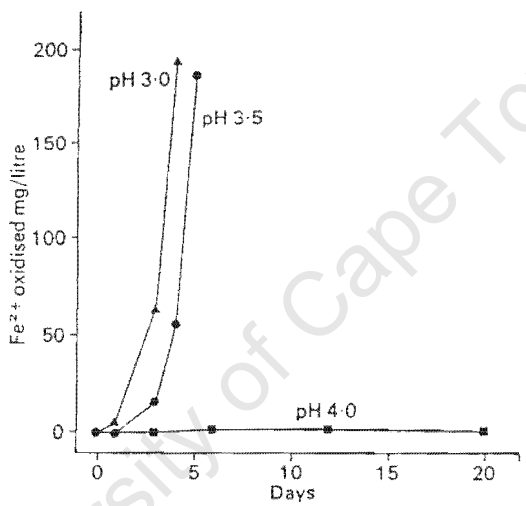

Figure 4. Maximum pH for growth of *T. ferrooxidans* (after Bloomfield, 1972).

S-contamination accelerates many processes that reduce the exchangeable base cation content of soils, and release phytotoxic elements such as Al^{3+} and Mn^{2+} into solution. A study by Terelak *et al.* (1996) showed that the addition of S to soil decreased the pH_{KCl} and increased the acidity and exchangeable Al content. There was also an associated decrease in the percentage of base cations, especially Ca^{2+} and Mg^{2+}, as well as an increase in the concentration of H^{+} on the exchange complex of the soil. In the most extreme case of applying the equivalent of 500 kg S $ha^{-1}yr^{-1}$ for 5 years, the base saturation dropped to 25% (Terelak *et al.*, 1996).

2.2.1.2 Mineralogy of acid sulphate environments

The ochreous precipitates of sediments associated with areas of acid mine drainage have been analysed by Bigham *et al.* (1992; 1996b). The results show that at pH > 6.5 the precipitates are composed of ferrihydrite and goethite, and at pH values between 2.8 and 4.5 the predominant mineral is schwertmannite with trace amounts of goethite. Between pH values of 4.5 and 6.5 the predominant minerals are schwertmannite and ferrihydrite. The mineral jarosite appeared at a pH of 2.6 (Figure 5). Due to the metastable nature of schwertmannite, it is transformed to goethite over a lengthy period of time by the following reaction (Bigham *et al.*, 1996b):

$$Fe_8O_8(OH)_6SO_4(s) + 2H_2O(l) \rightarrow 8FeOOH(s) + 2H^+(aq) + SO_4^{2-}(aq) \qquad (7)$$

Other work conducted by Bigham *et al.* (1996a) confirms the occurrence of jarosite at pH < 3 and shows that this mineral increases in abundance as the pH decreases. Schwertmannite was the only mineral precipitate found at pH = 3 while goethite appeared at pH > 3 and seems to increase as the pH increases, as can be seen in Figure 6 (Bigham *et al.*, 1996a). Minor changes in pH can thus have important impacts on mineral speciation within acid SO_4 systems. Goethite formation is also favoured by the presence of HCO_3^-, such as when acid mine waters are mixed with carbonate-rich surface or ground waters. The minerals forming in acid sulphate environments from the oxidation of Fe^{2+} are bacterially mediated at pH < 4. Mineralisation is extracellular and mineral speciation is controlled by geochemical parameters such as pH and $[SO_4^{2-}]$ (Bigham *et al.*, 1992).

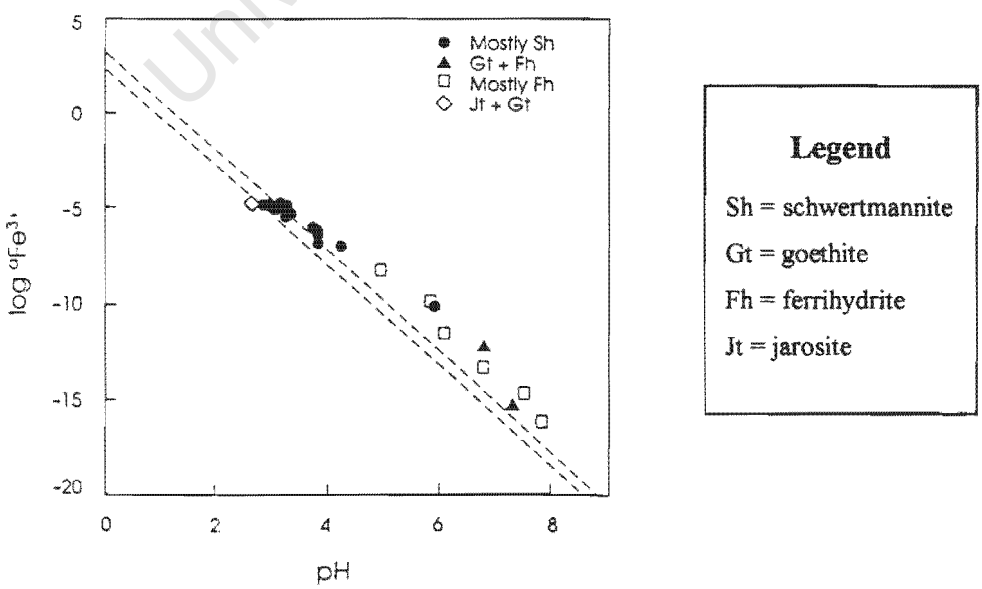

Figure 5. Ferric iron activity as a function of pH for mine drainage waters (after Bigham *et al.*, 1996b).

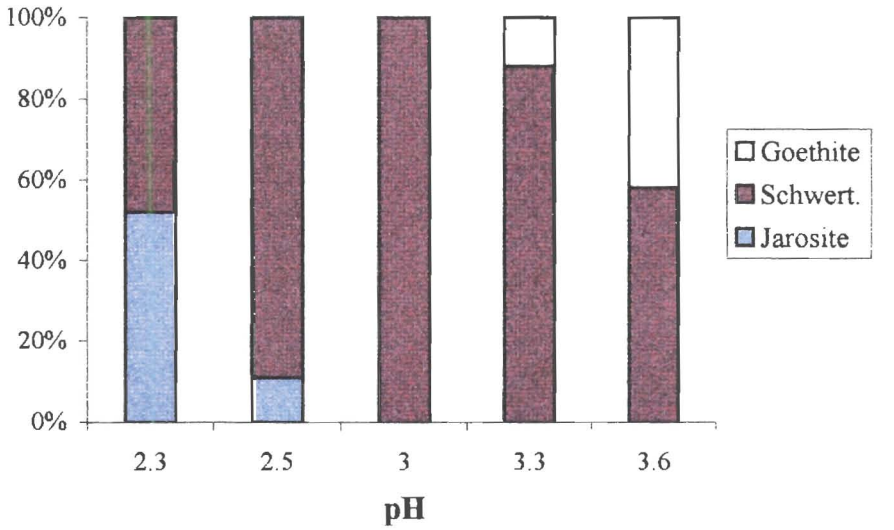

Figure 6. Relative abundances of mineral precipitates normalised to 100% (after data by Bigham *et al.*, 1996a).

The fine-grained weathering products of sulphide mining have been noted by Dinelli *et al.* (1998) to produce two distinctly different secondary mineral phases. The first phase of sediments have a typical ochreous colour and are associated with pyritic oxidation and the formation of goethite and ferrihydrite consistent with the discussions above. The second mineral is blue in colour and appears to be a Cu-Al hydrous sulphate mineral of the woodwardite group. These blue sediments are not detected in the aerated portion of the soil but are rather associated with a mixing zone involving reduced, low pH waters from within the waste deposit and aerated surface and phreatic waters from the outside of the waste dump. These precipitates are thus thought to represent an alkaline geochemical barrier in an oxidising environment (Dinelli *et al.*, 1998). This unusual blue mineral probably forms under specific redox conditions and is dependent on the presence of Cu and soluble Al for its make-up. It seems that the more stable ochreous precipitates will form preferentially under aerobic conditions and this may account for the rare occurrence of this woodwardite mineral in sulphide oxidising environments.

The occurrence of cemented layers within sulphide mine tailings has been documented by Blowes *et al.* (1991) and is of particular interest, as this is consistent with the industrial site near Somerset West where a continuous cemented horizon was encountered between 10 and 80 cm from the soil surface. Although a direct comparison between an anthropogenically-created tailings dump and an *in situ* soil profile should not be made, the processes involved in the formation of cemented layers in acid sulphate environments is likely to be similar. Two distinctly different horizons have been observed by Blowes *et al.* (1991), the first occurring near

the depth of active oxidation, which is cemented by gypsum and Fe(III)-bearing minerals like jarosite, goethite, lepidocrocite and ferrihydrite. The second horizon, which was encountered at a different site, occurred 20-30 cm below the depth of active oxidation and is cemented by gypsum and Fe(II)-bearing minerals, predominantly melanterite ($FeSO_4 \cdot 7H_2O$). At the Fe(II) site, high sulphide concentrations have caused atmospheric O_2 to be consumed near the tailings surface and the reduction of Fe(III) to Fe(II) at depth, allowing for high enough concentrations of Fe(II) and SO_4 to attain saturation with respect to melanterite. The Fe(III) site is oxygenated and thus characterised by the expected suite of Fe-oxyhydroxy-sulphate minerals mentioned above (Blowes *et al.*, 1991).

2.2.1.3 Metal mobility in acidic soils

One of the important concerns of the low pH of acid sulphate environments is the mobilization of heavy metals. An example of metal sorption on the Fe oxides, goethite and hematite, can be seen in Figure 7, clearly showing that sorption of metals by these oxides is strongly controlled by pH and only begins to occur at pH > 3 (Schwertmann and Taylor, 1989).

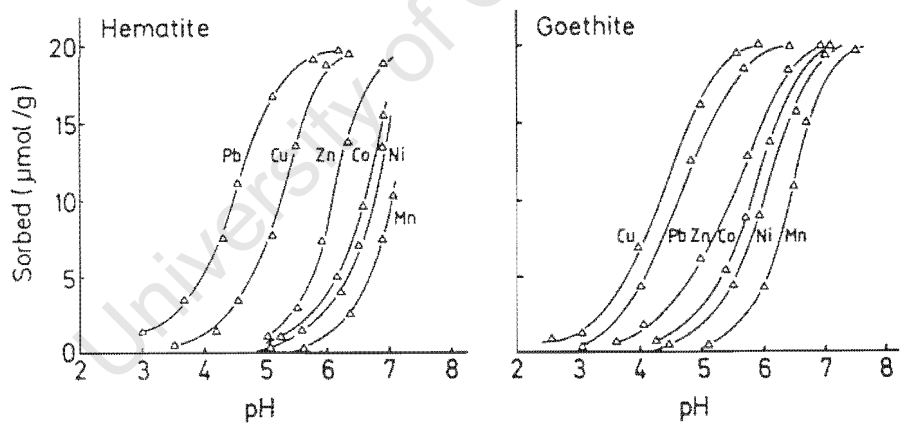

Figure 7. Effect of pH on metal adsorption by hematite and goethite (after Schwertmann and Taylor, 1989).

Metal ions are lost from solution by precipitation or adsorption, both processes being strongly controlled by pH. The minimum pH for the precipitation of metal hydroxides and other salts ranges from 4.2 for Sn to 10.6 for Mn(II) (Kelly, 1988). Acid sulphate waters are thus likely to contain elevated concentrations of heavy metals in solution, contributing to their toxicity to plants and animals.

2.2.2 Mine spoils

Mining activities may bring large quantities of sulphides to the surface, particularly those mines associated with coal and metal extraction. The sulphide-rich rocks are then stockpiled where they are well aerated and easily able to oxidise to SO_4^{2-}, generating acidity (Reactions 3 and 5), and substantially lowering the pH of the associated soils and ground water. The important sulphide oxidising reactions pertaining to AMD have been discussed in section 2.2.1.1 above (Reactions 3-5), as well as the bacteria that are able to utilize pyrite as a source of energy and facilitate the oxidation of Fe species like Fe^{2+}. The acidophilic chemo-autotrophic bacteria, *T. ferrooxidans* (iron-oxidising) and *T. thiooxidans* (S-oxidising), have been found in virtually all AMD environments (Kelly, 1988).

In terms of acidity, it is important to note that pH is neither a true indication of acidity, nor is it a good determining factor for the extent of AMD. It is the availability of H^+ ions to neutralise bases that is most important. This is referred to as the total acidity and is expressed in mg/L $CaCO_3$, thereby relating the total acidity to the amount of $CaCO_3$ required for its neutralisation. It is, however, generally found with AMD that there is a linear relationship between total acidity and pH, and that at pH values > 5, there is rarely very much acidity as can be seen in Figure 8. In fact, the key difference between AMD and other acid sulphate environments such as peat drainage and acid rain affected areas, is that in other acid sulphate environments, low pH is coupled with low acidity, whereas in AMD environments, low pH is linked to high acidity (Kelly, 1988).

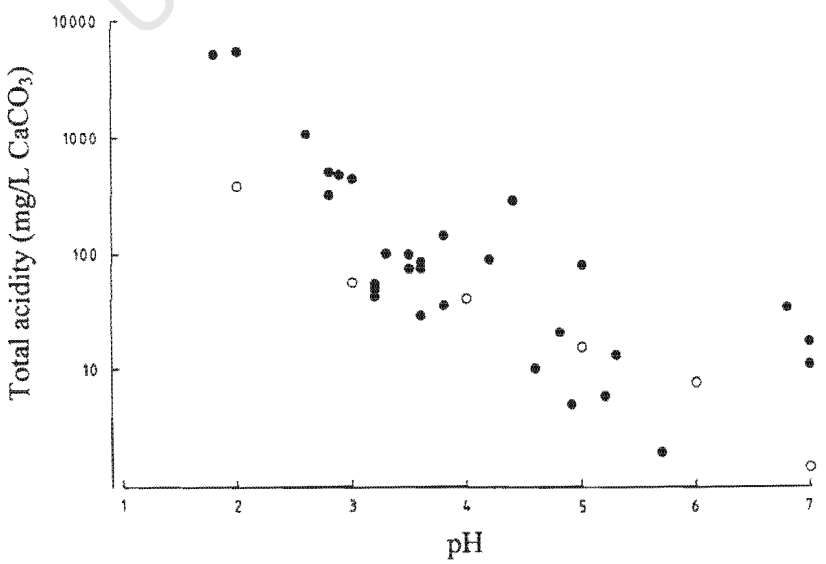

Figure 8. Total acidity as a function of pH in AMD environments (after Kelly, 1988).

One of the most important effects of low pH is to destroy the carbonate buffer system, which controls the magnitude of change in pH. At pH < 4.2, all carbonate and bicarbonate is converted to carbonic acid which easily dissociates to H_2O and CO_2. The important consequences of this are that the water loses its capacity to buffer changes in pH, and that plants use bicarbonate as their inorganic source of C and therefore, in its absence, need to use CO_2 for photosynthesis. What is also important is that once the alkalinity of a water body is destroyed, it can take a long time to recover, even without the addition of further acid to the system (Kelly, 1988).

The classic orange-hued iron precipitates associated with AMD have been discussed in 2.2.1.2 above and will thus not be covered in this section. In certain instances, some iron may be precipitated as phosphate, effectively stripping this nutrient from solution. Other flocs may form from Al oxides and hydroxides producing white coloured precipitates. These flocs form as the AMD becomes neutralised. At typical pH values for AMD, Fe(III) salts will remain in solution until a certain amount of neutralisation has taken place (Kelly, 1988).

2.3 Remediation of acid sulphate environments

2.3.1 Neutralising agents and techniques

A number of different neutralising agents and techniques can be used to remediate acid sulphate environments, the most notable being the application of liming materials such as carbonates, which provide a practical and effective means of neutralising severely acidic environments. An important consideration in terms of liming is the use of crushed cement, since it is often more easily available and is still an extremely effective neutralising agent (Fey and Abanda, 1998).

Another method of neutralisation is organic amendment using alkaline biosolids, which may provide another inexpensive and effective means of neutralising acidity. The use of electrochemical methods is a further option, which is unlikely to provide a practical solution to the remediation of soils, but may find some application in the treatment of effluent waters in mining operations. In these cases, the AMD produced by the constant production of sulphides over a long period of time could effectively be neutralised by setting up an electrochemical cell as part of the treatment process.

2.3.1.1 Cement waste

An experiment conducted by Fey and Abanda (1998) on the use of crushed cement in the treatment of S-contaminated soil demonstrated the effectiveness of this inexpensive liming material in the treatment of soil acidity. It was found that with a cement:soil ratio of 0.3 (i.e. 1 part cement to 3 parts soil) it was possible to increase the pH from <3 to >6, while the EC decreased to <3 μS/cm at cement:soil ratios of >1. Plant growth experiments were then conducted using leached mixtures of soil and cement with the concentration of cement varying from 0-33%. From these experiments it was found that the plant yield response correlated closely with the increase in pH and at cement levels of 25%, the pH was >6 and dry plant yield also increased dramatically. What is also important is that the salinity of the mixtures remained relatively uniform, suggesting the precipitation of phases such as gypsum, jarosite and ettringite. Salinity appears to have had no effect on plant growth in these experiments, as the maize plants appeared healthy at pH 6 to 7, suggesting that salinity was not a growth-limiting factor (Fey and Abanda, 1998).

2.3.1.2 Passive treatment with anoxic limestone drains

The technique of passively treating acid sulphate mine spoils with limestone is of particular interest as it does not require regular additions of chemicals, providing a long-term, low maintenance solution to AMD remediation. The basic concept is to set up an anoxic limestone drain (ALD), which is done by burying a bed of limestone beneath a mine spoil dump in order for the mine drainage to flow through the limestone before entering the environment. In this way the acid is neutralised before exiting the mine site. The critical factor for the effectiveness of this technique is that the Fe remains in the ferrous form, and thus the mine water in contact with the limestone should be in an anoxic environment. Under this condition, no armouring of limestone should occur (Hedin *et al.*, 1994). The results from a study by Hedin *et al.* (1994) showed that in two constructed ALDs, the effluent waters were characterised by increases in pH, alkalinity and Ca^{2+}. The concentrations of Fe^{2+}, Mn^{2+}, Mg^{2+}, Na^{+} and SO_4^{2-} changed little between the influent and the effluent of the first site but showed a slight decrease in the effluent of the second site. However, this was attributed to dilution with uncontaminated water from another source. This ALD system is expected to provide a simple long-term solution to the problem of AMD, but it is important to note that high concentrations of metals in solution, such as $Fe^{2+,3+}$ and Mn^{2+}, will need to be lowered for the water to be restored to an uncontaminated state. For this reason, it has been proposed that wetlands be constructed downstream of the ALDs. In this way, the alkalinity can facilitate the precipitation of metal contaminants, as aerobic conditions will promote Fe^{2+}

oxidation reactions and the precipitation of ferric oxyhydroxides (Hedin *et al.*, 1994). However, it should be noted that Fe^{2+} oxidation is, itself, an acid releasing process.

By contrast to the discussion above, Ziemkiewicz *et al.* (1997) proposed that open limestone channels can also provide a long-term maintenance free solution to AMD. The obvious negative consequence of this method is that the limestone will become armoured by Fe hydroxides, reducing its ability to dissolve and neutralise acidity. It was found that armoured limestone was 2 to 45% less effective in neutralising acid than unarmoured limestone, and that it was pH dependent. The effectiveness of armoured limestone appeared to decrease with the pH of the solution. The use of open channels could be optimised by minimising the amount of armouring of the channels. This could be achieved by constructing channels on steep slopes (>20%) where flow velocities keep metal hydroxides in suspension, limiting their precipitation and plugging of limestone pores in the channel (Ziemkiewicz *et al.*, 1997).

2.3.1.3 Barium carbonate

A study was conducted on the removal of sulphate from mine effluent waters by reaction with $BaCO_3$, with favourable results (Trusler *et al.*, 1991). It was found to effectively remove sulphate from solution and neutralise acid mine drainage. The drawbacks with the use of $BaCO_3$ are that it is too expensive, the reaction rate is too slow and that Ba contaminates the product water. The long reaction time, however, can be solved by using smaller particles of Ba, seeding the mixture with $CaCO_3$ and adding lime to ensure that the SO_4^{2-} ions are associated with Ca^{2+} ions (see Reaction 8). The Ba is recycled, producing Ba-salts and elemental S and lime as byproducts, which can then be sold to reduce costs. The product water also contains very little Ba.

$$BaCO_3 + CaSO_4 \rightarrow BaSO_4\downarrow + CaCO_3\downarrow \quad (8)$$

The benefits of using $BaCO_3$ over more easily accessible and cheaper alternatives such as $CaCO_3$ are related to the fact that the reaction product, $BaSO_4$, is highly insoluble and $BaCO_3$ is thus more successful in permanently removing SO_4^{2-} from solution than other carbonates. Due to the high cost of $BaCO_3$, however, it is essential that the substance is recycled to make it a feasible alternative. It is unlikely to be economically feasible to use this material for the remediation of acid sulphate environments but it may find some application in waterworks technology. It is also important to note that $BaCO_3$ was successfully used on an effluent from a zinc plant, not only to

neutralise the acidity, but also to rapidly remove metals such as Zn^{2+}, Cd^{2+} and Mn^{2+} from solution (Trusler *et al.*, 1991). $BaCO_3$ may thus be more effective in removing metals from solution than $CaCO_3$ alone, establishing its preference for use in water treatment.

2.3.1.4 Liming of sulphides

In a land reclamation study on the application of $CaCO_3$ to soils containing FeS_2, it was shown that lime treatment slowed the oxidation of FeS_2 but that oxidation increased once the lime was neutralised, indicating that larger amounts of lime were needed (Doolittle and Hossner, 1997). Residual FeS_2-CO_3 data and acid-base values, however, showed that lime was dissolving faster than the FeS_2 was oxidising, and thus all treatments would eventually become acidic.

2.3.1.5 Organic amendment

Organic amendment of acid soils has been considered by Sloan and Basta (1995), by using alkaline biosolids as neutralising agents. Biosolids are produced from wastewater treatment sewage sludge. Alkaline biosolids arise from sewage sludge that is treated with alkaline materials, such as lime, to kill pathogens. The relative effects of treating an acid soil with unlimed sewage sludge, alkaline biosolids and agricultural lime were compared. These materials were added to soil samples that had phytotoxic concentrations of Al and Mn prior to treatment. It was found that alkaline biosolids were as effective as agricultural lime for remediating acid soils. The soil pH increased linearly with the application of alkaline biosolids and soluble and exchangeable Al were decreased to nontoxic levels (<0.4 mmol/L). The concentration of soluble Mn also decreased to levels that eliminated the potential threat of Mn toxicity and the increase in pH minimized any increases in heavy metal bioavailability (Sloan and Basta, 1995).

The use of nonalkaline biosolids showed a slight increase in soil pH, coupled with a decrease in soluble and exchangeable Al, but these decreases were much smaller than for alkaline biosolid amendment, and thus did not eliminate the threat of Al toxicity to plants. Direct application of untreated sewage sludge is also likely to increase heavy metal bioavailability in soils. There was no effect on the concentration of soluble Mn from the use of unlimed sewage sludge. The application of alkaline biosolids to acid soils will thus have more of an agronomic benefit than nonalkaline sewage sludge (Sloan and Basta, 1995). The use of alkaline biosolids could thus provide another inexpensive and effective way of remediating acid soils and may serve as an alternative liming material to carbonates.

2.3.1.6 Electrochemical methods

A new technique for the amelioration of AMD employs a galvanic arrangement in which a block of massive sulphide rock is used as the cathode of an electrochemical cell with Al and Zn making up the sacrificial anodes. These experiments were designed to halt acid generating reactions and increase the pH of AMD by converting H^+ ions to H_2 (Shelp *et al.*, 1996).

The effectiveness of the cell in reducing the H^+ concentration of the acidic leachate to pH $\geq$ 5.5 is directly related to the precipitates of Al or Zn that are formed. The concentrations of toxic trace elements should also decrease by coprecipitation. The use of Al as an anode produced an increase of pH from 3.17 to 4.4, after which it remained constant until the termination of the experiment. This lower equilibrium pH is likely to be controlled by the formation of Al precipitates such as amorphous gibbsite or alunite. The only trace element showing a significant decrease was Cu, with a decrease of over 85%. The Zn anode, on the other hand, had a distinctly different effect, with the pH increasing from an initial value of 3 to a final value of 6.7. The solution concentrations of Al, Cd, Cr, Co, Cu and Ni also reduced significantly to below environmentally acceptable levels for mine effluent discharge. The drawbacks to this method of AMD amelioration include the cost of Zn metal and the fact that the concentration of Zn in solution was unacceptably high under the current Eh/pH conditions (Shelp *et al.*, 1996). Further work in this regard is needed before this method can be used effectively in treating acidic mine effluent waters.

A similar experiment was conducted by Shelp *et al.* (1995) with pleasing results, using an iron-sulphide rock as the cathode and scrap Fe as the anode. In this experiment, the pH was raised to 5.6 and there was a significant lowering of the concentrations of Al, Cd, Co, Cu and Ni in solution. In terms of the cost and relative success of the Fe anode, it may provide a more practical alternative to the Zn anode, and in addition to this, it is unlikely to produce environmentally hazardous concentrations of Fe in solution. It thus provides an inexpensive and effective means of remediating the AMD problems associated with mining effluent waters.

2.4 Conclusions

Acid sulphate soils result from the oxidation of reduced sulphidic materials, such as sulphides, and the subsequent generation of acidity in the form of H_2SO_4. The oxidation of sulphide-rich material is primarily a biochemically-driven process at pH < 4, with the acidophile bacterium *Thiobacillus ferrooxidans* catalysing the oxidation of Fe^{2+} and pyrite, and accelerating the

reaction by up to 10^6 times. The oxidation of elemental S is mediated by *Thiobacillus thiooxidans* producing acidity in the following way:

$$2S + 3O_2 + 2H_2O \xrightarrow{T.\ thiooxidans} 2H_2SO_4$$

S-contamination reduces the exchangeable base cation content of soils, and releases phytotoxic elements such as Al^{3+} and Mn^{2+} into solution. The addition of S to soil decreases the pH_{KCl} and increases the acidity and exchangeable H and Al content. Although pH is not a true indication of acidity, there seems to be a direct relationship between pH and acidity in AMD environments. The increase in acidity and subsequent lowering of pH also leads to the mobilization of potentially toxic metals, such as Al, Cu, Fe, Mn, Ni, Zn and As. A common problem caused by the oxidation of sulphides is AMD, which results from the oxidation of sulphide-rich waste materials produced by certain mining activities such as coal and metal extraction.

The most common minerals precipitating from acid SO_4 environments are the characteristic red, orange and yellow minerals including ferrihydrite, goethite, schwertmannite and jarosite. These ochreous precipitates are commonly associated with areas of AMD and their sequence of precipitation is strongly dependent on pH. At pH > 6.5, the precipitates are composed of ferrihydrite and goethite and at pH values between 2.8 and 4.5, the predominant mineral is schwertmannite with trace amounts of goethite. The mineral, jarosite, occurs at pH values of <3. Schwertmannite is a metastable, poorly crystalline mineral and transforms to goethite over time. Relatively minor changes in pH thus have important impacts on mineral speciation within acid SO_4 systems. The formation of cemented layers within acid sulphate soils seems to be a common phenomenon. The cemented horizons found in the oxic zone are composed of gypsum and Fe(III)-bearing minerals like jarosite, goethite, lepidocrocite and ferrihydrite, while the horizons encountered below the level of active oxidation include gypsum and Fe(II)-bearing minerals such as melanterite ($FeSO_4 \cdot 7H_2O$).

In terms of remediating acid sulphate environments, the most effective technique is that of liming, with the most practical and inexpensive liming material being crushed cement. This material effectively neutralises acid soils and eliminates the risk of phytotoxicity in terms of the concentration of metals in the soil solution. Because relatively large quantities of cement are needed to neutralise severely acidic soils, and waste concrete may not be readily available, the usefulness of this substance is largely site specific. The alternative to remediating acid soils is

the use of commercial liming materials such as CaO and $CaCO_3$. These substances are likely to be more effective in neutralising acidity, provided that they are finely crushed, however, they can be substantially more expensive and difficult to obtain, depending on location.

Anoxic limestone drains provide a moderately effective way of passively managing sulphide tailings dumps as they require little maintenance and provide a long-term solution to the ongoing problem of stockpiling sulphides produced from mining activities. The direct application of $CaCO_3$ to sulphide-rich soils slowed down FeS_2 oxidation, but it soon increased again once the lime was neutralised, indicating that larger amounts of lime were needed. In this type of treatment it was found that lime was dissolving faster than the FeS_2 was oxidising, and thus all treatments would eventually become acidic.

Other acid neutralising solutions include the use of barium carbonate, alkaline biosolids and electrochemical techniques. $BaCO_3$ was found to be effective in water treatment but would require recycling in order to reduce its cost, and it may thus find some application in waterworks technology where recycling plants could be set up as part of the process. Alkaline biosolids were found to be extremely effective in neutralising soils and removing metals from solution, providing another inexpensive and useful means of remediating acid soils as well as finding a use for biosolid material. Electrochemical techniques were found to be effective in treating acid mine effluent water with either Fe or Zn making up the anode for the electrochemical cell and sulphide rock providing the cathode.

3 Geochemical investigation of soil and water

3.1 Introduction

To fully appreciate the complexity of the chemical processes that are at play in this environment, it is important to consider both the solid phase and aqueous geochemistry of the site. A holistic approach was thus adopted, exploring the aqueous chemistry, the soil composition, mineralogy and solution chemistry as well as the mineralogy of any precipitates forming in this environment. A representative set of soil and water samples were therefore collected and analysed using standard techniques of soil and water chemistry. Chemical speciation of solutes and the solubility of relevant mineral phases was explored with the aid of the hydrochemical modelling program, PHREEQC. Where appropriate, comparisons have been drawn between the water and soil solution data from this study as well as data from other authors.

3.2 Sample collection

An initial sampling excursion was undertaken to the site in June 1999, prior to the initiation of a remediation program by an engineering consulting firm in Cape Town. On this occasion, 5 soil profiles were sampled across the site comprising 19 individual soil horizon samples. In addition to this, 5 water samples were taken from the site and the vicinity. A second visit was made in August 1999, by which time the site had been treated with approximately 450 tonnes of dolomitic limestone and 220 m^3 of cattle manure. Three composite topsoil samples were taken on this occasion in representative E-W traverses across the site. A further 5 surface water samples were also taken as well as 2 groundwater samples from strategically placed boreholes on the site. The initial sampling locations are labelled with the prefix A to denote 'acid' followed by the sample locations, labelled A to H. The post-liming sample locations have been labelled with a prefix L denoting 'limed' followed by locations A to E. The sampling locations are presented in Figure 9 with soil profile and water sample descriptions in Appendix A.

In order to obtain an estimation of the ferric/ferrous iron ratio, a further 4 water samples were taken and acidified in the field, as described in section 3.2.1 below. The sample locations are presented in Figure 10 (labelled LF to LI) and described in Appendix A. The water sample taken from site LE was also included in the Fe^{2+} analysis since it was preserved shortly after reaching the laboratory. No other water samples were selected for Fe^{2+} determination as they were not suitably preserved.

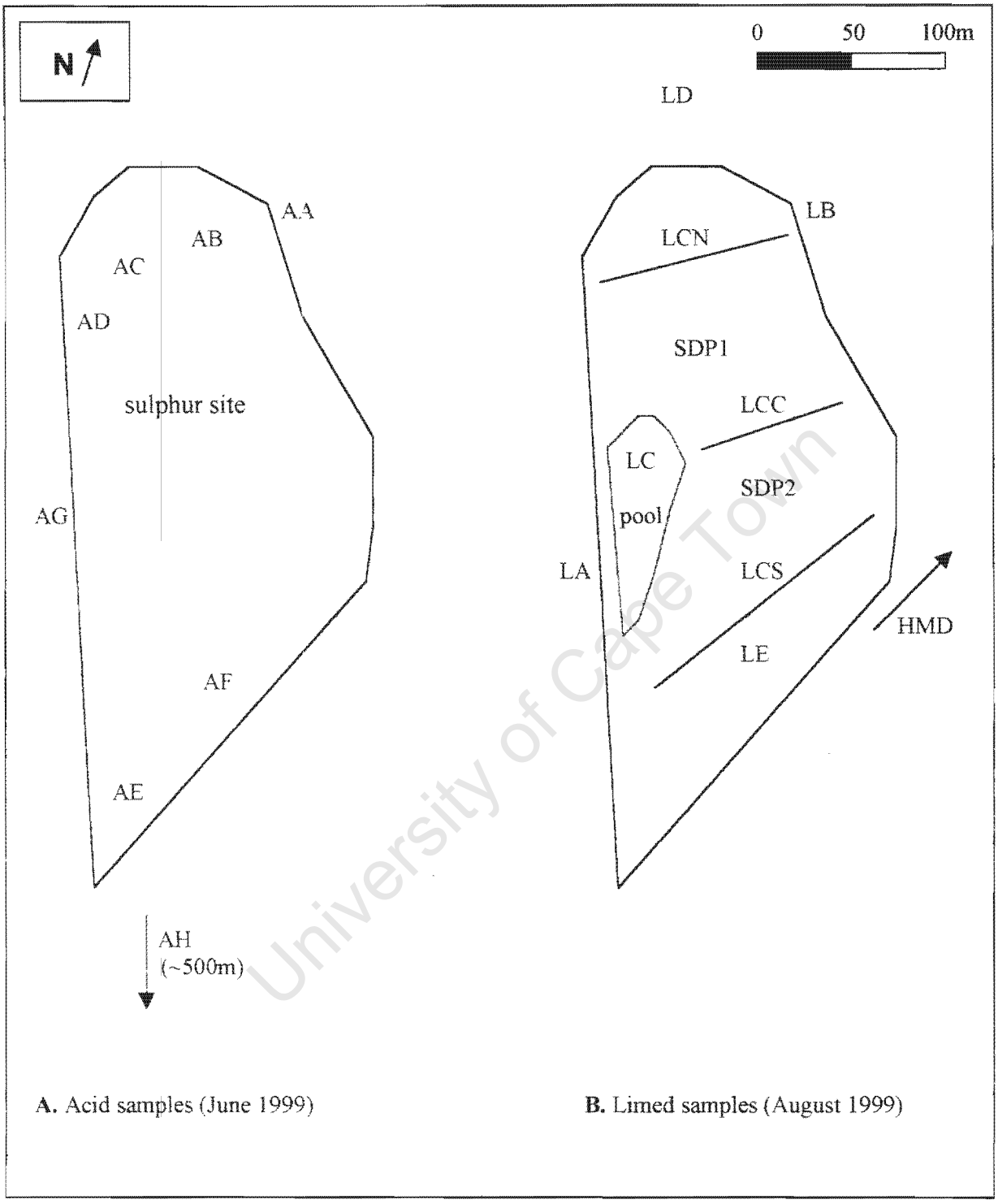

Figure 9. Sampling locations for all water and soil samples.

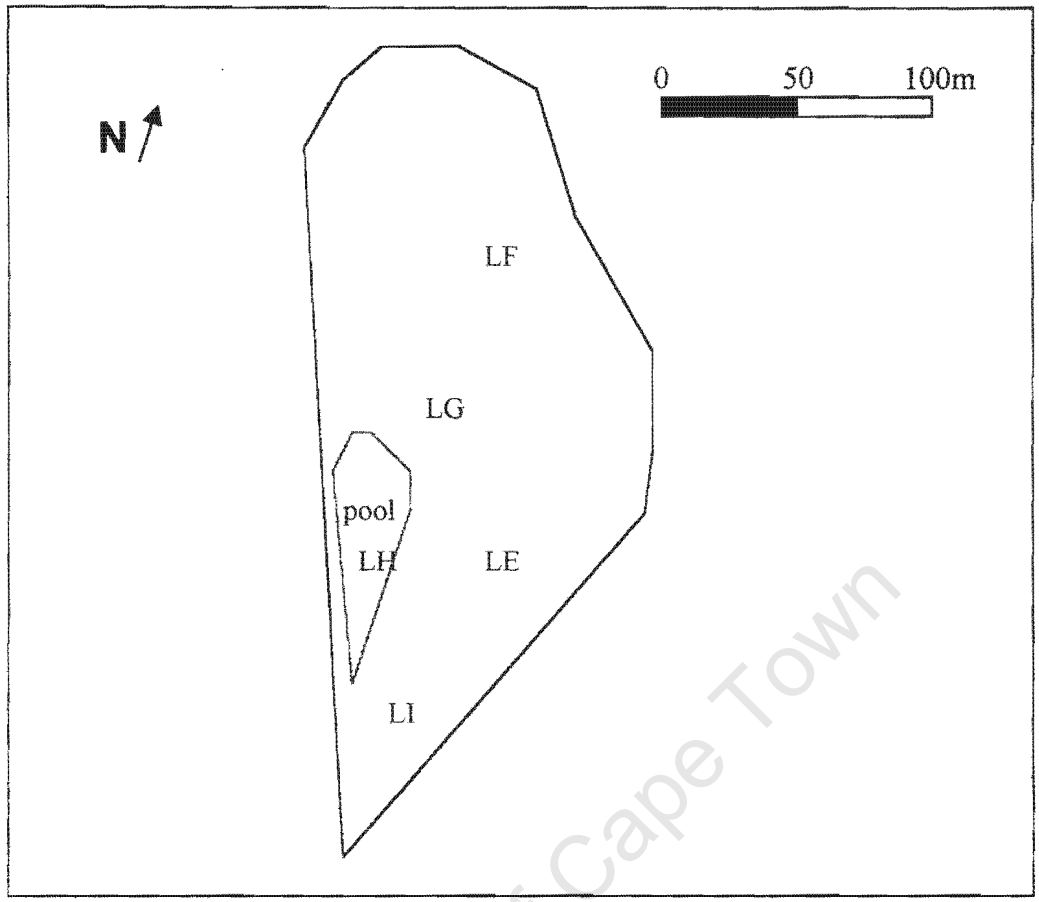

Figure 10. Sampling locations of waters taken for Fe^{2+} determination.

3.2.1 Water sampling

All water samples were collected in plastic bottles and the pH and EC were measured in the laboratory. In some cases, pH measurements were also made in the field. Each sample was filtered for further analysis using a 0.45 μm membrane filter and separate aliquots of each sample were acidified with 50% HNO_3 for trace element determination. The samples taken for Fe determination were filtered in the field and acidified with concentrated HCl in the ratio of 2ml HCl : 100 ml sample in order to prevent the oxidation of Fe^{2+} in solution.

3.2.2 Soil sampling

The soil profile sampling was performed on the side-walls of various pits that were excavated to introduce lime to the subsoil horizons. Each profile was subdivided into separate horizons, some of which have been markedly disturbed, such as the distinctly dark brown to grey ash-rich layers forming the surface layer of the soil at sites AA and AB. An informal description of each profile is presented in Appendix A1.

To perform representative experiments on the soil at this site, it was decided to combine the topsoil and subsoil samples from all the soil profiles into two composite samples. These composite samples were then used to conduct the incubation liming experiments on the soil (described in Chapter 4). A general characteristic of each soil profile was the occurrence of a cemented horizon between 10 and 47 cm from the surface. This cemented horizon was taken to represent a transitional zone between the topsoil and subsoil and was considered separately. The topsoil composite sample (ATSC) comprised equal sub-samples of all soil horizons occurring above the cemented horizon and the subsoil composite sample (ASSC) was similarly made up using the horizons below the cemented horizon.

The samples included in each composite were as follows:

Acid topsoil composite (ATSC): A2, B2, B3, C1, C2, E1, F1

Acid subsoil composite (ASSC): A4, B5, C4, E3, F3

The composite limed samples were taken along E-W traverses from the north, central and southern parts of the site and have been labelled LCN, LCC and LCS, respectively (Figure 9). These samples were used to provide some indication of the effects of liming the site.

3.3 Sample analysis

Standard analytical techniques were utilised for the analysis of the waters and soils from this site and these are described separately below. Where necessary, further details of the techniques are presented in Appendix B.

3.3.1 Water and soil solution analysis

3.3.1.1 pH and electrical conductivity (EC)

The pH of the water and soil samples was measured in the laboratory using a *Metrohm 691* pH meter. The pH electrode was stored in a pH 4 buffer solution and measurements were taken at room temperature. Some field measurements of pH were taken using a portable *Ciba-Corning M90* field pH meter which was calibrated on each occasion in pH 4 and pH 7 buffer solutions.

Soil pH measurements were conducted by mixing 2.5 g of soil with 25 ml M KCl in a centrifuge tube, shaking on a reciprocal shaker and centrifuging for 2 minutes. The pH of the supernatant liquid was then measured and recorded as soil pH.

Electrical conductivity (EC) of all water samples and soil solution extracts was measured in the laboratory using a *Crison micro CM 2201* conductivity meter which was calibrated using a standard 0.01 M KCl solution with an EC of 1412 µS/cm at 25°C.

3.3.1.2 Alkalinity and acidity

Alkalinity was determined by the titration method described in method 2320 B of Standard Methods (1995) using a Radiometer *ABU 80* autoburette and a *TTT 85* titrator fitted with a pH electrode.

Acidity titrations were performed on selected water samples using a digital autoburette with 0.01M NaOH and titrating to an end point of pH 8.3 with the *Ciba-Corning* field pH meter. This method is similar to that used for KCl extractable acidity, which is described in section 3.3.2.4 below.

3.3.1.3 Major ions

Two *Dionex* Ion Chromatography (IC) units were used to determine the ionic concentration of all the water samples. The columns were set up to measure the cations Na^+, K^+, Mg^{2+}, Ca^{2+} and NH_4^+ and the anions F^-, Cl^-, Br^-, NO_3^-, NO_2^-, SO_4^{2-} and PO_4^{3-}. Cation analysis was performed with a *Dionex* CS12A Separator and CG12A Guard column with H_2SO_4 (11 mM) eluent at a flow rate of 1 ml/minute and a sample loop volume of 25 µL. Cation samples were eluted for a run time of 15 minutes. Anions were analysed using a *Dionex* HPIC-AS4A Separator and HPIC-AG4A Guard column with a combined eluent of Na_2CO_3 (1.8 mM) and $NaHCO_3$ (1.7 mM). The flow rate for anion analysis was 2 ml/minute with a sample loop volume of 50 µL and the run time was 8 minutes.

All samples run through the IC were first filtered using a 0.45 µm membrane filter to remove the colloidal matter. Each sample was then diluted to bring the EC to within the range of operation of the IC (≤100 µS/cm). Before injection into the IC units, each sample was passed through an *Onguard-P* polyvinylpyrollidone cartridge to remove organic materials that might contaminate the IC columns.

3.3.1.4 Trace elements

Trace element analysis was performed with an *Elan 6000* Inductively Coupled Plasma Mass Spectrometer (ICP-MS). This technique is more accurate for the heavier elements on the periodic table and is not considered reliable for the lighter elements making up the major ions in solution. Samples run on the ICP-MS are first filtered through a 0.45 µm membrane filter and acidified with 50% HNO_3 to prevent metals precipitating from solution.

3.3.1.5 Ferrous and ferric iron

Selected water samples were chosen for total soluble Fe and Fe^{2+} determination by means of Fe colorimetry by the Phenanthroline method described in 3500-Fe D of Standard Methods (1995). A Sequoia-Turner model 340 spectrophotometer was used to measure the light absorbance with the wavelength set at 510 nm. Ferric Fe was determined by difference of total Fe and Fe^{2+}. The total soluble Fe concentration of selected samples was also determined by Flame Atomic Absorption Spectrometry (FAAS) to use as a comparison with the colorimetric results.

3.3.1.6 Dissolved organic carbon (DOC)

DOC analysis was performed on selected saturated paste extracts and water samples by the Council for Scientific and Industrial Research (CSIR) in Stellenbosch using the Persulphate-Ultraviolet Oxidation method as described in 5310 C of Standard Methods (1995). The technique of extracting soil solution from saturated pastes will be outlined in section 3.3.2.6 below.

3.3.2 Soil analysis

This section describes the analyses performed on the solid phase of the soil samples. Standard methods of routine soil analysis were utilised in most cases as outlined below.

3.3.2.1 Soil composition

An analysis of the major oxides in selected samples was performed using X-ray Fluorescence Spectrometry (XRFS) on fusion discs prepared in the standard way. In order to estimate the proportions of S to SO_4 in each sample, a powder briquette was also made of each sample and the K_β peaks for S and SO_4 were compared to obtain a ratio of each species. The full details of these analyses can be found in Appendix B2.1.

3.3.2.2 Soil texture

A sub-sample of each soil horizon was sent to the soil science laboratories of ARC-Infruitec in Stellenbosch for textural analysis. The analysis was performed by the Hydrometer method as documented in Gee and Bauder (1986).

3.3.2.3 Organic carbon

The organic carbon content of each sample was determined by ARC-Infruitec in Stellenbosch using the Walkley-Black method as documented in Rowell (1994).

3.3.2.4 Exchangeable acidity and basicity

The KCl extractable acidity method was used to determine the amount of exchangeable acidity in each sample. This method employs a simple extraction with unbuffered salt solution (M KCl) and is followed by titration of an aliquot of the extract with a base in order to estimate the amount of exchangeable acid cations in solution (McLean, 1982). The concentration of exchangeable base cations in solution is then estimated by determining the Ca^{2+} and Mg^{2+} concentration of the extract. The concentration of Ca^{2+} and Mg^{2+} was determined by Flame Atomic Absorption Spectrometry (FAAS) in the Department of Chemical Engineering at the University of Cape Town (UCT).

Once the concentration of acid and base cations in the sample has been determined, useful ratios such as the percentage of acid or base saturation can then be calculated, which serve to characterise the soil in terms of its toxicity towards plants (see Appendix B1.4).

3.3.2.5 Mineralogy of clay fraction

A selection of soil samples was chosen for analysis of the clay fraction using a *Philips PW 3890* X-ray diffractometer (XRD) with a graphite monochromator and scintillation detector with CuK_{α} radiation. Scanning was performed over a 2θ range of 3.5 to 65° with the XRD running at 25mA and 40 kV. Results were recorded using *Philips* PC-identity software (PW1876 Version 1.0E).

The samples chosen for clay fraction analysis included the composite topsoil and subsoil samples (ATSC and ASSC respectively) and the uncontaminated test pit samples (topsoil and subsoil) to

serve as a comparison. An abbreviated clay dispersion technique was utilised to collect enough clay and this was then prepared on a glass slide and analysed. The details of the clay dispersion technique are presented in Appendix B2.2.

A phase analysis of the cemented horizon was also performed using XRD although these samples were prepared in a simpler way to save time. Each sample was wet-sieved through a 63μm sieve and the mud fraction was collected, dried and crushed for XRD analysis. This more straightforward technique proved to be successful in identifying key phases even though the samples were understandably dominated by quartz in each case.

Samples of elemental sulphur and dolomitic limestone from the site were also analysed by XRD to verify the nature of these substances.

3.3.2.6 Saturated paste extraction

The chemistry of the solution phase of a soil is critically important in determining the geochemical character of the soil. The saturated paste extraction technique was used to obtain samples of the soil solution for further analysis. The method of extraction is after Rhoades (1982) and is described in detail in Appendix B2.3.

3.3.2.7 Micro-analysis of acid precipitates

Selected precipitates from the exposed soil surfaces were analysed using a *Leica S400i* Scanning Electron Microscope (SEM) fitted with an X-ray Energy Dispersive Spectrometer (EDS). In this way it was possible to take advantage of the high resolution of the SEM to study the morphology of these precipitates as well as obtaining a qualitative appreciation of the elemental composition of the precipitates with the use of the EDS capability.

Samples are routinely coated with Au or Pd, providing strongly conducting surfaces and allowing for well-defined topographical images but Au and Pd interfere with the EDS of the sample. For this reason, specimens are generally coated with carbon when EDS analysis is required since carbon-coated specimens normally provide acceptable topographic images but also allow for elemental analysis.

3.4 Results and discussion

3.4.1 Historical results

Limited geochemical work was conducted at this site prior to the sulphur fire in December 1995. In fact, it was the fire itself and the devastation that it caused that prompted detailed investigations of the site. For this reason, it is difficult to quantify the effect that bacterial oxidation may have had in acidifying the soil in this area prior to the fire. However, it is likely that the environmental impact the S has had on the soil is a combination of bacterial oxidation as well as the conversion of S to SO_3^{2-} by melting and burning.

A study of the soil and water at the site was conducted by Simpson and Morris (1996) subsequent to the S fire. Surface and groundwaters varied in pH from values of 0.2 in the canal forming the western boundary of the site to values of 9 in the Helderview main drain (marked HMD in Figure 9). The Helderview water, however, drains from an area upgradient of the S stockpile and therefore represents water from an entirely different system. The on-site pH values are generally in the acidic range with values of pH < 5 being common. There is also a wide variation in salinity with EC values ranging from 1.0 to 19.5 mS/cm.

The soil samples taken from the site at this time were also found to be acidic, with pH values ranging from 2.7 in the topsoil samples to 6.9 in the subsoil horizons. The EC of the soil ranged in value from 0.3 to 4.2 mS/cm.

The results of Simpson and Morris (1996) emphasise the heterogeneous nature of this site in terms of salinity and pH. Their study also found the waters to contain elevated concentrations of SO_4^{2-} with values of up 8000 mg/L being recorded in surface water samples. The groundwater samples were dominated by Na^+, Cl^- and SO_4^{2-} in solution.

A further geochemical investigation of the S stockpile site was conducted by Doel in 1997. The sampling for this study was undertaken in August and September 1996. One water sample was collected from the extreme southern apex of the site. This water is extremely acidic with a pH of 1.5 and a total acidity of 328 mmol/L. It is also highly saline with an EC of 20.7 mS/cm. The ionic composition of the water is dominated by SO_4^{2-} and Na^+ with concentrations of 13600 and 1440 mg/L, respectively. The acidic nature of the water is emphasised by the trace element composition which is dominated by the characteristic acid cations, Al^{3+} and $Fe^{2+,3+}$, with

concentrations of 845 and 423 mg/L, respectively. Other trace elements in solution occurring in concentrations of over 1 mg/L include Si, Mn, Zn, Cu, Ni, As, Cr and Co.

3.4.2 Surface and groundwater geochemistry

3.4.2.1 Chemical composition

The chemical composition of a selection of surface and groundwater samples from the site and vicinity is presented in Table 1 and the complete data set of water results can be found in Appendix C. Once again, the samples with prefix 'A' were taken prior to liming and those with prefix 'L' were sampled after liming had taken place. It is quite evident from Table 1 that the liming has had little effect as can be seen in sample LWE where the pH is still below 2 and the SO_4^{2-} concentration is in excess of 45 g/L. However, the site is heterogeneous in character, with pools of highly acidic water occurring sporadically across the area and often in close proximity to piles of limestone gravel which are associated with less acidic waters and characteristic ferric oxyhydroxide precipitates with occasional signs of algae. This scenario is illustrated in Figure 11 where a pool of characteristic red-brown acid sulphate water (pH 1.7) occurs a few meters away from a slightly higher pH water (pH 3.8) with Fe precipitating from solution. The waters depicted in Figure 11 are in the vicinity of sample location LE (Figures 9 and 10) where the water sample LWE was taken.

Table 1. Geochemistry of surface and groundwater from the site and vicinity.

Sample No.	**SDP1**	**AWC**	**AWF**	**AWH**	**LWD**	**LWE**
Description:	ground-water	surface water	surface water	wetland nearby	test-pit nearby	surface water
Date sampled:	24/08/99	02/06/99	02/06/99	02/06/99	17/08/99	24/08/99
pH	3.6	3.4	1.8	7.3	6.2	1.7
EC (mS/cm)	45.6	22.0	40.0	2.4	2.4	66.8
Solutes (mg/L):						
Major ions:						
Na^+	160	1460	591	176	251	110
Ca^{2+}	450	386	261	173	55.4	550
Mg^{2+}	2460	908	759	55.2	28.6	1485
K^+	40	18	24	10.2	4.2	40
NH_4^+	40	nd	9	nd	nd	65
F^-	45.5	4.6	49.2	0.2	3.24	24.5
Cl^-	211	501	304	236	360	79
SO_4^{2-}	25300	11100	23000	522	219	45800
Trace elements:						
Fe	212	124	141	0.7	0.61	1900
Al	413	146	1390	1.34	0.978	1370
Mn	33.4	5.1	20.1	0.064	0.147	14.6
Li	0.82	0.718	2.04	0.007	0.017	1.43
Si	12.6	24.0	22.1	6.42	nd	32.6
Cr	0.166	nd	1.24	nd	nd	2.46
Ni	1.4	0.502	1.69	0.008	0.014	1.03
Cu	6.56	1.46	2.35	0.179	0.031	3.31
Zn	6.45	2.3	3.57	0.165	0.078	5.8
As	0.014	0.008	0.078	0.003	0.006	0.903
Se	0.016	0.142	0.180	0.011	nd	0.016
Rb	0.030	0.024	0.123	0.020	0.004	0.289
Sr	0.995	5.90	4.02	1.01	0.502	2.10
Mo	0.002	0.206	0.105	0.004	nd	0.007
Cd	0.05	0.022	0.048	0.0006	0.0006	0.017
Cs	0.003	nd	0.0048	nd	0.0002	0.041
Ba	0.025	0.40	0.144	0.058	0.036	0.045
Pb	0.046	0.458	1.11	0.055	0.153	0.358
U	0.033	0.007	0.045	0.005	0.0002	0.101

nd = not detected

A. Red-brown acid sulphate water (pH 1.7).

B. Limed water (pH 3.8) with Fe precipitates forming on the surface of limestone grains.

Figure 11. Characteristic acidic red-brown water occurring in close proximity to limed water with Fe oxyhydroxide precipitates.

The major ion chemistry of the acidic water samples is expectedly dominated by SO_4^{2-} with the most prevalent basic cation being Mg^{2+}. The basic cations, however, are understandably not adequate in balancing the charge of the sample. It is the contribution of the acidic cations, such as Al, Fe and Mn, as well as the role of H^+ that are important in balancing the charge of highly acidic systems. For this reason, it is instructive to measure the total acidity of such extremely acidic samples before attempting to calculate the charge balance. The total acidity of samples LWE and SDP1 was measured as 560 and 130 $mmol_c/L$ respectively. Including the acidity with the basic cations gives a charge balance of 14.2% for LWE and 18.8% for SDP1. It is likely that the severe dilution of most of the samples from this study has had some effect on the accuracy of the IC analyses. It is possible that the SO_4^{2-} concentrations, in particular, have been overestimated since SO_4^{2-} is generally an order of magnitude higher than most other anions even after dilution. This may partly explain why the charge balance is out by more than 10% in both cases above. By comparison, the charge balance of the test pit sample (LWD) is 3.9%, supporting this argument. The concept of waters being electrically neutral and hence, the calculation of charge balance is described by Murray and Wade (1996).

It is expected that most water samples from this study will be of a similar character, perhaps closely resembling waters emanating from acid mine drainage environments. A convenient way of characterising waters into hydrochemical facies is with the use of Piper diagrams. A Piper plot of the waters from this study is presented in Figure 12. All the acidic samples plot in a cluster with SO_4^{2-} as the dominant component and they approach the apex marked AMD on the quadrilateral part of the diagram. This region is characteristic for acid mine drainage samples. The only samples deviating from the general trend in Figure 12 are the control samples which plot slightly away from the clusters of acidic samples.

The dominant trace elements in solution are expectedly represented by Al, Fe and Mn with other metal cations such as Cu, Zn, Ni and Sr also coming into solution as a result of the low pH (Table 1). Trace metals are commonly adsorbed by clay and Fe oxide surfaces as can be seen in Figure 7, but since this adsorption only begins at pH > 3, most trace elements will thus become soluble below pH 3.

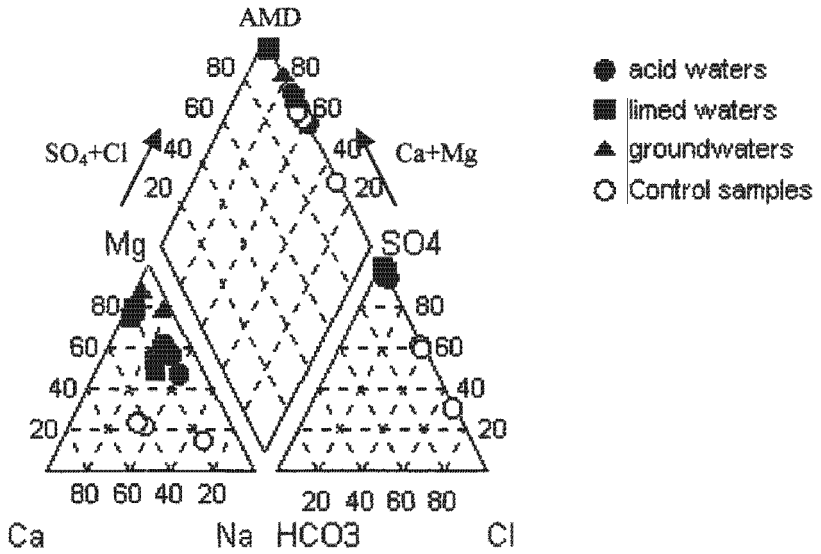

Figure 12. Water samples plotted on a Piper diagram using AQUACHEM, showing the distinctive geochemical facies of the samples from this environment.

3.4.2.2 Chemical speciation and saturation indices

In order to fully understand natural systems and the effects that various components will have on one another, it is important to appreciate the complexity of the reactions and processes that are potentially important in aqueous systems. Due to the vast number of reactions and mineral equilibria that are often at play, and because of the complexity of the thermodynamics governing each reaction, it becomes increasingly difficult to predict chemical speciation and mineral saturation in natural environments. For this reason, a number of geochemical modelling programs have been written which calculate activities of species in solution and predict mineral saturation using extended Debye-Hückel theory. Programs of this nature include MINTEQA2, PHREEQC and WATEQ4F (Allison *et al.*, 1990; Parkhurst, 1995; Ball and Nordstrom, 1991). For the purposes of this study, the PHREEQC modelling program was chosen (Parkhurst, 1995), using the WATEQ4F database of reactions since the PHREEQC database was not considered as thorough with respect to the mineral saturation of certain potentially important species in this system. All data was initially entered into the program, AQUACHEM (Calmbach, 1998), which was then used as an interface for running PHREEQC.

Because of the excessively high ionic strengths of most waters and soils from this study, the standard models mentioned above become somewhat inappropriate since it is postulated that in concentrated solutions, the formation of ion pairs is responsible for a departure of the behaviour

predicted by the Debye-Hückel equation (Drever, 1997). Ion-pair formation decreases the concentration of free ions since some of the ions are tied up in ion pairs and the ionic strength of the solution is decreased because the ions are converted to uncharged species. The net effect is that the activities of the individual ions are lower than would be predicted by the Debye-Hückel equation. The ion pair model is sufficiently accurate to predict the activities of solutions less concentrated than seawater. However, to accurately predict the activity-concentration ratio of more concentrated brines, the Pitzer model is more appropriate. This model postulates that departures from ideality in ionic solutions are due to the interaction of the various ions in solution (Drever, 1997).

A program that is in some way able to interpret the behaviour of concentrated solutions is PHRQPITZ (Plummer *et al.*, 1988). This program is, however, written in DOS format and, although being available on the Internet, no supporting literature was available for its operation. Because the program was poorly understood and time was not sufficient in this study to interpret the operating commands, the value of the potential output was considered dubious. It was considered more instructive to use PHREEQC for modelling the samples from this study. In this way it was possible to predict trends in the data, even though the absolute values produced may not be completely accurate in light of the above discussion.

Two important elements occurring in solution under extremely acid conditions are Al and Fe, emphasising the importance of secondary mineral phases containing these elements in soil environments. Aluminium is one of the most abundant elements in soils, since the earth's crust contains approximately 7% Al. During the weathering of primary minerals, Al is released and precipitated as secondary minerals, mainly aluminosilicates. These minerals often contain metal ions such as Fe^{2+}, Fe^{3+}, Mg^{2+} and K^{+}. Silicon is removed more rapidly than Al during weathering in soils, causing Al and Fe to precipitate as oxides and hydroxides. In acid soils, Al is also important as an exchangeable ion (Lindsay, 1979).

Aluminium minerals that are of importance in soil environments include gibbsite, kaolinite, alunite and jurbanite, the latter two being particularly important in acid sulphate soils. The Al^{3+} activities of all the waters from this study have been plotted against pH in Figure 13, since Al^{3+} activity in equilibrium with any of these minerals is a function of pH (Lindsay, 1979). In this way, it may be possible to predict whether or not the waters are in equilibrium with one or other solid mineral. The saturation indices of salient mineral phases are plotted in Figures 14 and 15 as a function of pH and will be discussed below.

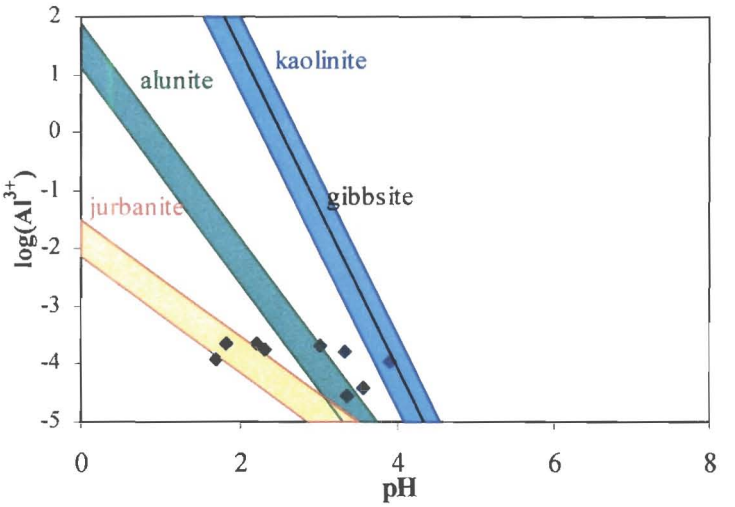

Figure 13. The activity of Al^{3+} as a function of pH for all water samples containing measurable concentrations of Al.

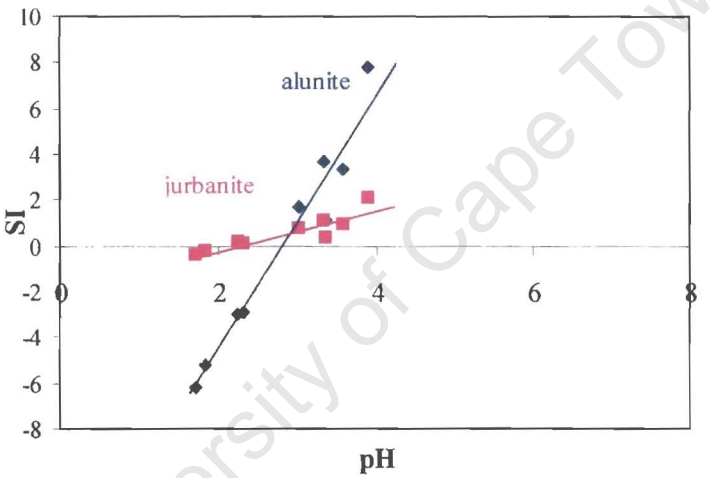

Figure 14. Saturation indices of Al-sulphate mineral phases as a function of pH for all water samples containing measurable concentrations of Al.

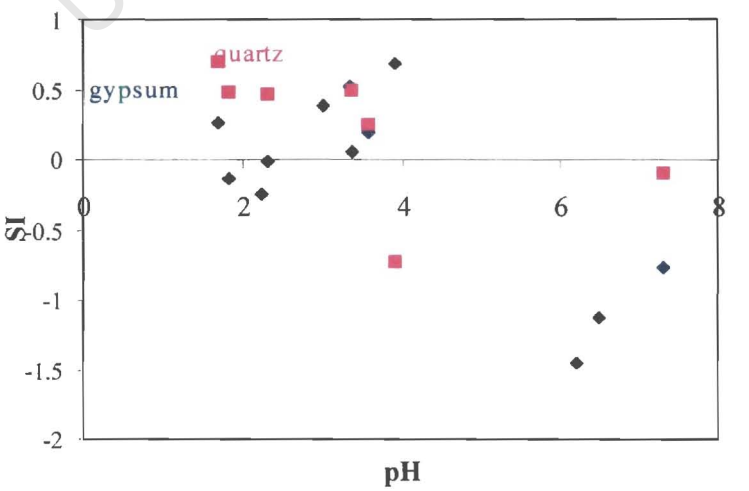

Figure 15. Saturation indices of gypsum and quartz as a function of pH for all water samples.

The mineral solubility lines in Figure 13 have been calculated using the equilibrium reactions and derivations presented in Appendix C1.2 which are taken from Lindsay (1979). The coloured fields marked with mineral names represent the upper and lower limits for each mineral based on the maxima and minima of the relevant species in each case. The activity data for the relevant species are presented in Appendix C1.1. The activity of Al^{3+} in soils is often below that of gibbsite due to the presence of aluminosilicates (Lindsay, 1979) as is the case with the data in Figure 13. The general trend of the data suggests that the activity of Al^{3+} for these water samples is controlled by jurbanite or alunite with the slope of the data tending more towards the former. The generation of H_2SO_4 and subsequent lowering of pH in acid sulphate soils leads to the precipitation of Al-sulphate phases rather than phases like gibbsite as can be seen by the relative positions of the fields in Figure 13. This is confirmed by a plot of Saturation Indices (SI) versus pH for Al-sulphate phases (Figure 14) where it can be seen that the waters are supersaturated with respect to both alunite and jurbanite above pH 3. The data plotted in Figure 14 show a remarkably linear trend for both minerals suggesting that all the samples, although taken from different locations and at different times, are controlled by the solid phases with which they co-exist.

The saturation indices for quartz and gypsum have been plotted against pH in Figure 15. From this diagram it can be seen that the solution is close to being in equilibrium with both these minerals, especially at pH < 4. Gypsum becomes undersaturated at neutral pH although the samples at neutral pH are the control samples which have much lower concentrations of SO_4^{2-} and a slightly different character to the acid samples (Figure 12).

An important and often difficult consideration when dealing with Fe species is the concept of redox since, unlike with Al where the system can effectively be defined in terms of Al^{3+}, Fe is affected by redox, occurring as Fe^{2+} in reducing environments and as Fe^{3+} in well oxidised environments. This is complicated by the fact that both redox and Fe^{2+} are difficult to measure, and furthermore, most environments will not maintain a constant redox since there is normally some degree of exchange of oxygen in most systems. Although the solubility of Fe in soils is largely controlled by Fe^{3+} oxides (Lindsay, 1979), the redox of the system is important since this will determine the proportion of ferrous to ferric Fe in solution. Rather than attempting to measure p*e* in the field, it is more instructive to determine the relative proportions of Fe^{2+} and Fe^{3+} in solution and then calculate p*e*. This was achieved with the aid of the modelling program PHREEQC (Parkhurst, 1995).

In this study, a selection of waters were chosen for Fe^{2+} determination following the method outlined in Appendix B1.7 and the results are presented in Table 2. Because the purpose of this sampling exercise was merely to determine Fe speciation, a full analysis of the major ion and trace element concentrations was not performed on these samples. The results from the other water sampling exercises were considered representative of the study site. From Table 2 it can be seen that the proportion of ferrous Fe varies from 11 to 84%, although sample LWE was not preserved in the field and some oxidation may have taken place before the measurement of Fe^{2+}.

Table 2. The iron composition and speciation of surface waters.

Sample	pH	Fe^{2+}	Fe^{3+}	Fe_{total}	Fe^{2+}(%)
LWE	1.7	201	1705	1906	11
LWF	3.1	102	19	121	84
LWG	2.3	908	382	1290	70
LWH	2.0	222	352	574	39
LWI	2.2	609	138	747	82

NOTE: all Fe values in mg/L

Having some knowledge of the approximate percentage of Fe^{2+} in solution and using the data for the range of p*e* of most soils from Baas Becking *et al.* (1960), it was possible to predict a likely redox window using PHREEQC. This was achieved by running a series of simulations with different p*e* values on a specific sample. The proportions of Fe^{2+} to Fe^{3+} were then determined by the PHREEQC program. A simulation of this nature was performed on sample AWC which was considered to represent an average acidic water in the area. The results of this are presented in Figure 16 from which it can be seen that for the range of Fe^{2+} of 11 to 84% determined in this study, the p*e* range was between 10 and 12. Since this represents a rather narrow range in redox and it was assumed that at least some oxidation of Fe was likely to have taken place between sampling and analysing for Fe^{2+}, it was decided to extend the range of p*e* to a limit of 4 for all further discussion. A p*e* of 4 represents an extreme state for the soil in this environment as, with the general drainage of the site and the absence of sulphide phases, it is considered that there is sufficient O_2 to prevent any further reduction in p*e* and subsequent formation of sulphide minerals.

The curve in Figure 16 was applied to the Fe^{2+} water samples from this study to predict a likely p*e* for each sample. This was done to establish whether or not a trend exists between p*e* and pH as was found by Lindsay (1979). A plot of this nature is presented in Figure 17 and, although there is insufficient data for the evidence to be conclusive, there is an apparently negative

correlation between pe and pH. Refined diagrams of this nature could prove to be extremely useful in systems such as this, where Fe is an important controlling phase. By simply measuring the relative concentrations of Fe^{2+} to Fe^{3+}, a 'calibration curve' for pe can be developed and thus by merely measuring the pH of a sample, a relatively accurate estimation of pe can be made. This is important because direct measurements of pe are far less reliable.

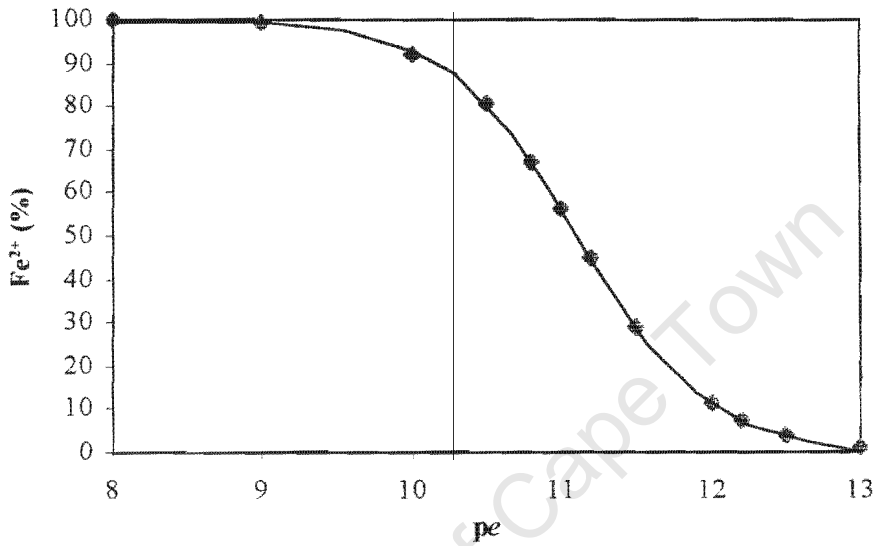

Figure 16. The proportion of Fe^{2+} in solution as a function of pe for water sample AWC as calculated by PHREEQC.

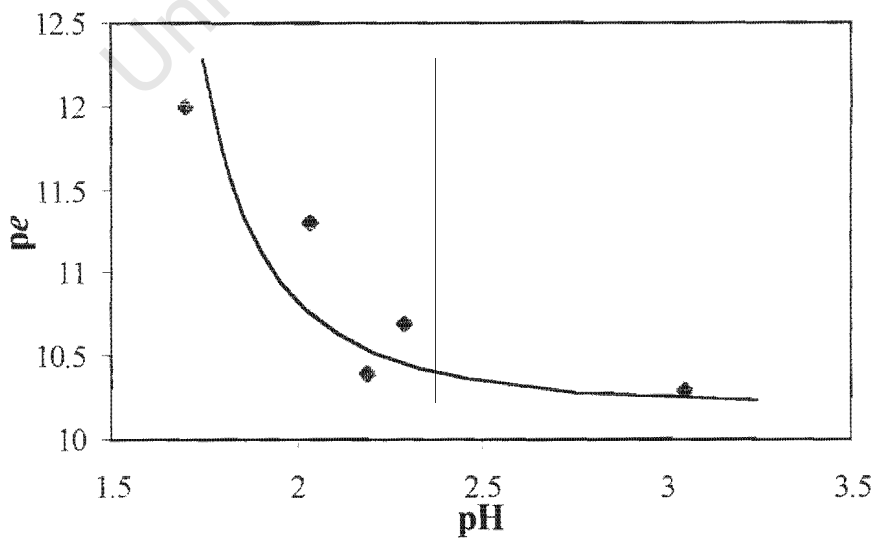

Figure 17. A comparison of pe and pH for all water samples in which Fe^{2+} was determined.

The electron activity in soils controls the ratio of Fe^{2+} to Fe^{3+} in solution by the following reaction:

$$Fe^{3+} + e^- = Fe^{2+} \qquad \log K = 13.04 \qquad (9)$$

Combining Reaction 9 with the solubility reaction for soil-Fe gives

	log *K*
$Fe^{3+} + e^- = Fe^{2+}$	13.04
$Fe(OH)_{3\ soil} + 3H^+ = Fe^{3+} + 3H_2O$	2.70
$Fe(OH)_{3\ soil} + 3H^+ + e^- = Fe^{2+} + 3H_2O$	15.74

(10)

from which the following derivation is obtained (Lindsay, 1979):

$$\log Fe^{2+} = -2pH + 15.74 - (pe + pH) \qquad (11)$$

In this way, activity data for Fe^{2+} can be represented on diagrams with predicted solubility lines for Fe^{3+} minerals. The maximum and minimum *pe* and pH limits from this study were used in Reaction 11 to create the windows in Figure 18 for soil-Fe and goethite. The data in Figure 18 have been plotted for the two extremes of *pe* (4 and 12) with the data points for each extreme plotted in blue and magenta, respectively. In this figure, it can be seen that all the data fall between the predicted boundaries of soil-Fe and goethite suggesting that this data may be in equilibrium with one of these phases. The data at *pe* 12, in particular, appear to follow a trend parallel to that of the boundary lines. This is consistent with the measured ratios of Fe^{2+} to Fe^{3+} which translate to *pe* values of between 10 and 12.

The saturation indices of two common Fe minerals, goethite and jarosite, were calculated using PHREEQC and are presented in Figure 19 as a function of pH, showing a clear linear trend with change in pH. These data are plotted for *pe* = 12, although the trend would be similar at different *pe* values. A *pe* of 12 is likely to be representative of the site as it occurs at present. Jarosite is a common mineral in acid sulphate environments and was found as a precipitate on soil surfaces at the S site (see section 3.4.3.4). It can be seen from Figure 19 how the waters in this study become supersaturated with respect to jarosite at pH > 2 and to goethite at pH > 1.

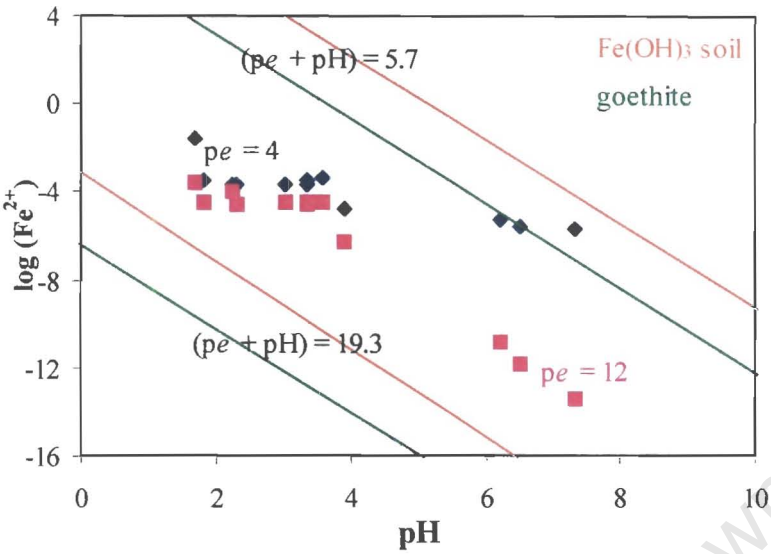

Figure 18. Activity of ferrous Fe as a function of pH for all water samples at p*e* values of 4 and 12 (presented in blue and magenta, respectively).

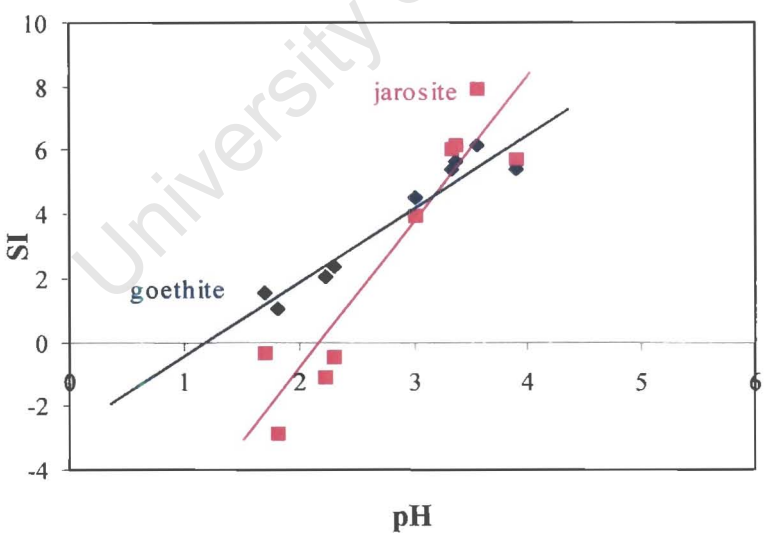

Figure 19. Saturation indices of goethite and jarosite as a function of pH for all water samples (assuming a p*e* of 12).

3.4.3 Soil geochemistry

3.4.3.1 Chemical composition

The chemical composition of a selection of soil samples is presented in Table 3. The samples chosen for chemical analysis include three individual topsoil samples, namely A1, B1 and C1, as well as the composite topsoil and subsoil samples and the test pit topsoil sample. Although the topsoil is generally sandy, samples A1, B1 and C1 contain a fairly large proportion of ash from the S fire which may be responsible for suppressing the SiO_2 values, particularly in A1, which has the most prominent ash component (a textural analysis of each soil sample is given in Appendix C2.1). As expected, the subsoil composite contains less SiO_2 and more Al_2O_3, Fe_2O_3 and MgO due to the higher clay content of the subsoil as opposed to the more sandy topsoils. The most notable component of these soils occurring in excessive concentrations is SO_3 and this was the main purpose for performing XRFS analysis. A more thorough discussion of the S content of the soils is presented in section 3.6.

Table 3. Composition of selected soil samples by XRFS.

Component	A1	B1	C1	ATSC	ASSC	TPT
SiO_2	57.03	77.12	74.83	75.64	66.38	79.28
TiO_2	1.00	0.41	0.48	0.20	0.25	0.16
Al_2O_3	19.20	4.83	4.42	3.61	6.48	2.05
Fe_2O_3	2.01	1.33	3.03	2.06	3.43	1.61
MnO	0.02	0.01	0.01	0.01	0.03	0.01
MgO	0.64	0.07	0.09	0.40	1.20	0.10
CaO	4.31	2.22	0.17	0.22	0.13	0.18
Na_2O	nd	nd	nd	nd	0.20	nd
K_2O	0.33	0.31	0.40	0.31	0.64	0.24
P_2O_5	0.34	0.08	0.03	0.04	0.03	0.05
SO_3	8.72	11.31	11.96	3.33	0.38	nd
H_2O^-	1.87	1.76	1.92	1.63	1.59	0.54
LOI	4.15	1.59	4.00	14.21	20.16	16.94
Total:	**99.61**	**101.04**	**101.33**	**101.65**	**100.91**	**101.16**

nd = not detected

3.4.3.2 Soil solution chemistry

An analysis of the extracts of the control samples of topsoil and subsoil that were prepared for inclusion in the liming incubation study is presented in Table 4 as a close approximation of the

composition of the unlimed soil solution. The results obtained from saturated paste extracts for the short and long-term incubation experiments were combined in each case for the topsoil and subsoil.

Table 4. Geochemical data from composite topsoil and subsoil samples.

	Topsoil			Subsoil		
Sample ID	**TS0**	**TL0**	**Avg**	**SS0**	**SL0**	**Avg**
pH	1.8	1.9	1.85	3.5	3.9	3.7
EC (mS/cm)	107	85.9	96.5	30	22.2	26.1
Solutes (mg/L):						
DOC	250	246	248	na	na	na
Na^+	690	744	717	1420	1260	1340
Ca^{2+}	2140	1980	2060	494	506	500
Mg^{2+}	1670	1740	1705	1380	1110	1245
K^+	20	144	82	24	28	26
NH_4^+	50	48	49	10	14	12
F^-	184	80	132	53.8	46.8	50.3
Cl^-	452	154	303	299	210	254.5
SO_4^{2-}	47500	51800	49650	13900	12200	13050
Al	4800	5240	5020	397	427	412
Si	30.3	49.7	40.0	57.4	60.1	58.8
Mn	29.9	32.0	31.0	59.6	60.4	60.0
Fe	1890	1490	1690	2.4	0.1	1.25
Li	5.8	6.57	6.19	6.46	5.59	6.03
Cr	5.28	6.54	5.91	nd	0.63	0.32
Ni	3.95	4.3	4.13	3.53	3.08	3.31
Cu	7.33	8.99	8.16	0.78	0.05	0.42
Zn	21.0	28.7	24.9	3.95	2.93	3.44
As	1.0	0.9	0.95	0.11	0.06	0.09
Se	0.32	0.83	0.58	nd	0.23	0.12
Rb	0.25	0.28	0.27	0.16	0.07	0.12
Sr	6.82	7.68	7.25	6.94	6.45	6.70
Mo	0.13	0.21	0.17	0.92	0.11	0.52
Cd	0.12	0.24	0.18	0.08	0.01	0.045
Cs	0.05	0.06	0.055	0.05	0.01	0.03
Ba	0.78	0.72	0.75	1.62	0.01	0.82
Pb	0.51	1.55	1.03	1.41	0.14	0.78
U	0.32	0.38	0.35	0.04	0.02	0.03

nd = not detected; na = not analysed

From Table 4 it can be seen that the soil solutions are similar in composition to the water samples but that in most cases, the soils are even more concentrated than the waters. The EC of the topsoil is over 90 mS/cm, which is almost twice that of seawater. The dominant solutes in the topsoil are SO_4^{2-}, Al^{3+}, Ca^{2+}, Mg^{2+} and Fe with trace elements such as Si, Mn, Zn, Li, Cu, Cr, Ni and Sr also occurring in substantial concentrations. The subsoil is expectedly far less contaminated than the topsoil as the acidity is associated with the S that was stockpiled on the surface and must first leach through the profile before affecting the subsoil horizons. There appears to be some evidence of such leaching as the subsoil is still dominated by SO_4^{2-} but the basic cations are now more prevalent than the acidic cations, Al^{3+}, Fe and Mn, which occur in much lower concentrations. The subsoil pH is also much higher explaining the lower concentrations of trace metals while the EC has dropped to a quarter of that of the topsoil.

3.4.3.3 Soil acidity

Acidity is a major limitation to soil productivity and, although acidification is a natural process in many soil environments, human activities have accelerated the process (McBride, 1994). The most diagnostic chemical measurement that is made on soil is pH. Soil pH is rarely low or high enough to indicate direct harmful effects of H^+ or OH^- on micro-organisms and roots. It does, however, signal potential harm from the indirect effects of extreme H^+ activities. Extreme pH values signify the presence of particular minerals with pH values below 3 usually indicating the oxidation of metal sulphides (McBride, 1994). Acid mine drainage environments represent a special case in which the oxidation of sulphides creates acidity, driving the pH down to extreme values. A similar case exists at the site in this study where oxidation of elemental S is the cause of extreme acidification.

The pH of a soil reflects the H^+ activity in the solution in the soil pores which is in equilibrium with the negatively charged surfaces of the soil particles (Alloway, 1995). The measurement of soil pH normally involves mixing dry soil with water, allowing it to equilibrate and measuring the pH. If the soil particles have negatively charged surfaces, then the value measured will be higher than the soil solution close to the solid surfaces. This effect is overcome by measuring the pH in a solution of a neutral salt such as KCl. For this reason, the pH measured in water for these soils is higher than that measured in KCl (Appendix C2.2.1). This also indicates that these soils have a dominant cation exchange capacity (CEC) as opposed to anion exchange capacity (AEC).

An important form of acidity in soils is the amount of exchangeable H^+ and Al^{3+} released by cation exchange and hydrolysis according to the following example (McBride, 1994):

$$K^+ + Al^{3+}\text{-smectite} = AlOH^{2+} + K^+\text{-smectite} + H^+ \quad (12)$$

The concentration of H^+ and Al^{3+} is the active acidity which is a measure of the acid intensity of the soil. The hydrolysis of Al^{3+} generates 3 moles of acidity per mole of Al^{3+} as follows:

$$Al^{3+} + 3H_2O = Al(OH)_3 + 3H^+ \quad (13)$$

Kaolinite and gibbsite are two of the principal solid phases that control the activity of Al^{3+} in naturally acidic soils. Below a pH of 4.5, Al converts to the soluble cation, Al^{3+}, and as the pH is reduced further, the above reaction proceeds in reverse, but since this reaction only occurs over a very narrow pH range, it will not substantially lower the pH (McBride, 1994).

The importance of pH as a 'master variable' that can be used to compare with other processes and parameters is widely recognised in soil science. For example, the adsorption of metals onto mineral surfaces is a function of pH as can be seen in Figure 7. More importantly in this study, pH is compared with the saturation indices of various minerals and the activity of cations such as Al and Fe (section 3.4.2.2). These results show clear trends with pH providing a useful tool for interpreting mineral saturation and the speciation of solutes.

Exchangeable acidity has been measured on all the soil samples from this study as well as the concentration of exchangeable Ca^{2+} and Mg^{2+} which was taken to represent the total suite of exchangeable base cations. In this way, the acid or base saturation can be estimated according to the formula presented in Appendix B1.4. The acid saturation of all the soil samples is presented as a function of pH_{KCl} in Figure 20. The individual soil horizon samples are presented in blue with the soil samples from the limed incubation study in orange and the composite samples taken subsequent to the liming of the site in magenta. The test pit topsoil and subsoil samples are represented as green triangles. The results in Figure 20 show a logarithmic relationship between pH and acid saturation which is expected. Some of the soil horizon samples at $pH < 2$ deviate slightly from the trend, with acid saturation values lower than expected. These samples were taken from the top of the soil profiles and had a relatively high ash content as well as relatively high concentrations of inert S. The proportion of available soil particles for ion exchange (clay and oxide surfaces) is thus smaller and this may explain why the acid saturation is lower than

expected. The two bounding lines in Figure 20 represent data from Thomas and Hargrove (1984) for natural soils, clearly showing that acid saturation reaches above 60%, even above pH 4. The acid saturation values of the soils from this study are thus depressed compared with the extreme pH of the soils. However, it is important to note that the data in Figure 20 is plotted against pH_{KCl} and not pH_{water}. The values of pH measured in water are higher for each sample (Appendix C2.2.1). A plot of Acid saturation versus pH_{water} would thus fit more closely with the data of Thomas and Hargrove (1984).

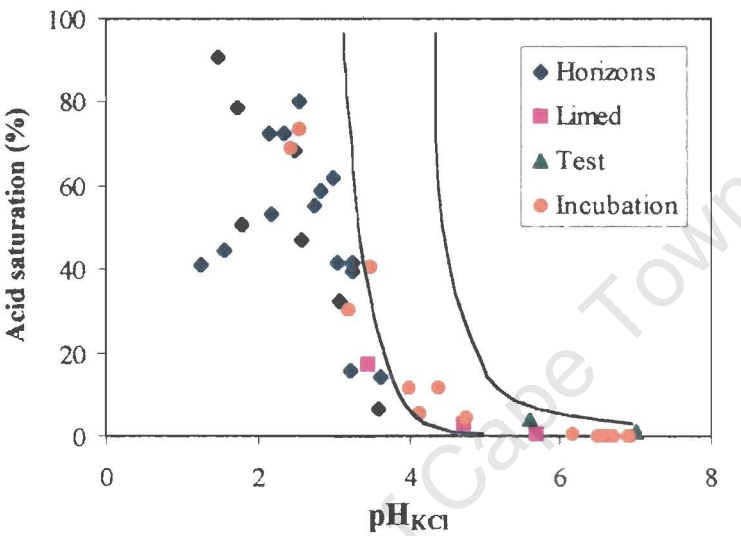

Figure 20. Acid saturation as a function of pH for all soil samples, with bounding lines based on data of Thomas and Hargrove (1984) for natural soils.

3.4.3.4 Mineralogy of the clay fraction

Soils are complex materials, reflecting the variability of the parent rock and the organic material from which they form. Even so, their elemental composition, particle size and mineralogy can be related almost systematically to the nature of the parent material and the degree to which it has weathered (McBride, 1994). Physical weathering processes decrease the particle size and increase the surface area of the mineral grains while chemical weathering dissolves or alters primary rock minerals to secondary layer silicates and oxides. These mineral products of weathering are typically clay sized (< 2μm) and because of their large surface area, they contribute substantially to the chemical reactivity of the soil (McBride, 1994). For these reasons, it is instructive to analyse the clay fraction of a soil and interpret its composition.

It was observed from sampling at the site that the dominant soil type in the subsoil horizons was composed mainly of a pale yellow swelling clay. The fact that the clay has a swelling and

shrinking nature is suggestive of a 2:1 layered silicate such as smectite. The silicate layers are separated by interlayer exchangeable cations and since smectites have a relatively low layer charge, the individual layers may separate to large dimensions in water producing the dramatic swelling properties of this mineral group (McBride, 1994).

In order to characterise the clay from this site, the method of glycerol solvation was used, according to the procedures of Novich and Martin (1983). Organic substances such glycol and glycerol form organic complexes from hydrated clay. These complexes are stable and provide an unequivocal spacing that can be verified by XRD. An example of this expansion is shown in Figure 21 where the original clay sample (shown in blue) has been treated with glycerol and re-analysed by XRD showing a distinctive expansion of the *d*-spacing from 15 to 18 Å (shown in magenta in Figure 21). This diffractogram also shows a minor peak on the expanded layer at 9 Å which represents the 002 spacing of expanded smectite. The kaolinite peak at 7.2 Å (marked K in Figure 21) serves as reference since the position of this peak remains unchanged with glycerol solvation.

A comparison was made of the test pit topsoil and subsoil samples and the acidic composite samples, the results of which are presented in Figure 22. Both the composite and test pit samples appear to have a similar composition in terms of clay mineralogy, with the dominant phases being smectite, kaolinite and quartz. The only notable difference is that the composite topsoil sample is less crystalline than the other samples but the mineralogy is similar. The hardened material of two soil profiles, as well as a characteristic pale yellow precipitate, was also analysed using XRD and the diffractograms pertaining to this are presented in Figures 23 and 24.

The hardened layer was analysed to establish whether or not the minerals making up this cemented horizon are distinct from the surrounding layers. The hardened horizons, A3 and B4 were selected for interpretation and the distinctly different horizons above each were also analysed to serve as a comparison (Figure 23). In the case of soil profile A, horizons A2 and A3 appear to be almost identical in composition with A2 being slightly more crystalline than A3. The mineralogy is dominated by quartz, kaolinite and smectite with jarosite appearing in A2 but not in A3. In profile B, it was decided to compare the hardened layer, B4, with horizon B2 since the horizon directly above B4 appeared to be similar in character and it was thus expected that this layer would not be dissimilar to B4 in composition. For this reason, horizon B2 was chosen for comparison. However, although B2 appears to be more crystalline than B4, it was not found to differ in composition. Both horizons contain quartz, kaolinite, smectite and jarosite.

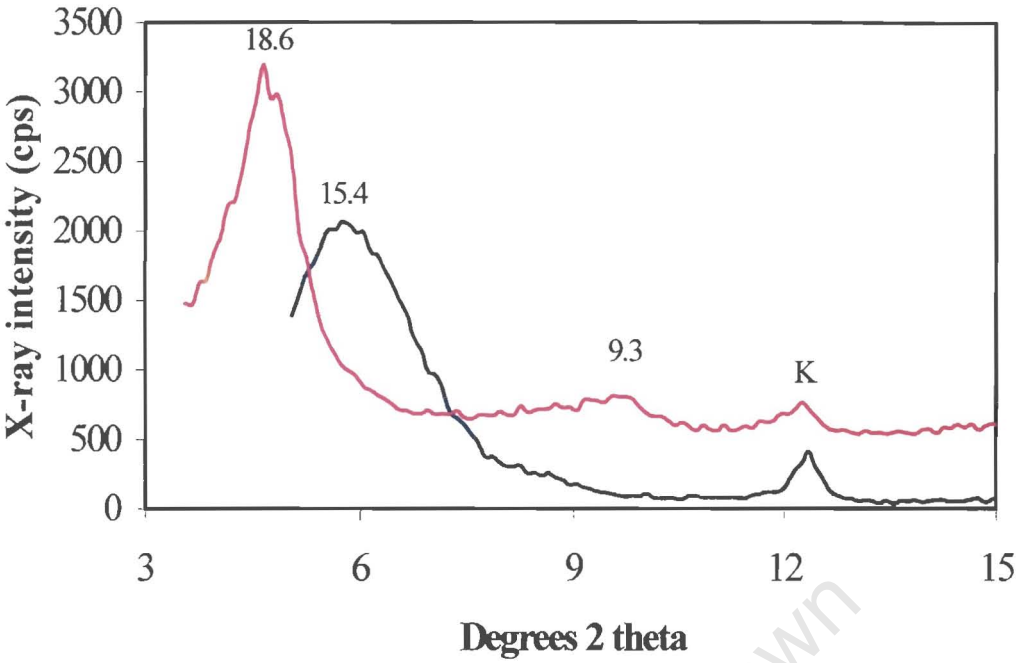

Figure 21. X-ray diffractogram of the clay fraction from the acidic subsoil composite sample (ASSC) showing expansion of smectite by glycerol solvation (K = kaolinite; 7.2 Å).

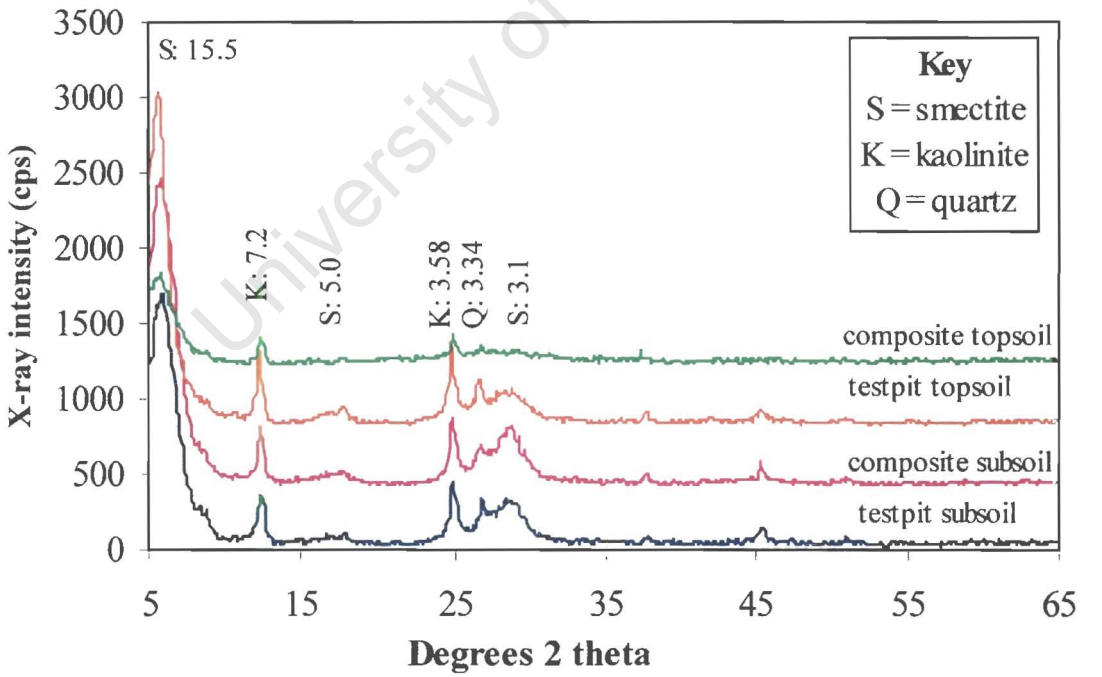

Figure 22. X-ray diffractograms comparing the acidic topsoil and subsoil composite samples (ATSC and ASSC respectively) with uncontaminated samples taken from a test pit adjacent to the site (*d*-spacings of major peaks in Å).

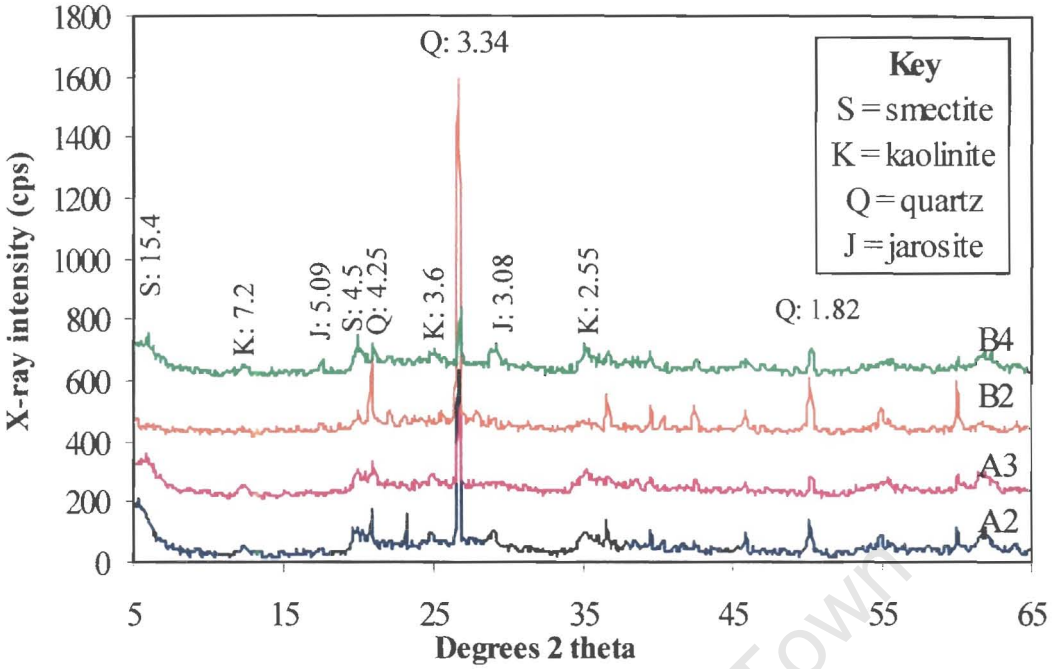

Figure 23. X-ray diffractograms comparing the hardened horizons of two soil profiles (A3 and B4) with the horizons above in each case being A2 and B2, respectively (*d*-spacings of major peaks in Å).

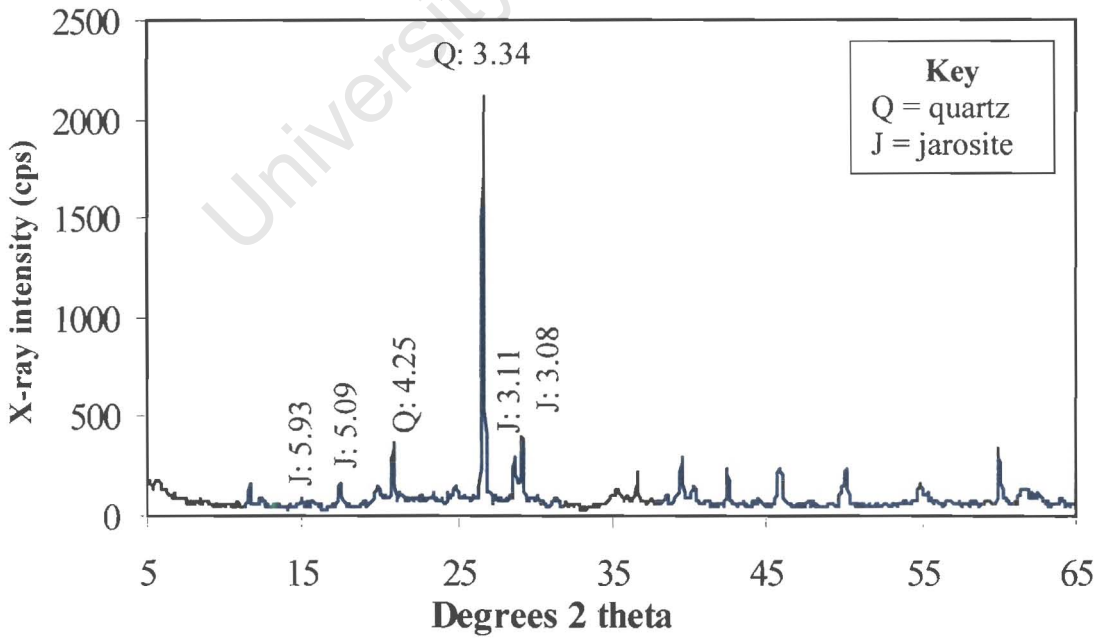

Figure 24. X-ray diffractogram of pale yellow precipitate from the surface of a hardened soil sample showing characteristic jarosite peaks at *d*-spacings of 3.08, 3.11, 5.09 and 5.93Å.

A sample of pale yellow precipitate was scraped from the surface of a piece of hardened material collected at the site. This precipitate was then crushed and analysed by XRD to verify its nature and the results are presented in the diffractogram in Figure 24. The diagnostic reflections for jarosite at *d*-spacings of 3.08, 3.11, 5.09 and 5.93 Å are all visible confirming the presence of this mineral phase. Pale yellow precipitates of this nature are common throughout the site and it is also evident from the discussion in section 3.4.2.2 and from Figure 19 that jarosite is likely to be of significance in this environment. The colour corresponds to a Munsell hue of 5Y 8/2, which is consistent with the colour of jarosite found by Bigham *et al.* (1992), further confirming the presence of this mineral.

Apart from the precipitation of acid sulphate minerals such as jarosite, alunite and jurbanite, which may have contributed to some extent in forming the cemented horizons, it is also possible that cementation within the soil profile may have occurred as a natural soil-forming process. A brittle sample of cemented material was cast in epoxy resin and prepared as a thin section for analysis by optical microscopy. On visual inspection, this material had the optical properties of amorphous silica (Frimmel, *pers. comm.*) and this was confirmed by SEM-EDS analysis which revealed that the sample was entirely composed of Si and O with a weight ratio of 43.5 to 56.5%, respectively. This material may thus represent a duripan horizon of cemented illuvial silica since it is firm and brittle and this is consistent with the material found in this study. Soils that have a duripan have a moisture regime in which soluble silica is translocated to lower horizons but not out of the soil (Buol *et al.*, 1997). At the S site, the water table is less than 1m from the surface in the rainy season and the subsoil is dominated by clay, providing an environment conducive to duripan formation. However, even though the climate is strongly evaporative, it is somewhat less arid than might normally be associated with duripan formation.

Vertisols are a characteristic soil order consisting of 2:1 expanding clays. Common features of Vertisols include evidence of soil movement such as slickensides, clay content of at least 30% to a depth of at least 50 cm, or a duripan horizon if shallower (Buol *et al.*, 1997). All of these features have been observed at this site, except for the fact that the topsoil is composed of considerably less than 30% clay (Appendix C2.1). The soil at this site can therefore not be classified as a Vertisol but does, however, show strong characteristics of this soil order.

3.4.3.5 Micro-analysis of acid precipitates

The scanning electron microscope (SEM) is a versatile and useful instrument for the examination and analysis of microstructural characteristics of solid objects. The primary reason for its usefulness is its high resolution, with images of the order of 5nm usually obtainable with commercial instruments. Another important feature of the SEM is the three-dimensional appearance of the image, which is the result of the large depth of field (Goldstein *et al.*, 1981). In order to obtain an indication of the elemental composition of individual particles, the SEM may be fitted with an X-ray energy dispersive spectrometer (EDS), allowing electrons to penetrate the particles causing X-rays to be emitted. In this way, a spectrum of X-ray intensity can be created, with individual peaks being proportional to the atomic number of the various elements within the particle and the X-ray intensity providing an estimation of the relative proportion of each element.

In order to understand something of the crystallinity of the precipitates forming at the surface of the soil as well as gaining an understanding of their chemical makeup, selected samples were analysed using SEM-EDS. Images of these acid sulphate precipitates are shown in Figures 25 to 27 with EDS spectra presented in Figures 28 to 30. In most cases, the spectra correspond to the images as will be alluded to in the discussion below.

Figure 25 shows a secondary and a backscatter image of a characteristic ochreous precipitate taken from the surface of an acidic soil sample. The highly crystalline and well-formed gypsum crystal is clearly evident and is surrounded by agglomerates of soil particles. The backscatter image emphasises the heterogeneous nature of these agglomerates as higher atomic number elements show up more clearly under backscatter. The small bright grains adhering to each agglomerate are thus likely to differ in mineralogy from the duller matrix. An EDS spectrum of one of these agglomerates is presented in Figure 28 (EDS-1) showing that it is composed mainly of Al, Si and O with lesser amounts of S and Fe. This probably indicates an aluminosilicate phase together with quartz. The small bright grains (shown in Figure 28 as EDS-2) are dominated by O, S and Fe, and are indicative of some Fe oxyhydroxide sulphate phase.

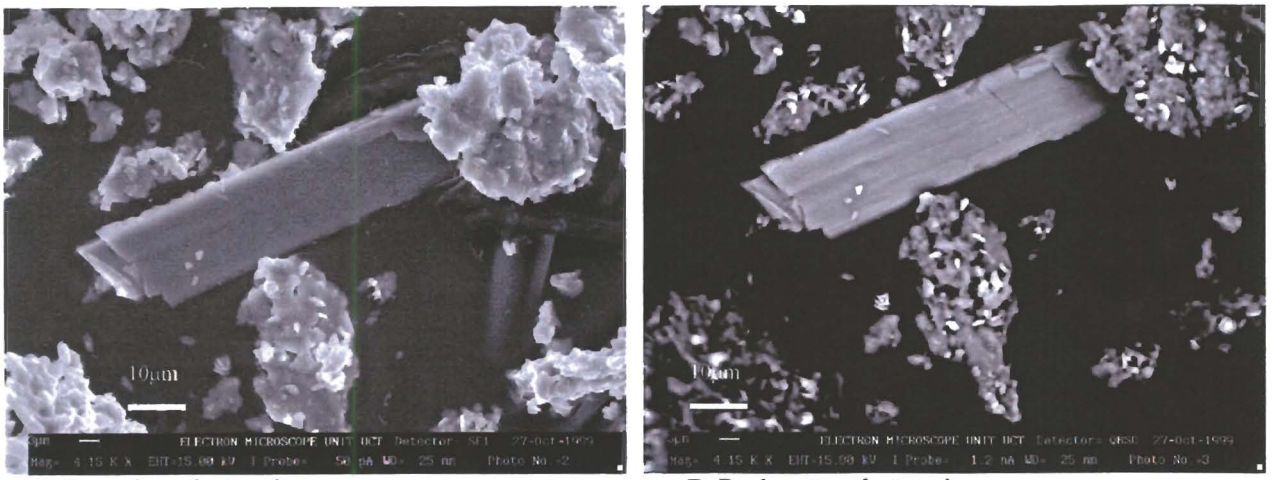

A. Secondary electron image **B.** Backscatter electron image

Figure 25. SEM image of Fe oxide precipitates and gypsum formed at the soil surface.

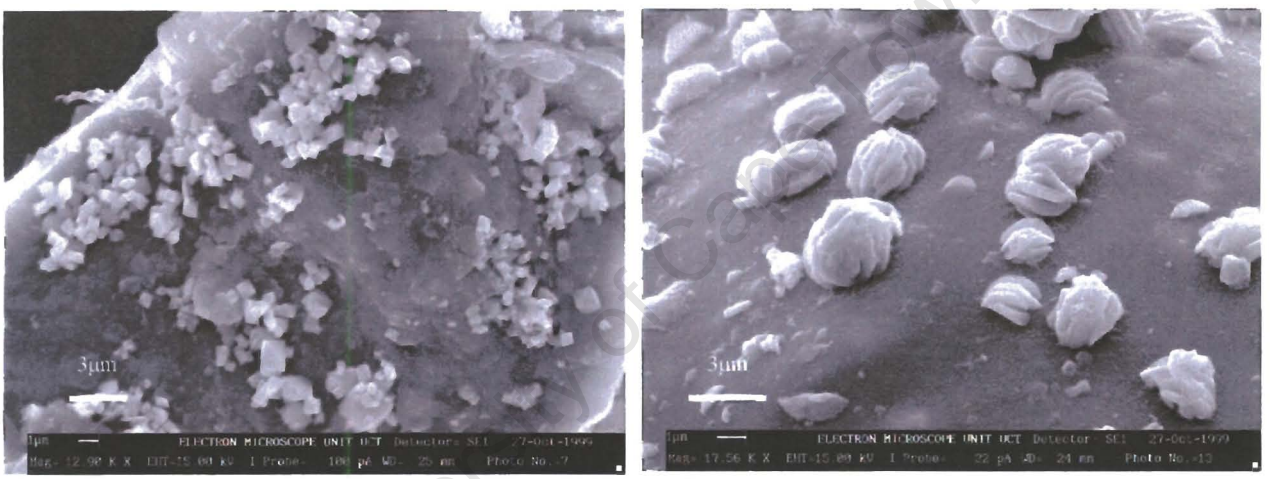

A. **B.**

Figure 26. SEM images showing different morphologies of acid precipitates adhering to larger grains.

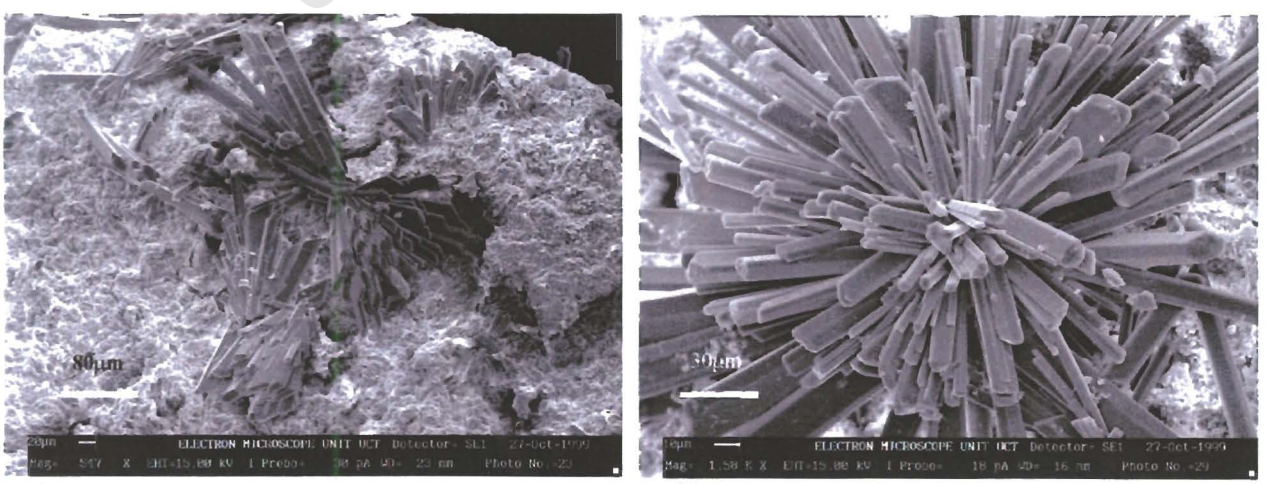

A. **B.**

Figure 27. SEM images of gypsum crystals growing from the surface of a lime grain coated with an Fe oxide precipitate.

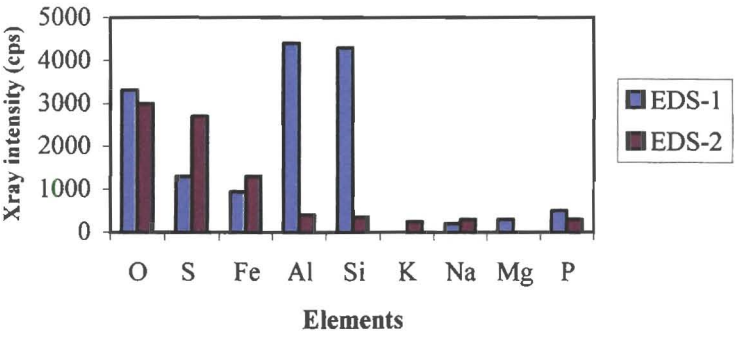

Figure 28. SEM-EDS spectra of ochreous precipitate from the site shown in Figure 25.

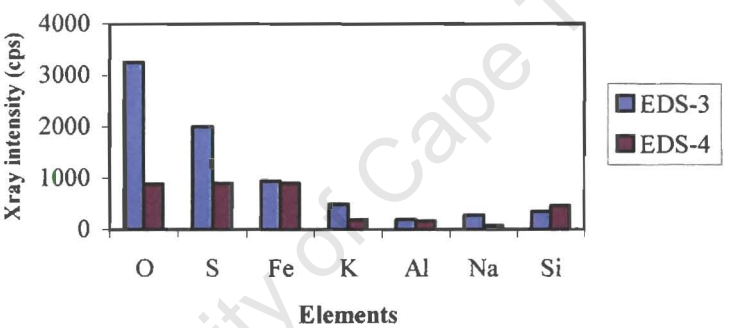

Figure 29. SEM-EDS spectra of acid sulphate crystals (possibly jarosite) shown in Figure 26.

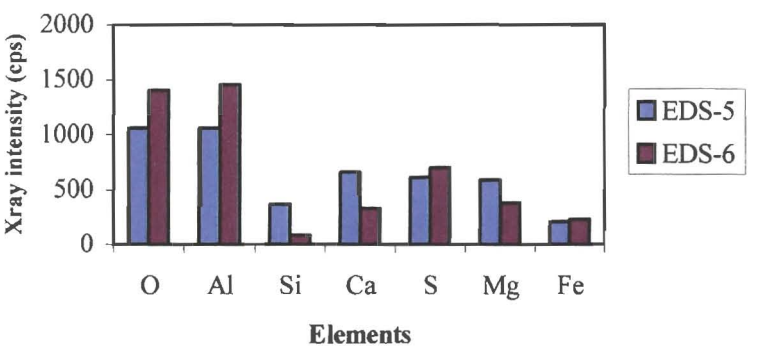

Figure 30. SEM-EDS spectra of Fe oxide coating of a lime particle from the site (Figure 27A).

The jarosite precipitate to which Figure 24 (section 3.4.3.4) refers, was also analysed by SEM-EDS and a small sample of this material is shown in Figure 26A. The large grain acting as a substrate is probably quartz with the small cubic-shaped crystals likely to represent jarosite. The EDS spectrum (Figure 29; EDS-3) reveals that these crystals are dominated by O, S, Fe and K, which is consistent with the composition of jarosite. It is also reported by Bigham *et al.* (1992) that the typical morphology of jarosite crystals is pseudocubic. The crystals shown in Figure 26B attached to the surface of a larger grain are composed of O, S and Fe with lesser amounts of Si, K, Al and Na (Figure 29; EDS-4). This precipitate is orange in colour, indicative of minerals such as goethite, lepidocrocite or ferrihydrite but the composition points more towards jarosite or possibly schwertmannite. There was insufficient material to perform XRD analysis in this case to confirm the mineral phases present in this precipitate.

The precipitate to which Figure 11 refers is also illustrated in Figure 27, showing the roughened texture of the Fe oxyhydroxide surface with rosettes of gypsum crystals growing from the surface. The EDS spectra of the surface are shown in Figure 30 with EDS-5 being a regional scan of the surface and EDS-6 displaying a scan of a single grain. The surface is composed of Al, O, Ca, S, Mg, Si and Fe, representing a combination of mineral phases, probably including quartz, aluminosilicates, Fe oxides, gypsum and dolomite. Gypsum crystals are abundant throughout the site since the waters are in near equilibrium with gypsum for most samples in this study (Figure 15).

3.5 Comparison between water and soil chemistry

In order to draw a comparison between the water and soil at the site, a selection of surface water, groundwater and acidic soil samples was chosen for discussion. The soil data were obtained from the saturated paste extracts of the control topsoil samples that were used in the liming incubation study.

A comparison of the major ions in solution is presented in Figure 31. The acidity of each sample was also determined by titration with NaOH and is shown together with the major ions. Sample LWE is a surface water sample taken from site LE, while SDP1 and 2 are groundwater samples, the locations of which are shown in Figure 9. The soil samples, TS0 and TL0, are composite topsoil samples used as controls in the liming incubation study, with TS0 being incubated at field saturation for 14 days and TL0 for 28 days. It is interesting to note that the dominant ion in solution, SO_4^{2-}, is almost linearly balanced by acidity as the dominant 'cation suite' (Figure 31). The SO_4^{2-} concentration of the water samples is slightly higher than their acidity while that of the soil samples is almost exactly balanced by acidity. The sample that appears to be anomalous to all others is SDP2, which is a yellow concentrated brine enriched in all ions and elements compared with other samples. A closer approximation of the groundwater at the site can probably be taken from SDP1, which is less contaminated than the other acidic samples. The major ion composition of surface water LWE is similar to that of the topsoil samples, suggesting that this water is probably in equilibrium with the surrounding soil.

The trace element concentration of the topsoil is in most instances higher than that of the water samples (Figures 32 and 33) with the exception of the Mn concentration of SDP1. Since all the samples are below pH 3, there is unlikely to be any adsorption of metals onto oxide surfaces as can be seen in Figure 7. Most metals are therefore in solution making a direct comparison between samples possible even though the pH values are slightly variable.

The chemical speciation and saturation indices of the limed soil samples will be discussed in Chapter 4 (section 4.2.2.7), at which stage a comparison between the waters and soils will be made.

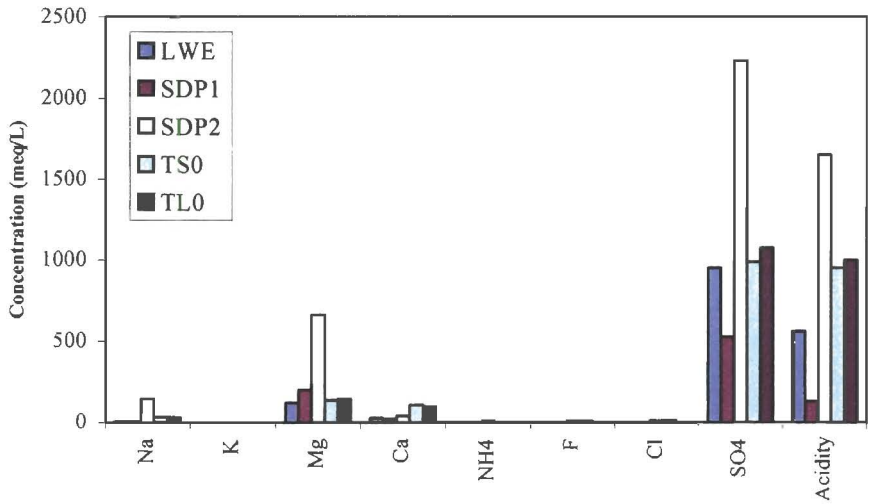

Figure 31. A comparison of the major ions in solution between water and soil samples.

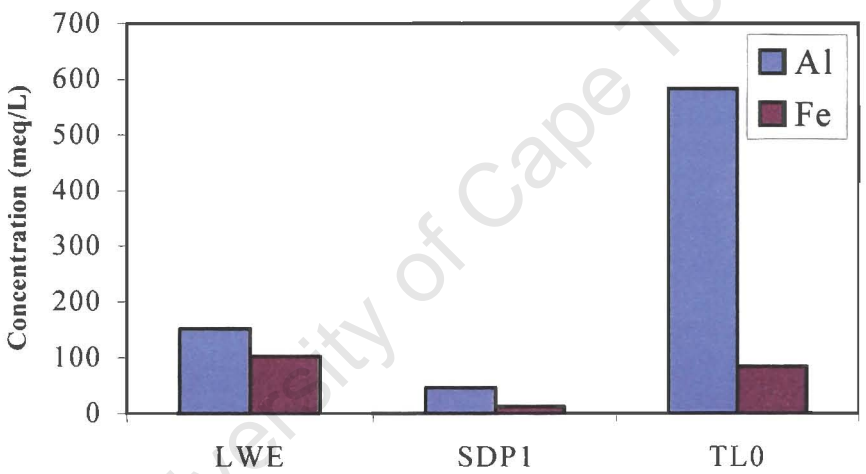

Figure 32. A comparison of the Al and Fe concentrations between selected water and soil samples.

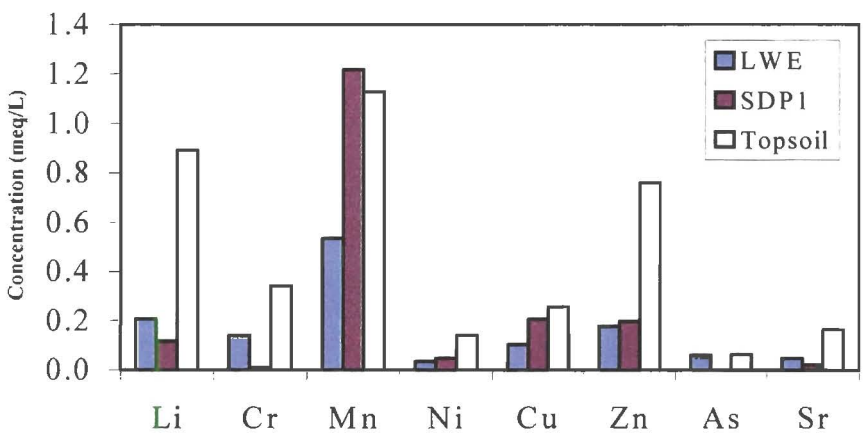

Figure 33. A comparison of trace elements in solution between selected water and soil samples.

3.6 Potential processes involved in soil acidification

It is apparent from the work conducted in this study that, although it is intuitively evident that the acidification has arisen from the oxidation of S, there are two possible processes by which this may have occurred. The first is the bacterially mediated oxidation process that occurs constantly over a long period of time provided that there is a supply of oxygen and S-oxidising bacteria, as was discussed in Chapter 2. The second oxidation event may have occurred as a result of the S fire and would have been much more rapid. Both of these pathways of S oxidation will be briefly explored in this section.

3.6.1 Sulphur content of soil

The unoxidised S content of the soil provides an estimation of the potential amount of acidity that can be generated in the future. For this reason, XRFS analysis was performed on selected samples and the ratio of S to SO_4^{2-} was determined so as to isolate the unoxidised proportion of the sample. These S speciation results are presented in Figure 34 for four topsoil samples, the first three being individual samples from soil profiles A, B and C, and the fourth being the composite topsoil sample (ATSC). The concentration of S in these samples varies from 0.2 to 3.5%. Samples lower down in the soil profile are not expected to contain higher concentrations of S. If sample ATSC is selected as a reasonable average S composition for the topsoil, a calculation can be made to determine the amount of acidity that is potentially stored in the soil. It can be seen from Reaction 2 (Chapter 2) that each mole of S that is oxidised produces 2 moles of acidity (H^+). Therefore, if the soil contains 0.5% S, that translates to 5 g S / kg soil and the amount of acidity generated can be calculated as follows:

$$5g / 32.07gmol^{-1} = 0.156 \text{ mol S}$$

i.e. $0.156 \times 2 = 0.312 \text{ mol } H^+ / \text{kg soil}$

i.e. Acidity = 312 $mmol_c$ / kg soil

It is important to note, however, that S is relatively inert and that large S particles will resist oxidation, thus slowing down the acidification process.

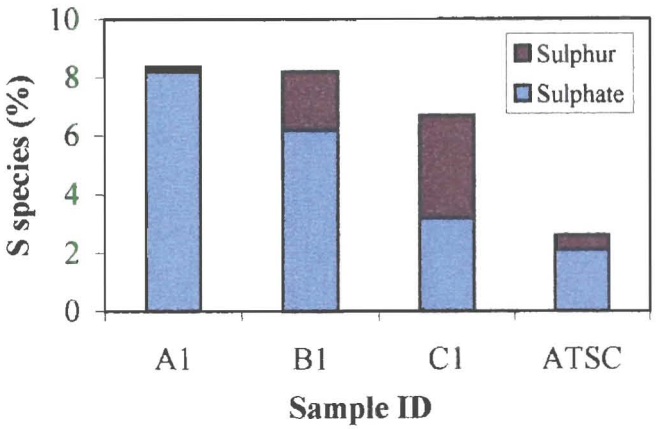

Figure 34. Proportions of different S species in selected soil samples.

3.6.2 Sulphur oxidising bacteria

Although the role of the acidophile bacterium *Thiobacillus thiooxidans* in oxidising elemental S is well understood, the rate at which this reaction takes place is quite variable (Tisdale *et al.*, 1985). There was insufficient time in this study to perform kinetic studies to assess the rate of oxidation in the natural environment. Since the S stockpile was in existence for several years prior to the fire in 1995, it is likely that bacterial oxidation has been continuous over this period. The fact that elemental S is a relatively stable compound may inhibit the process of oxidation but the S is unlikely to remain totally unoxidised due to the manner in which it was stored.

3.6.3 Sulphur melting experiments

The stable form of elemental S occurs as a lattice of crown-shaped S_8 molecules and is known as rhombic sulphur. A sample of the S stored at this site was analysed using XRD and it was found to consist of pure rhombic S (Figure 35). This compound melts at 113°C to form an orange-coloured liquid (Ebbing, 1987). S burns in air giving off highly noxious SO_2 gas. During the S fire at the site in 1995, a great deal of the S was driven off as SO_2 affecting a nearby community. A molten mass of S 'lava' was also formed and this travelled in a southerly direction as the fire continued to blaze. Fire-fighting efforts to douse the flames with water probably aided in the formation of H_2SO_3.

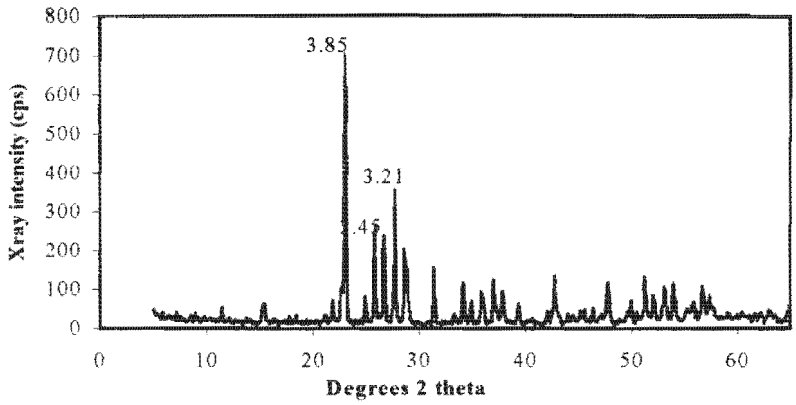

Figure 35. X-ray diffractogram of rhombic S from the site showing the distinctive S reflections at *d*-spacing values of 3.85, 3.21 and 3.45 Å.

In this study, an attempt was made to determine the effects of melting S in soil. An experiment was conducted where increments of S ranging from 0.1 to 1.0 g were added to 10g of uncontaminated topsoil and heated on a hot plate until the S had melted. The test pit topsoil (TPT) was used for this purpose together with crushed S from the site. In approximately 15 minutes, all the S in each beaker had melted and the samples were removed from the heat. The pH_{KCl} of each sample was then measured, the results of which are presented in Figure 36A and Appendix C2.2.2. This figure shows a clear reduction in pH even with the smallest addition of S of 0.1 g (1% S). The pH decreases gradually to pH 3.8 at 1.0 g S. The experiment was repeated in a similar way to determine whether the results obtained are consistent and it was found that, although the pH initially drops by approximately two pH units, there is some variability in pH with further addition of S. The results of all the burning experiments are presented in Figure 36B. A separate set of samples was also used to determine acidity and the results are tabulated in Appendix C2.2.2. Once again, there is some variability with the acidity data. However, since only 2.5 g of the sample was used in each case, this may not have been representative of the whole sample. The acidity values ranges from 3.0 to 17.3 $mmol_c/kg$ for samples containing various increments of S.

Although the results from these experiments do not show clear trends of amounts of S added with pH and acidity, it is evident from the results that at least some degree of acidification does occur. The amount of acidification will depend on how much S is released as SO_2 (g) and how much is converted to H_2SO_4. What is important to note is the speed at which this process takes place. Whereas bacterial oxidation of S slowly releases acidity over time, one catastrophic

burning event can release massive amounts of acidity in an extremely short space of time to the detriment of the surrounding environment.

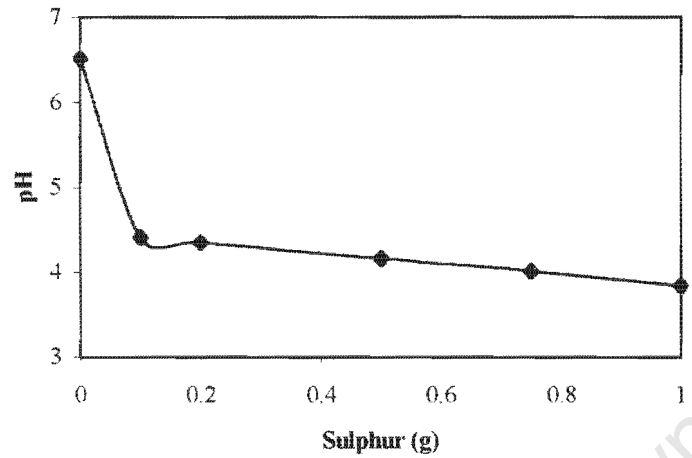

A.

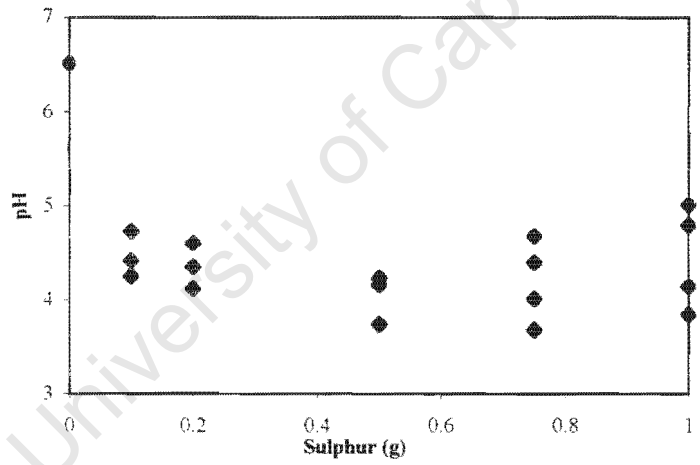

B.

Figure 36. The effects of molten S on soil pH.

3.7 Summary and conclusions

The environment associated with the S stockpile has become severely acidified, partly due to bacterially mediated oxidation of S and partly as a result of the sulphur fire that caused the rapid oxidisation of S to H_2SO_4. The waters in this environment are highly acidic with pH < 3 being common. The dominant ion in solution is SO_4^{2-} and this is balanced by acidity with Al^{3+}, Fe^{2+}, Fe^{3+} and Mn^{2+} comprising the bulk of the acid cation suite. The most significant basic cation is Mg^{2+}, with smaller amounts of Ca^{2+} and Na^{+}. The salinity of the water is also extreme with EC values reaching 67 mS/cm for the surface waters and as high as 179 mS/cm for the groundwater. The low pH of the water has also led to elevated concentrations of other trace elements in solution such as Cr, Ni, Cu, Zn, Sr, Ba and Pb.

The Al^{3+} activity of the water samples suggests that the waters may be in equilibrium with the mineral phases, jurbanite and alunite. This is supported by the saturation indices for these minerals which show that the solutions become supersaturated with respect to both jurbanite and alunite at pH > 3. The saturation indices for quartz and gypsum indicate that the solutions close to being in equilibrium with both of these phases, especially at pH < 4.

Ferrous Fe data were used to predict a p*e* window for this environment based on the modelling program, PHREEQC. According to the Fe^{2+} constraints, the p*e* of the water from this site was estimated to fall between 10 and 12. At a p*e* of 12, the Fe^{2+} activity data for all the water samples plotted against pH follow the solubility lines for soil Fe and goethite in an almost linear fashion suggesting equilibrium with a phase of their basicity. At a p*e* of 12, the waters are supersaturated with respect to goethite and jarosite above pH 1 and 2, respectively.

The composition of the soil is variable with the topsoil being capped by an ash-rich layer in places. The subsoil contains less SiO_2 and more Al_2O_3, Fe_2O_3 and MgO due to a higher clay content as opposed to the more sandy topsoil. The most notable component of these soils occurring in anomalous concentrations is the SO_3 originating from the S stockpile.

In terms of the chemistry of the soil solution, the topsoil horizon is expectedly more contaminated than the subsoil in terms of both acidity and salinity, with pH values as low as 1.2 and EC values as high as 107 mS/cm being recorded. The soil solutions are again dominated by the SO_4^{2-} anion and acid cations, including Al^{3+} and $Fe^{2+,3+}$. The base cation suite of the topsoil is dominated by Ca^{2+} with slightly lower concentrations of Mg^{2+} while the subsoil bases are

dominated by Na^+ and Mg^{2+}. Trace metals in solution occurring in significant concentrations include Zn, Cu, Ni, Cr, Sr and Pb in the topsoil and Sr, Ni and Zn in the subsoil. Soil acidity data show a logarithmic trend of acid saturation with respect to pH_{KCl} as would be expected.

The dominant clay mineral in the soil profile is smectite, which imparts distinctive swelling and shrinking properties to the soil. The mineralogy of both the topsoil and the subsoil comprises kaolinite, quartz and smectite as the dominant phases. The hardened horizons have a similar mineralogy but with minor occurrences of jarosite also being evident. Precipitate analysis with SEM revealed the occurrence of gypsum crystals on the soil surface with Fe sulphate phases (probably jarosite) also occurring as well as silicates and aluminosilicates. The EDS capability of the SEM was also used to verify the nature of a brittle duricrust-type sample taken from the hardened horizon, which was found to comprise Si and O, possibly representing amorphous silica.

4 Amelioration of the site

4.1 Introduction

An important consideration in assessing the geochemistry of acid environments is establishing a means of rehabilitation. This is commonly achieved by liming, as was the case at this site. To determine the effects of the liming, it was decided to conduct laboratory experiments using the same limestone product as was used at the site. By applying progressive increments of specially prepared limestone to samples of contaminated soil, it was possible to establish trends in pH, EC, major ions, trace metals and DOC. In addition to this, plant growth experiments were conducted in limed soils to establish the response of plants to liming. Furthermore, the mobility of certain mineral phases was monitored by modelling the soil solution data using PHREEQC, and in so doing, an understanding of the chemical processes potentially controlling this system was obtained.

4.2 Liming of acidic soils

The most effective ameliorating materials in treating acid soils are basic agents such as carbonates. Soil acidity can be divided into two broad groups, the reserve acidity which represents the buffer capacity of the soil and the active acidity which is the acidity associated with the solution phase of the soil and is dominated by free Al^{3+} and H^{+} ions. The reaction of bases such as lime with soils occurs with the active acidity first after which reserve acidity is slowly released into the active form (McBride, 1994).

In acid soils, 1 mole of $CaCO_3$ will neutralise 2 moles of acidity (H^{+}) or $^{2}/_{3}$ moles of Al^{3+}. The Ca^{2+} is immobilised at the exchange sites made available by the neutralising reaction, making the Ca^{2+} relatively immobile (McBride, 1994).

4.2.1 Liming agent used in this study

It was decided to utilise a locally available commercial limestone product for the amelioration of the soil at the site. The texture of the chosen limestone was heterogeneous, spanning a wide range of particle size fractions with over 85% of the material comprising sand and gravel (Table 5). Coarse limestone fragments are relatively ineffective in neutralising acidity since the outer surface of the grain may react with the acid to form an armoured coating rendering the inside of

the grain useless for further neutralisation (Fey, *pers. comm.*). It is generally the mud fraction (<63 μm) of the limestone that is most effective in acid neutralisation. It is also important to note that any lime that is applied to soil needs to be well mixed into the soil to maximise its effectiveness.

A sample of the limestone was analysed by XRD and was found to be composed of dolomite with trace amounts of quartz (Figure 37). Due to economic constraints, pure $CaCO_3$ could not be utilised at this site. The relative cost of dolomite over $CaCO_3$ probably warrants the use of the former.

Table 5. Particle size distribution of the limestone used at the site.

Size fraction	Particle size (mm)	Mass %
gravel	> 2	30.2
very coarse sand	2.0 – 1.0	28.0
coarse sand	1.0 – 0.5	14.0
medium sand	0.5 – 0.25	6.5
fine sand	0.25 – 0.125	4.5
very fine sand	0.125 – 0.0625	3.5
silt and clay	< 0.0625	13.2
Total:		**99.9**

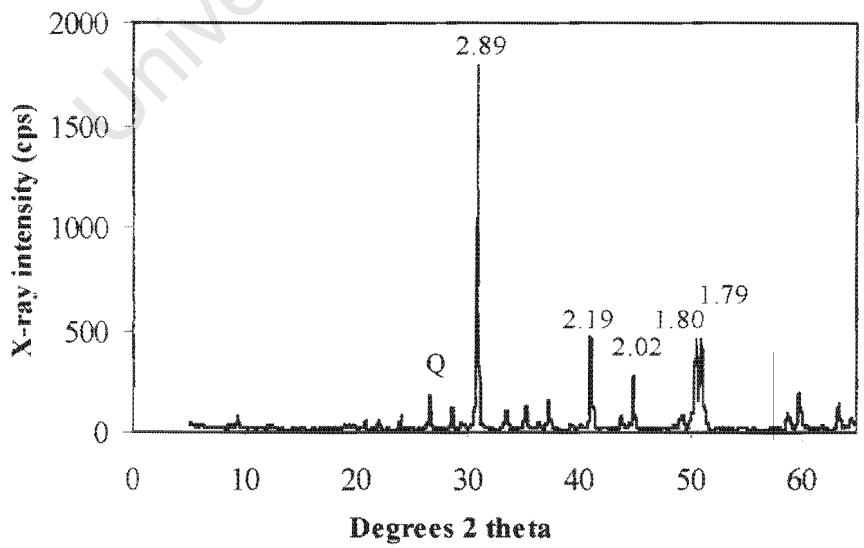

Figure 37. X-ray diffractogram of dolomitic limestone used to neutralise the acidity of the soil at the site (*d*-spacings of major dolomite peaks are shown in Å; Q = quartz).

It was decided that in order to provide results that are consistent with the work conducted at the site, it would be instructive to conduct all liming experiments using the same limestone that was used to ameliorate the site. Before this product could be used in meaningful experiments, it was thus necessary to determine its effective neutralising capacity. This is simply achieved by mixing a small sample of crushed limestone with a standard HCl solution and titrating the excess acidity with a base (NaOH in this case) as outlined in method 1.004 of Horwitz (1975) which is described in Appendix B3. The neutralising value of the limestone is then expressed as the $CaCO_3$ equivalent (CCE) with pure $CaCO_3$ having a value of 100% and most other products having CCE values of less than 100%. A determination of this nature was performed on crushed limestone from this study and it was found to have a CCE value of 58% (Appendix B3).

4.2.2 Lime requirement of soil

The lime requirement of the soil is strictly defined as the amount of alkaline material required to neutralise all the exchangeable acidity and bring the soil to a base saturation of 100%. The lime requirement should, however, be considered in the context of the land use for a particular soil. It is generally considered sufficient to neutralise the soluble and exchangeable Al^{3+} to a non-toxic level for the crop to be grown on the soil (McBride, 1994; McLean, 1982). The approach outlined above is more appropriate than merely considering the pH of a soil, since H^+ ions may form a relatively small fraction of the total acidity and this will vary from soil to soil. In acid soils, it is frequently the concentrations of Al, Fe and Mn that are high enough to be toxic to plants and any amount of lime added will decrease the solubility and consequently the toxicity of these elements (McLean, 1982).

To determine the lime requirement of the composite soils that were to be used in the limed incubation experiment, their acidity was first measured. This was done using the standard KCl extractable acidity method outlined in Chapter 3 (section 3.3.2.4). The exchangeable acidity of the topsoil and subsoil was thus determined as 342 and 136 $mmol_c/kg$, respectively. The CCE value for the limestone was then used to determine the amount of lime that was required for each soil. This was found to be 29.3 and 11.6 g lime / kg soil for the topsoil and subsoil, respectively. The calculations pertaining to this are presented in Appendix B3.

4.3 Limed soil incubation experiments

4.3.1 Method of preparation and analysis

4.3.1.1 Liming of soils

It was decided that to accurately assess the effects of liming at the site, a series of soil samples should be prepared and incubated in a standard way with appropriate increments of lime (based on the experiments of Engelbrecht, 1983). The composite topsoil (ATSC) and subsoil (ASSC) samples were thus prepared and used for this purpose. A set of 16 samples of 300 g each was prepared for the incubation experiment of which 8 were incubated for a short-term period of 2 weeks and the other half for a long-term period of 4 weeks. The experiment was conducted in a controlled environment chamber at 25°C. The samples were divided into 4 groups of 4 samples as follows:

Group	Description	Sample ID
Group 1:	topsoil short-term	TS
Group 2:	subsoil short-term	SS
Group 3:	topsoil long-term	TL
Group 4:	subsoil long-term	SL

Each group of 4 samples comprised a control sample and 3 samples containing lime in the ratios of ½, 1 and 2 times the lime requirement of the soil. The precise make-up of each sample is presented in Appendix B3.3. Before the lime was applied to the soil samples, it was crushed using a standard carbon steel *Sieb* mill to ensure that all samples were consistently treated. The particle size of the crushed lime comprised 87% mud-sized grains (<63 μm) with the remainder being in the very fine sand fraction (<125 μm).

The samples were moistened to field water capacity using deionised water with field capacity being estimated as half the amount of water needed for a saturated paste. The sample containers were loosely sealed to allow for exchange of gases with the atmosphere and the moisture content was maintained on a daily basis. On termination of incubation, an aliquot of each sample was extracted for pH_{KCl} measurement and acidity titration using the methods outlined in Chapter 3 (section 3.3.2.4) after McLean (1982). The balance was prepared in the standard way for saturated paste extraction (Rhoades, 1982).

4.3.1.2 Plant growth experiments

The soils recovered from the saturated paste extraction process were dried and retained for use in a plant growth experiment to illustrate the response of plants to these limed soils. Individual pots of soil were prepared using 300 g of each soil from the limed incubation study moistened to field capacity with five seeds of maize (*Zea mays*) added to each pot. The pots were then placed in a controlled environment chamber at 25°C for a period of 21 days. A solution of NH_4NO_3, $NaH_2PO_4 \cdot 2H_2O$ and KCl (NPK solution) was added in small equal increments for the first 6 days so as to provide 100 mg N, 20 mg P and 60 mg K per kg of soil. The plants were watered each day to field capacity. After the 3-week growth period, the maize plants were harvested and dried at 60°C and the dry mass of shoots was recorded for each pot.

4.3.2 Results and discussion

4.3.2.1 pH, exchangeable acidity and EC_e

The pH_{KCl} was measured for each sample subsequent to terminating the incubation experiment and the results are plotted in Figure 38 and presented in Appendix C2.2.1. The pH_{KCl} results for the short and long-term study appear to be similar as can be seen in Figures 38A and B, with a notable difference being the slight decrease in pH for the long-term incubation period of both the topsoil and subsoil. It is likely that the longer period of incubation allowed for further release of acidity and subsequent decrease in pH as was found to be the case, even though the decrease is slight. The addition of half the theoretical lime requirement increased the pH to above 4 in each case for both the topsoil and subsoil, with further additions of lime bringing the soils to near neutral pH values of over 6. The amount of exchangeable acidity similarly followed the trend of pH, decreasing dramatically with half the lime requirement (Appendix C2.2.1). The acid saturation decreased to below 20% for the topsoil and to below 10% for the subsoil (Figure 39). There was little difference in the rate of decrease in acid saturation for the short and long-term incubation. This is consistent with the liming results of Engelbrecht (1983) for a wide range of dolomitic limestone products varying in CCE from 37-79%, in which acid saturation was found to decrease sharply after two weeks of incubation with further incubation having little effect.

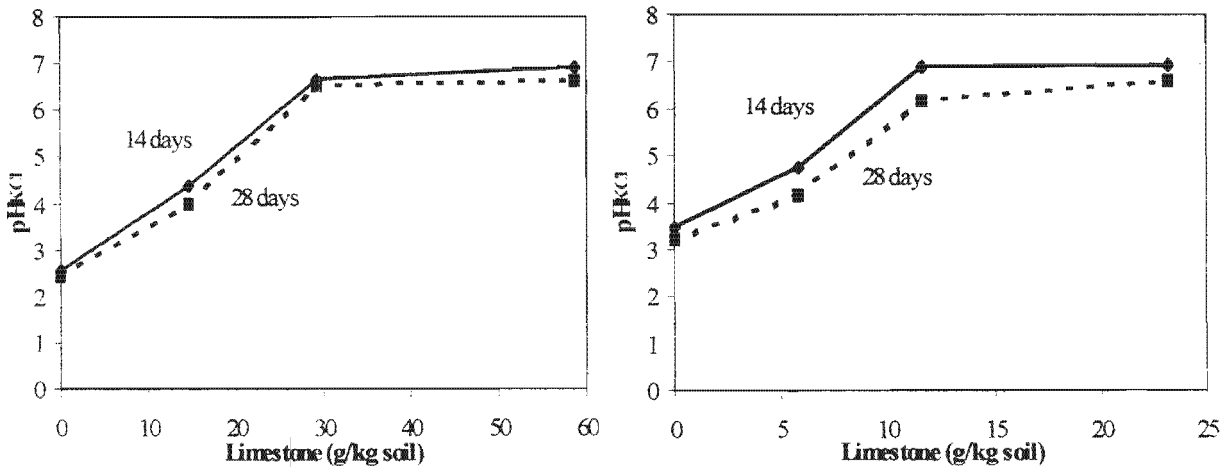

Figure 38. pH_{KCl} of limed topsoil and subsoil samples for short and long-term incubation as a function of the amount of limestone added.

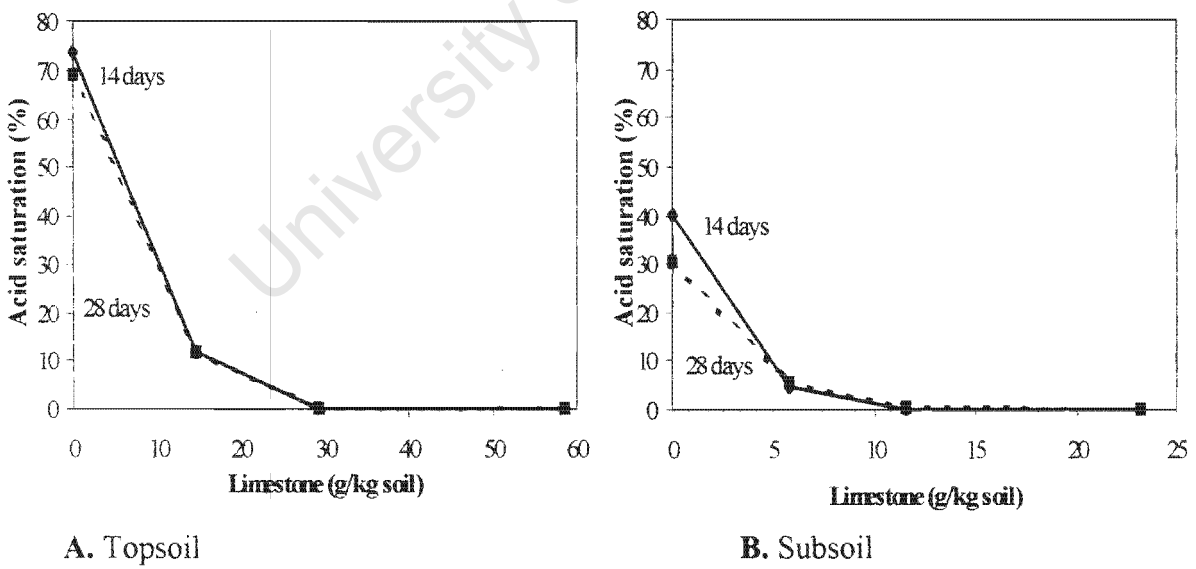

Figure 39. Acid saturation of limed topsoil and subsoil samples for short and long-term incubation as a function of the amount of limestone added.

In light of the discussion in section 4.2.2, it is instructive not only to consider the acidity of the system, but also to investigate the change in soluble Al with liming. The Al concentration of the saturated paste extracts has thus been presented in Figure 40 and although the levels of Al in solution are still extremely high after half the lime requirement has been applied, there is still a marked decrease from the original concentrations. In terms of Al toxicity to plants, it is probably necessary to apply the full lime requirement to the soils in this study to restore them to non-toxic levels. As was seen from Reaction 13 in Chapter 3, the hydrolysis of Al^{3+} generates 3 moles of acidity per mole of Al^{3+}. It is thus necessary to restore the pH to at least > 5 to eliminate Al in solution since the hydrolysis of Al buffers the soil pH in the region of 4.5 to 5. Above pH 5, the Al tends to precipitate as solid $Al(OH)_3$ and below pH 4.5, the Al occurs as the free ion Al^{3+} (McBride, 1994).

It is interesting to note that the EC of the soil solution (EC_e) decreases markedly with the addition of lime (Figure 41). This may not be intuitively obvious since it may be expected that applying lime to the soil will introduce more ions into solution and consequently maintain the salinity. However, in the context of this discussion it is important to consider the equivalent conductance of separate ions. The majority of ions in solution have a specific conductance of <80 at 25°C but the contribution of H^+ is 350 (Weast, 1969). Thus removing H^+ from solution has a significant effect on the EC of the sample. A further consideration with respect to the decrease in EC with increased liming is the fact that the increase in pH induces the precipitation of solid mineral phases and this may decrease the charge of the solution.

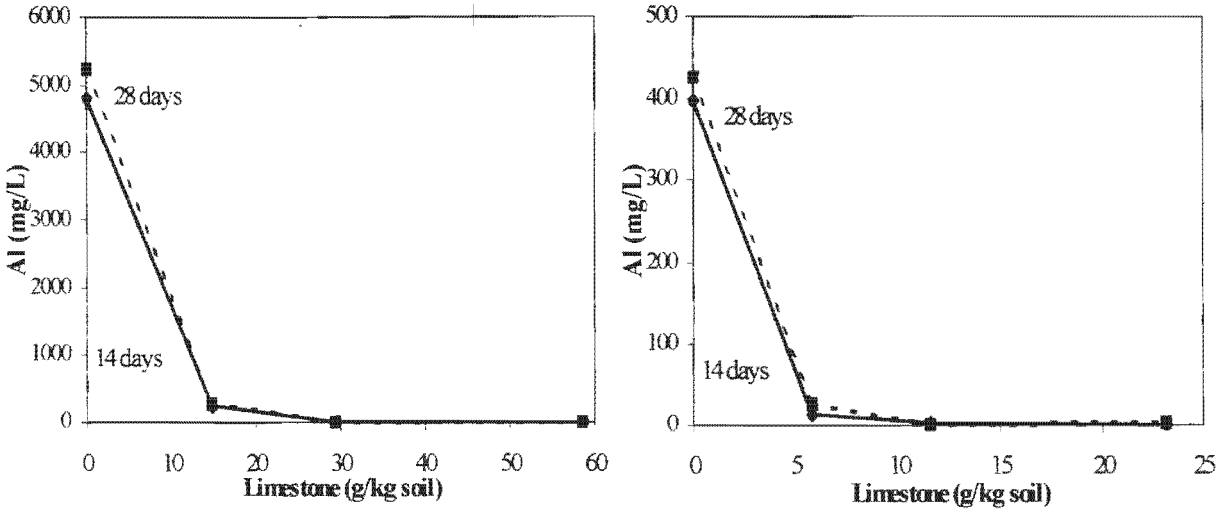

A. Topsoil **B.** Subsoil

Figure 40. Al concentration of limed topsoil and subsoil saturated paste extracts for short and long-term incubation as a function of the amount of limestone added.

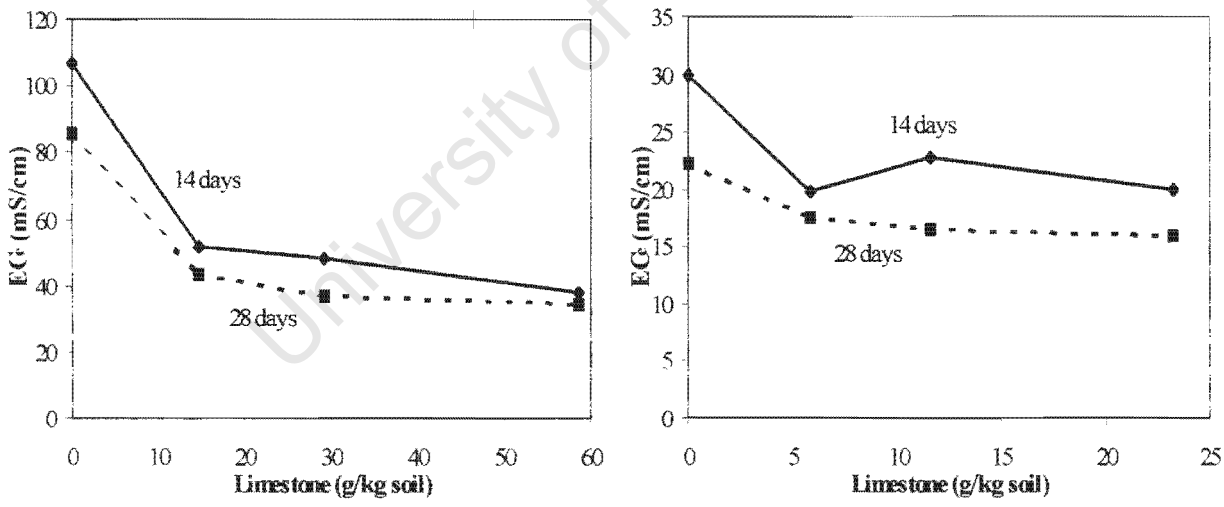

A. Topsoil **B.** Subsoil

Figure 41. EC_e of limed topsoil and subsoil saturated paste extracts for short and long-term incubation as a function of the amount of limestone added.

4.3.2.2 Major ions in solution

It has been seen from various discussions in this work that the concentration of SO_4^{2-} in solution is almost linearly balanced by acidity. The rapid decrease in acidity with liming is consequently balanced by a decrease in SO_4^{2-} as can be seen in Figure 42. In the topsoil horizon, half the lime requirement is responsible for decreasing the SO_4^{2-} by 2/3 of its original concentration with further additions of lime only having a slight effect. Likewise, the SO_4^{2-} in the subsoil decreases significantly with the application of limestone.

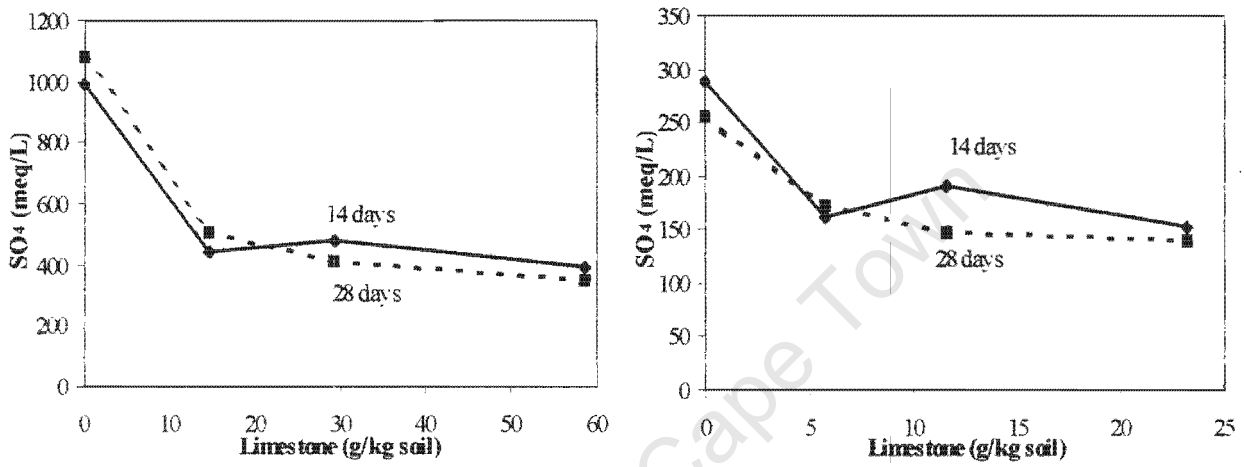

A. Topsoil **B.** Subsoil

Figure 42. SO_4 concentration of limed topsoil and subsoil saturated paste extracts for short and long-term incubation as a function of the amount of limestone added.

One mechanism for the removal of SO_4^{2-} with liming, also accounting for Al precipitation, is based on the following reaction:

$$Al^{3+} + OH^- + SO_4^{2-} = AlOHSO_4 \qquad (14)$$

Solutions from acid sulphate soils were found to be in equilibrium with jurbanite at extremely low pH (Reddy *et al.*, 1995), supporting this argument. The potential importance of the mineral jurbanite in this study, was seen in Chapter 3 (section 3.4.2.2) and further treatment of the solubility of this mineral will be explored with respect to liming of soils in section 4.3.2.6 below.

Another important consideration with respect to the solubility of SO_4^{2-}, is the fact that in a study by Rose and Elliot (2000), SO_4^{2-} concentrations in solution were found to increase with excessive liming. Aluminium and Fe oxyhydroxides that precipitate within acid sulphate environments often sorb high concentrations of SO_4^{2-}, a significant percentage of which is

desorbed with liming (Rose and Elliot, 2000). An example of the potential adsorption of SO_4^{2-} onto Al complexes is shown below:

$$Al^{3+} + 3OH^- = Al(OH)_3 \quad (15)$$

$$Al(OH)_3 + SO_4^{2-}(aq) = Al(OH)_3\text{–sorbed } SO_4 \quad (16)$$

Under acidic conditions, $Al(OH)_3$ precipitates will be positively charged and will therefore adsorb anions such as SO_4^{2-}.

Although Fe and Al phases play a significant role in acid sulphate environments and ferric precipitates, in particular, are evident at this site, they make up a relatively small proportion of the soil surface. It is thus unlikely that the desorption of SO_4^{2-} will play a major role in this environment as can be the case in AMD environments (Rose and Elliot, 2000). However, merely from an economic point of view, over-liming acidic soils is impractical and is thus likely to be avoided.

The Ca and Mg results from the saturated paste extracts of the incubation study are presented in Figures 43 and 44. There is an initial decrease in the concentration of Ca^{2+} in the topsoil with the addition of lime after which Ca^{2+} remains fairly stable with further limestone application. The Mg^{2+} concentration shows an initial increase after which it appears to stabilise with liming. A reaction that might explain the mobility of Ca^{2+} and Mg^{2+} in this system is as follows:

$$CaMg(CO_3)_2 + 2H_2SO_4 = CaSO_4\,(s) + MgSO_4\,(aq) + 2H_2O + 2CO_2 \quad (17)$$

This is substantiated by the fact that the saturation indices for the topsoil solutions indicate that the solutions are supersaturated with respect to gypsum (section 4.3.2.6) and slightly undersaturated with respect to the hydrated $MgSO_4$ phase, epsomite. The solutions in the subsoil behave somewhat differently, with the Mg^{2+} decreasing and the Ca^{2+} remaining constant with liming. Since the subsoil horizon is more clay-rich than the topsoil, the amount of ion exchange and adsorption between cations on the clay surfaces will be greater in the subsoil. This is particularly significant at this site since the clay is mainly composed of smectite which has a very high surface area (700-800 m^2/g) and a cation exchange capacity (CEC) of between 70 and 120 cmol/kg (McBride, 1994). The Al^{3+} on the smectite exchange surfaces may thus be replaced by Ca^{2+} and Mg^{2+} from the soil solution.

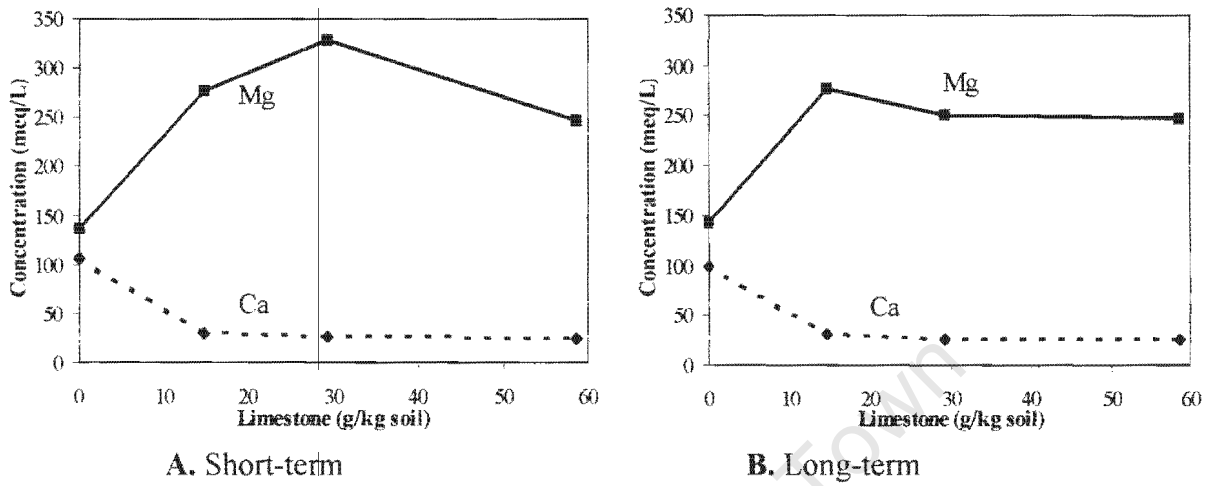

Figure 43. Ca and Mg concentration of limed topsoil saturated paste extracts for short and long-term incubation as a function of limestone added.

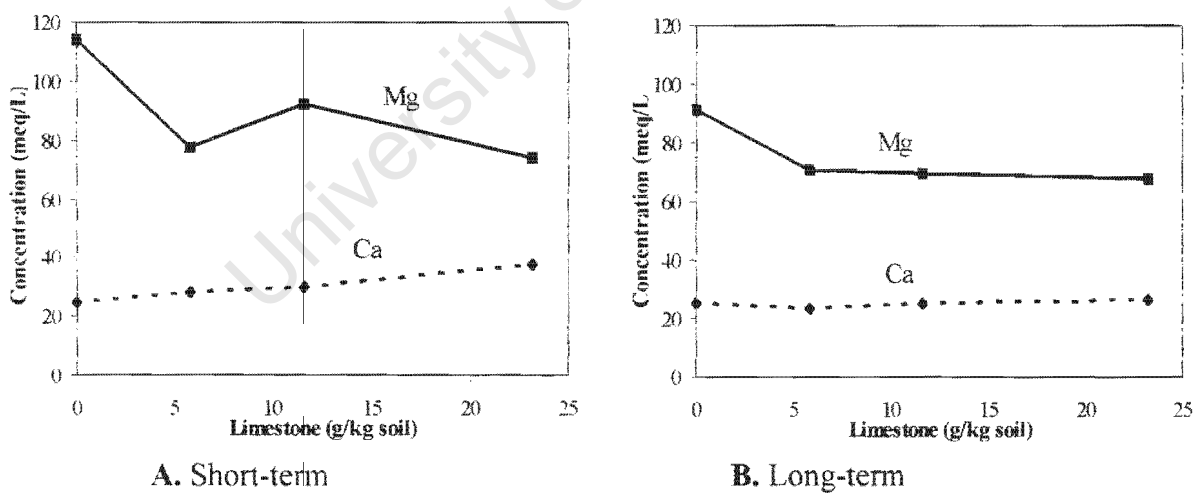

Figure 44. Ca and Mg concentration of limed subsoil saturated paste extracts for short and long-term incubation as a function of the amount of limestone added.

It is instructive at this point to consider the importance of solid solution formation in controlling cation and anion solubility in soils. The theory of solid solutions predicts that the solubility of an ion can be lowered in a mixed ionic compound relative to the solubility of the pure compound (McBride, 1994). This is particularly important when considering the formation of co-precipitates. A key factor controlling which cations are able to form solid solutions is the ionic radius, which must be small enough for the cations to enter the octahedral sites of the mineral structure. Small divalent cations, including Zn^{2+}, Cu^{2+} and Mg^{2+}, form solid solutions with Al hydroxide, whereas larger cations such as Pb^{2+}, Mn^{2+} and Ca^{2+} do not (McBride, 1994). An example of such a reaction is the formation of a Mg-Al double hydroxide, which is presented below:

$$Mg^{2+} + Al^{3+} + 5OH^- = MgAl(OH)_5 \qquad (18)$$

This reaction lowers the solubility of Mg^{2+}, accounting for its decrease in solution with liming. Solid solutions with the general formula $[M^{2+}_{1-x}Al_x(OH)_2]^{x+}A^{n-}_{x/n}$ where A^{n-} is an anion, are well known and referred to as *hydrotalcites*. The A^{n-} anion is represented by SO_4^{2-} in this case and, since *hydrotalcites* possess the unusual property of permanent positive charge, this is manifested as a high anion exchange capacity (McBride, 1994). Therefore, in addition to decreasing the solubility of Mg^{2+}, *hydrotalcite* formation also provides another mechanism for lowering the solubility of SO_4^{2-}.

Other major ions in the soil solution occurring in decreasing order of abundance are Na^+, Cl^-, F^-, NH_4^+, and K^+, although the contribution of these ions is far less than that for SO_4^{2-}, Ca^{2+} and Mg^{2+} (Appendix C2.3). Sodium occurs as the next most significant basic cation in the soil solution, and decreases in concentration with progressive liming in both the topsoil and subsoil. Successive liming reduces the concentration of H^+ and Al^{3+} in solution, possibly allowing for Na^+ replacement on the exchange surfaces of negatively charged clay and oxide surfaces. There is also a decrease in the concentrations of NH_4^+ and F^- in solution with liming (Appendix C2.3). Fluorine is known to form strong complexes with Al^{3+} (Lindsay, 1979), and the precipitation of Al minerals may consequently be accompanied by co-precipitation of F^-. Ammonium and K^+ may also be adsorbed to negatively charged surfaces of clay minerals, although the behaviour of K^+ in solution does not appear to follow any particular trend (Appendix C2.3).

A more rigorous discussion of the solubility of specific mineral phases, as modelled by PHREEQC, will be attempted in section 4.3.2.6.

4.3.2.3 Other trace metals in solution

The solubility of metal cations at low pH is well known and has been discussed at various points in this work. Increases in pH promote the adsorption of cations onto clay and oxide surfaces (Figure 7) consequently removing them from solution. The trace element data for the limed soil solutions from the incubation study are presented in Table 6.

It can be seen from this table that in almost all instances for both the topsoil and subsoil, the trace metal concentration decreases with progressive liming. This is particularly evident for the important acid cations Fe and Al where the levels in solution are especially high in the control samples and the decrease in concentration with liming is dramatic. Some Fe and Al appears to remain in solution, even at neutral pH, especially in the subsoil horizon, however, it is unlikely that there are detectable concentrations of either of these metals above pH 5. It is more likely that since these samples were filtered using a 0.45 μm filter, some colloidal material would have passed through the filter and would thus have been detected by ICP-MS as being in solution. It is especially important to consider this when modelling data with PHREEQC, for example. Colloidal Al or Fe that may be present at neutral pH should be excluded in the input of modelling programs, since any values that are entered, will be treated as being in solution. This will consequently affect the output that is obtained with respect to the speciation and saturation indices of phases including these elements.

Other trace metals in solution will follow a similar path to the major cations in this system, such as Mg^{2+}, Ca^{2+}, Al^{3+}, Fe^{3+} and Fe^{2+}. The addition of limestone to the soils and the subsequent increase in pH promotes the adsorption of metal cations onto negatively charged mineral surfaces, removing these cations from solution (Table 6).

Table 6. Trace element data for the saturated paste extracts of limed samples from the incubation study.

A. Short-term incubation (14 days):

Sample ID	TS0	TS1	TS2	TS3	SS0	SS1	SS2	SS3
Lime (g/kg soil)	0	14.7	29.3	58.6	0	5.8	11.6	23.2
Li	5.8	0.6	0.1	0.1	6.5	0.8	0.2	0.3
Al	4799.5	245.2	nd	nd	396.8	12.2	1.5	0.3
Si	30.3	37.4	nd	0.7	57.4	39.5	8.2	16.9
Cr	5.3	nd	nd	nd	nd	nd	nd	0.3
Mn	29.9	38.7	16.0	11.3	59.6	27.5	13.3	5.7
Fe	1837.5	3.4	9.4	10.6	0.2	9.4	10.6	10.9
Ni	3.9	1.9	0.1	0.1	3.5	1.2	0.1	0.1
Cu	7.3	nd	nd	0.2	0.8	nd	nd	nd
Zn	21.0	7.2	1.2	1.8	3.9	2.4	0.3	0.3
Sr	6.8	2.0	1.3	1.2	6.9	3.4	2.4	2.4
Ba	0.8	0.1	0.1	3.7	1.6	0.1	1.0	0.1
Pb	0.5	0.1	0.3	0.4	1.4	0.3	0.2	0.2

B. Long-term incubation (28 days):

Sample ID	TL0	TL1	TL2	TL3	SL0	SL1	SL2	SL3
Lime (g/kg soil)	0	14.7	29.3	58.6	0	5.8	11.6	23.2
Li	6.6	0.8	0.4	nd	5.6	1.4	0.5	0.3
Al	5239.4	276.8	nd	nd	427.0	24.4	0.5	2.9
Si	49.7	1.3	11.1	nd	60.1	19.4	15.5	7.0
Cr	6.5	0.3	0.3	nd	0.6	0.1	0.2	nd
Mn	32.0	39.1	9.0	7.8	60.4	30.1	7.2	14.4
Fe	1424.2	nd	nd	nd	139.2	112.1	2.6	nd
Ni	4.3	1.9	0.1	0.1	3.1	1.4	0.1	nd
Cu	9.0	nd	nd	0.1	nd	nd	nd	nd
Zn	28.7	7.8	0.4	0.3	2.9	1.5	0.5	1.2
Sr	7.7	2.4	1.0	1.0	6.4	3.4	1.7	1.6
Ba	0.7	0.1	nd	nd	nd	0.4	nd	1.2
Pb	1.6	0.1	0.1	0.3	0.1	0.2	0.3	0.2

nd = not detected; all values in mg/L.

NOTE: all trace elements with concentrations less than 1mg/L have been omitted.

4.3.2.4 Dissolved organic carbon (DOC)

An interesting trend was noted in the DOC concentrations of the saturated paste extracts from the limed topsoil samples (Figures 45 and 46). The DOC was found to be high at low pH showing an initial decrease with liming followed by a subsequent increase to the original concentration with neutralisation of pH (Figure 45). The saturated paste extracts showed a particular variation in colour, which was repeatable for the short and long-term limed study. At low pH in the absence of lime, the extracts had the characteristic red-brown hue indicative of Fe^{3+} in solution. Once the pH was brought to above 4 and the Fe^{3+} removed, the extract solutions became clear, and further addition of lime and increase in pH produced a distinctly yellow colour in the extract solutions (Figure 46).

The trivalent ions, Al^{3+} and Fe^{3+} form highly stable complexes with organic matter (McBride, 1994; Reddy *et al.*, 1995) possibly explaining the high concentrations of DOC at such low pH. Once these metals are removed from solution, the solubility of organic matter is consequently reduced and the concentration of DOC decreases. Further increases in pH promote the dissolution of organic matter since organic polymers tend to disperse at higher pH (McBride, 1994) as can be seen in Figure 45. The analogous subsoil samples at neutral pH have DOC concentrations from 25-30 mg/L which is expected, since the organic matter content of a soil generally decreases downwards in the soil profile. The organic carbon content decreases from 0.8% in the topsoil to 0.1% in the subsoil composite sample (Appendix C2.1).

It is important to note that organic matter, as with 2:1 aluminosilicates, has a substantially high CEC (Oades, 1989). At low pH, organic acids will thus have a strong affinity for soluble cations, forming complexes in solution. These organic complexes are thus likely to play an important role in the soil solution of the topsoil, as opposed to the subsoil, in which the role of 2:1 layer silicates will probably be more significant.

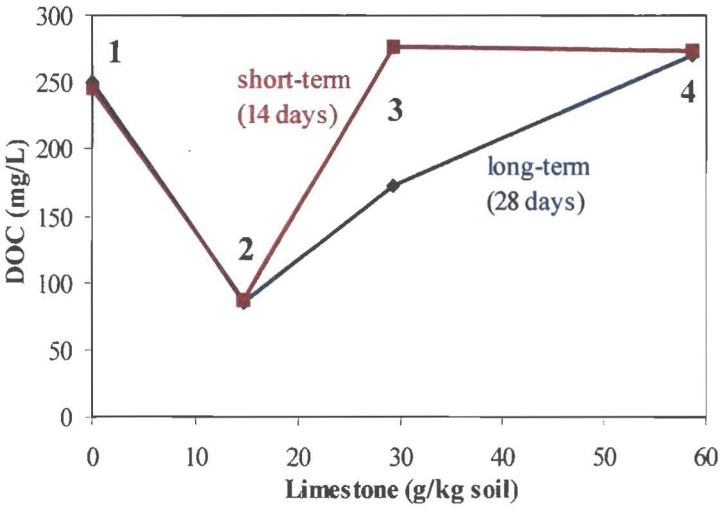

Figure 45. Dissolved organic carbon (DOC) of topsoil saturated paste extracts after incubation with limestone (No's 1-4 refer to equivalent solutions in Figure 46).

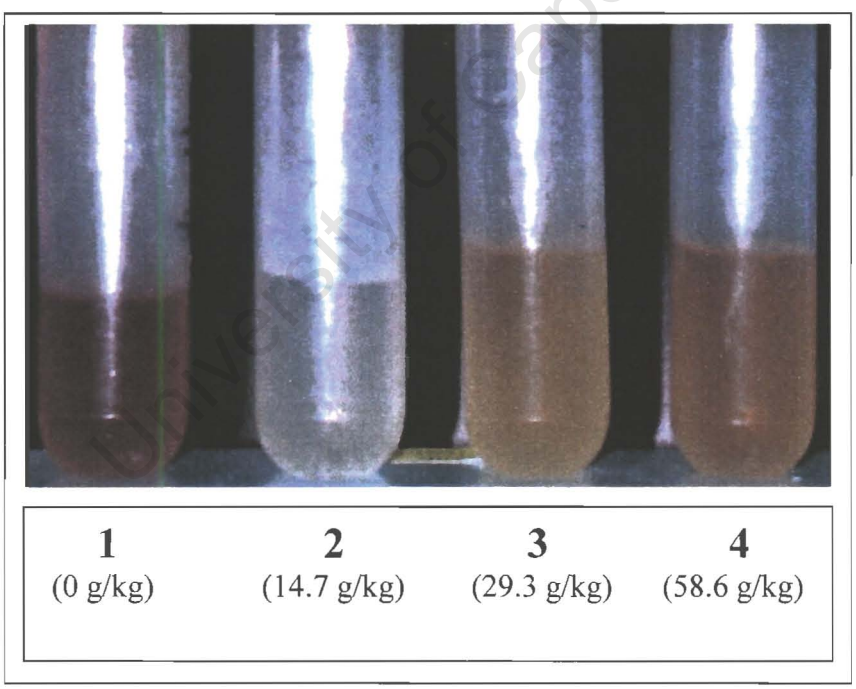

Figure 46. Saturated paste extracts of topsoil samples after incubation with limestone, showing changes in solution colour with variation in DOC (values in brackets represent amount of limestone added to sample per kg of soil with DOC concentrations plotted in Figure 45).

It is generally considered uninstructive to consider organic matter in computer modelling programs since there are such a wide variety of organic complexes that can occur in solution and their behaviour may be very different. The program MINTEQA2 allows for the input of dissolved organic matter (DOM) which is calculated on the basis of the DOC concentration of the sample. The precise relationship between DOC and DOM is not well constrained with DOM merely being estimated from DOC. Nowicki (1997) has explored this problem and has presented an empirical relationship between DOC and DOM. Furthermore, the thermodynamic data for DOM, as presented in MINTEQA2, is based on the composition of fulvic acids from the Suwannee River as characterised by Leenheer *et al.* (1994) and may therefore be inappropriate when considering other systems. For these reasons, modelling data with DOM was not attempted since the potential output was considered to be dubious.

4.3.2.5 Alkalinity

Free carbonate minerals in soils such as Ca and Mg carbonates constitute a reserve of alkalinity that can neutralise natural and anthropogenic forms of soil acidity. Acid neutralisation reactions generate bicarbonate salts as in the following example:

$$H^+ + CaCO_3 = HCO_3^- + Ca^{2+} \qquad (19)$$

This reaction and the subsequent leaching of HCO_3^- salts from the soil surface slowly depletes the carbonate buffering capacity and will eventually lead to a lowering of pH (McBride, 1994). Since the soils in this study are highly acidic, a prolonged application of lime may be necessary to maintain a level of carbonate buffering to counteract acidity. A further problem at this site is the fact that dolomite has been used for liming instead of more soluble calcite. Since dolomite has an equilibrium constant of $K = 10^{-17.2}$ compared with that of $10^{-8.5}$ for calcite (Drever, 1997), the rate of neutralisation with dolomite will be far slower than with calcite.

Alkalinity of the saturated paste extracts was determined on all incubation samples with pH > 4.5 and the results are presented in Figure 47 showing a clear linear relationship between alkalinity and pH. It is thus evident that crushed dolomite is successful in, not only neutralising the acidity, but also imparting free soluble alkalinity to the soil. The results achieved in the 14-day incubation were similar to those for the 28-day period apart from one long-term sample with an anomalously high pH and alkalinity (Figure 47 and Appendix C2.3). This suggests that the limestone has reached its maximum efficiency by the end of the short-term cut-off period of 14

days. The anomalous result may indicate heterogeneity within the soil or the limestone since proper splitting apparatus was not used to apportion either the samples or the lime. The rate of the reaction is also likely to have been increased by the moist warm conditions of the controlled environment chamber, the fine grain-size of the material and the fact that the lime was thoroughly mixed with the soil before incubation. In reality, this lime would be less effective in neutralising acid soils. It is important to note, however, that even though dolomite is far less soluble than calcite, it is still effective in introducing alkalinity to the soil in a relatively short period of time provided that the conditions are kept at an optimum as discussed in this section.

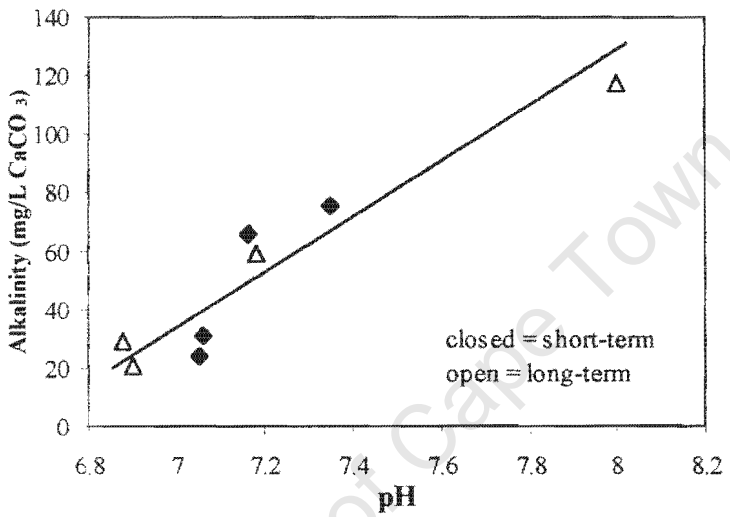

Figure 47. Alkalinity as a function of pH for all the saturated paste extracts of the limed incubation samples with pH > 4.5 (short and long-term samples shown as closed and open shapes, respectively).

4.3.2.6 Chemical speciation and saturation indices

In Chapter 3 (section 3.4.2.2), a discussion of the chemical speciation and saturation indices of various mineral phases was made for all the water samples in this study. Apart from the systematic effect that liming will have on the soil samples, the results in this section should be similar to those from Chapter 3 since both the soil and water samples are from the same system.

The activities of Al^{3+} and Fe^{2+} have again been considered in this context since minerals containing these cations are the most important in acid systems. The behaviour of Al and Fe in low pH soil environments is controlled by a number of chemical processes, including the formation of soluble inorganic and organic complexes and solid phase equilibria (Reddy *et al.* 1995). To predict possible controls on these chemical processes, the data in this study were modelled using PHREEQC with the WATEQ4F database and the relevant activities and

saturation indices are presented in Appendix C2.5. The solubility lines were, once again, calculated using the derivations from Appendix C1.2. The activity of Fe^{2+} was considered at different conditions of redox and the data are presented accordingly.

The Al^{3+} data for all samples below pH 5 are presented in Figure 48. The solubility regions for the two prominent Al-sulphate minerals, jurbanite and alunite, are also depicted together with the solubility line for gibbsite. The jurbanite and alunite zones are based on the minima and maxima of the SO_4^{2-} and K^+ activities (Appendix C2.5). In Figure 48 it can be seen that all samples plot above the solubility zone of jurbanite and most plot above that of alunite, indicating that the solutions are supersaturated with respect to both these minerals above pH 3. The data points are approximately parallel to the jurbanite solubility field suggesting equilibrium with this phase rather than alunite. This is consistent with the work of Reddy *et al.* (1995) on pyritic soils undergoing oxidation, where it was found that at extremely low pH (~2), jurbanite was the equilibrium phase. In soils at neutral pH, Al^{3+} activities are generally low and are assumed to be controlled by gibbsite, however, in acid sulphate soils, it is suggested that the Al^{3+} activities are not controlled by gibbsite but rather by jurbanite (Reddy *et al.*, 1995; Nordstrom, 1982). It can be seen from Figure 48 that at low pH, the solutions are undersaturated with respect to gibbsite but not to jurbanite.

The Fe^{2+} activities of all the acidic samples are shown in Figure 49 as a function of pH. These data were calculated at pe = 12 as this appeared to represent a reasonable estimation of redox based on the Fe^{2+} concentration of the water samples and the data presented in Figure 18 (Chapter 3). An attempt was made to estimate the Fe^{2+} concentration of the soils but, in all cases, the soluble Fe content of the saturated paste extracts was composed entirely of Fe^{3+}. This suggests that the process involved in extraction, including the mixing with oxygenated water and the vacuum extraction has caused complete oxidation of the samples. For these reasons, to estimate realistic conditions of redox for the soil solutions, the Fe^{2+} concentrations of the water samples from Chapter 3 (section 3.4.2.2) were used to calculate pe instead. The (pe + pH) windows in Figure 49 have thus been calculated using the pe range of 10 to 12 as determined in Chapter 3, with $Fe(OH)_3$ representing an average soil Fe and goethite chosen as a common Fe^{3+} mineral. Reaction 11 was once again utilised to obtain the bounding solubility lines for $Fe(OH)_3$ and goethite in Figure 49. It can be seen from the data in this figure that for $Fe(OH)_3$, the data fall between the (pe + pH) range whereas the solutions all appear to be supersaturated with respect to the goethite window.

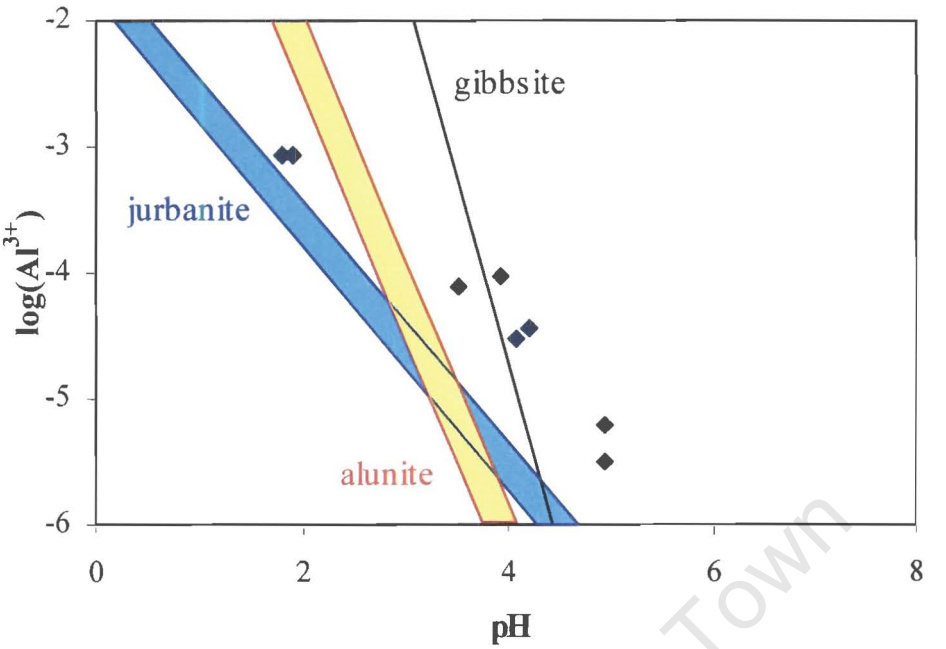

Figure 48. Al^{3+} activity as a function of pH for all saturated paste extracts containing soluble Al (the solubility line for gibbsite is shown in black and the solubility windows for jurbanite and alunite are shown in blue and orange, respectively, based on minimum and maximum activity data from this study).

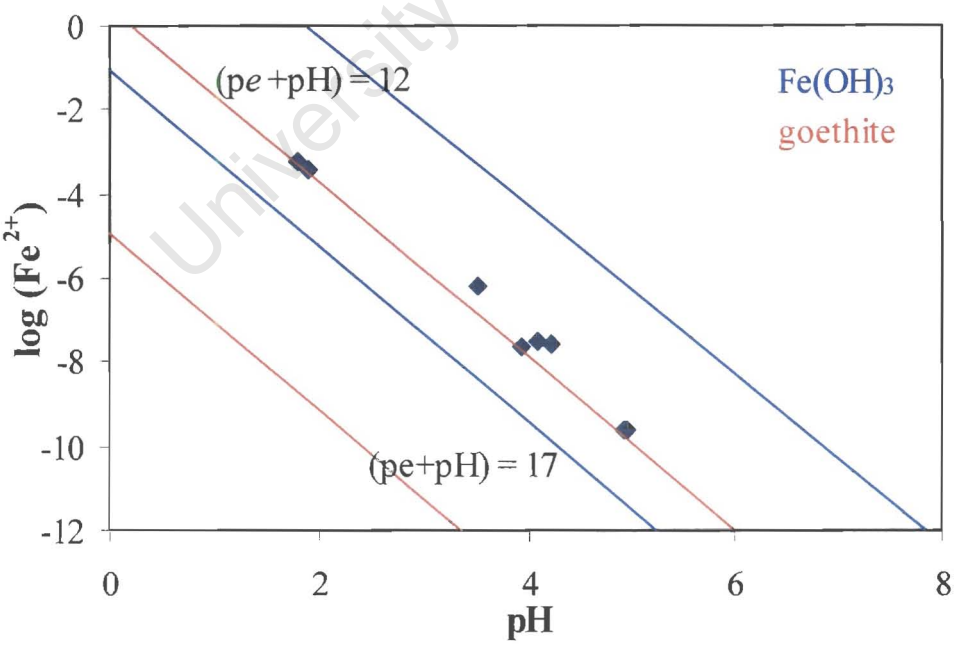

Figure 49. Fe^{2+} activity as a function of pH for all saturated paste extracts containing Fe at p*e* = 12 (estimated maximum and minimum (p*e*+pH) windows for $Fe(OH)_3$ and goethite are shown in blue and orange, respectively).

The saturation indices of a selection of Al minerals are depicted in Figure 50, the trends for which are consistent with the results from Figures 48 and 49. What is interesting to note, however, is the fact that the topsoil and subsoil samples follow the same trend in all cases. The soils making up the two composite samples are highly variable as can be seen by the composition of each horizon (Table 3) as well as the textural data in Appendix C2.1. It may thus be expected that the chemical processes controlling each horizon would be distinctive and follow different trends. However, the solid phases that control the dissolved Al and Fe concentrations in these soils appear to be dominating this system, as is evidenced by the trends in saturation indices. The data appearing at neutral pH (circled in Figure 50) should be ignored since it is unlikely that the Al determinations at this pH are reliable in terms of reflecting monomeric Al in solution, as was discussed in section 4.3.2.3. The system is thus slightly supersaturated with respect to jurbanite over the full acidic pH range with all other Al minerals being undersaturated at low pH and becoming supersaturated above pH 5.

The saturation indices pertaining to selected silicate, carbonate and basic sulphate phases are presented in Figure 51 and show that the solution has a composition which is approximately in equilibrium with respect to quartz and gypsum. At neutral pH, the soil solution becomes supersaturated with respect to dolomite as would be expected with the progressive addition of this mineral to the soil. The mineral, sepiolite, has been chosen to represent a Mg-silicate phase and shows a strong linear trend, being highly undersaturated at low pH and approaching equilibrium at neutral pH.

The saturation indices for the ferric Fe phases, goethite, jarosite and amorphous $Fe(OH)_3$ are presented in Figure 52 as a function of pH under a variety of redox conditions. Figure 52A is the most reduced scenario and shows that the solution is highly undersaturated with respect to all the minerals below pH 5. However, the occurrence of jarosite at the site (Chapter 3; section 3.4.3.4) and the range of *pe* estimated in Chapter 3 (section 3.4.2.2), points to a more oxidising environment. The scenario depicted in Figure 52C is thus the most accurate estimation of Fe^{3+} mineral saturation as well as possible *pe*, with the system being approximately in equilibrium with respect to jarosite and supersaturated with respect to goethite. These results are also consistent with those of Figure 49.

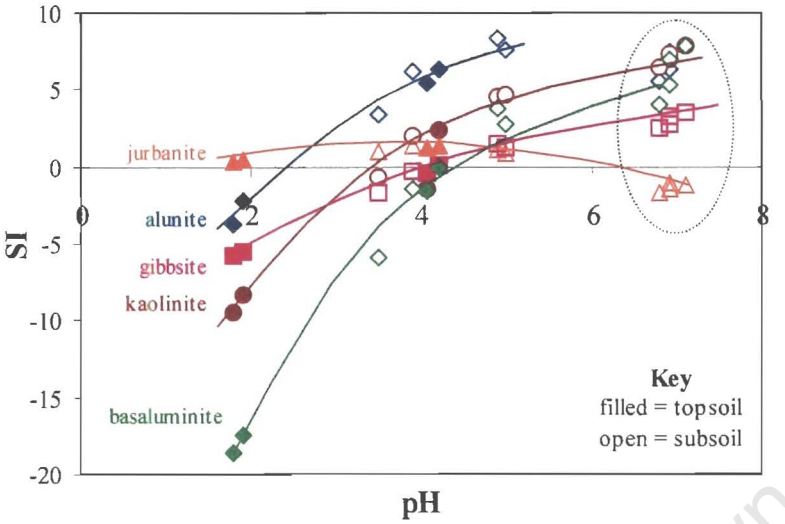

Figure 50. Saturation indices of selected aluminium mineral phases as a function of pH.

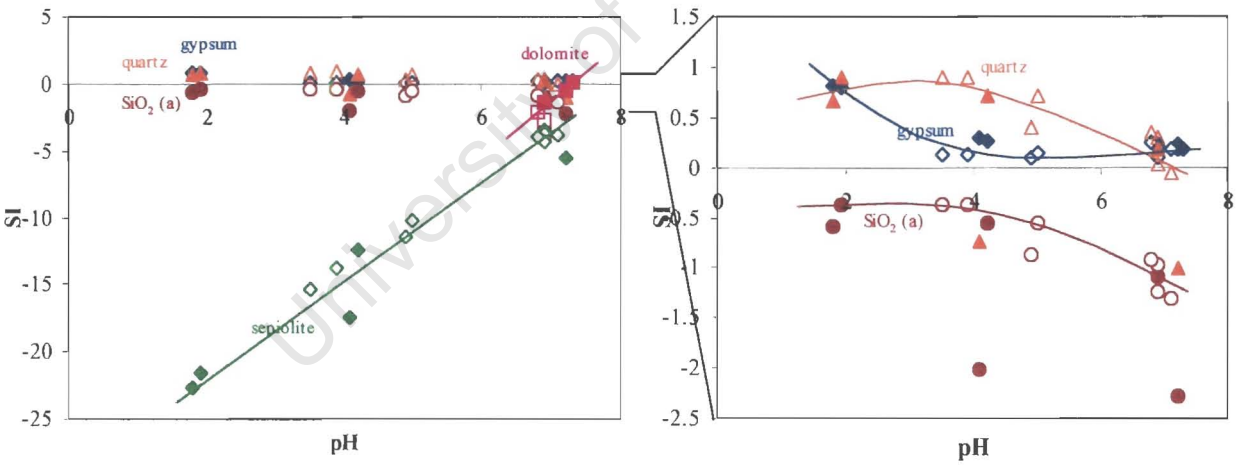

Figure 51. Saturation indices of selected silicate and carbonate mineral phases as a function of pH.

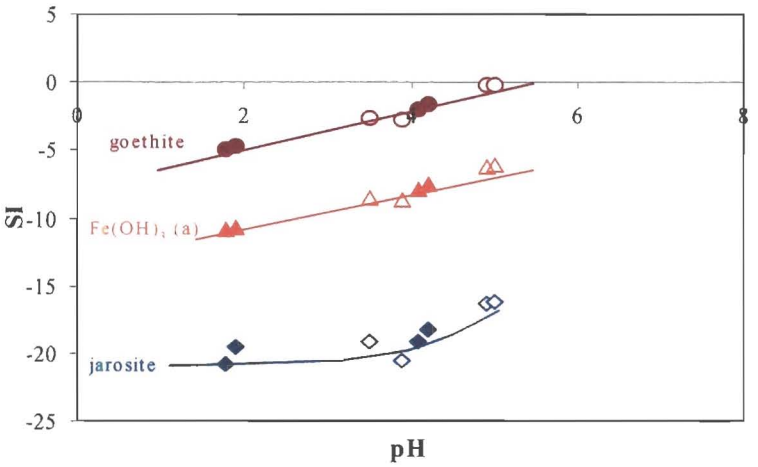

A. p*e* = 4

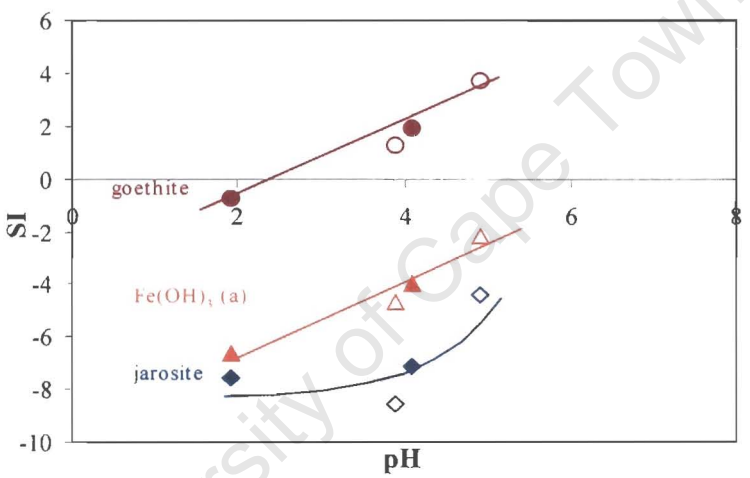

B. p*e* = 8

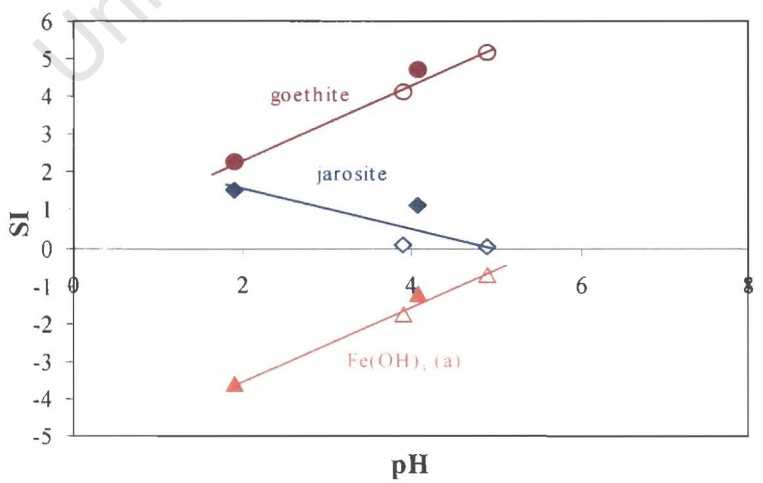

C. p*e* = 12

Figure 52. Saturation indices of Fe^{3+} mineral phases as a function of pH under various p*e* conditions.

4.3.3 Plant growth experiments

A small unreplicated plant growth trial experiment was performed using maize seeds in residual saturated pastes from the incubation study to determine the response of plants to liming. This experiment was conducted as a preliminary demonstration and any conclusions drawn from it are thus provisional. The biomass data for the plant growth experiments are shown in Figure 53 with an illustration of the response of plants to liming shown in Figure 54. These figures show the positive response of plants to liming with seeds germinating in all but the most acidic topsoil sample.

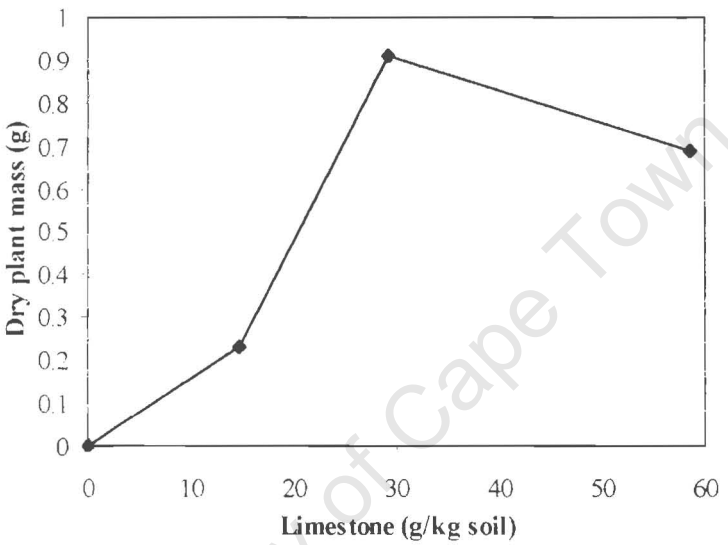

A. Topsoil

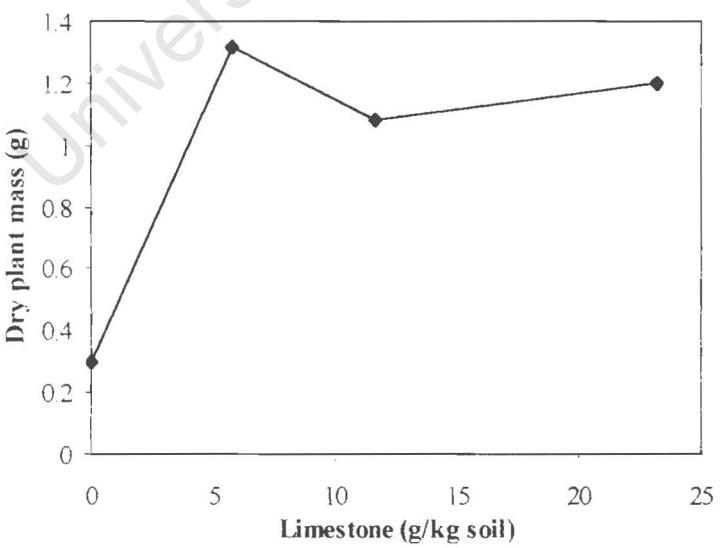

B. Subsoil

Figure 53. Dried maize biomass of limed topsoil and subsoil samples as a function of the amount of limestone added.

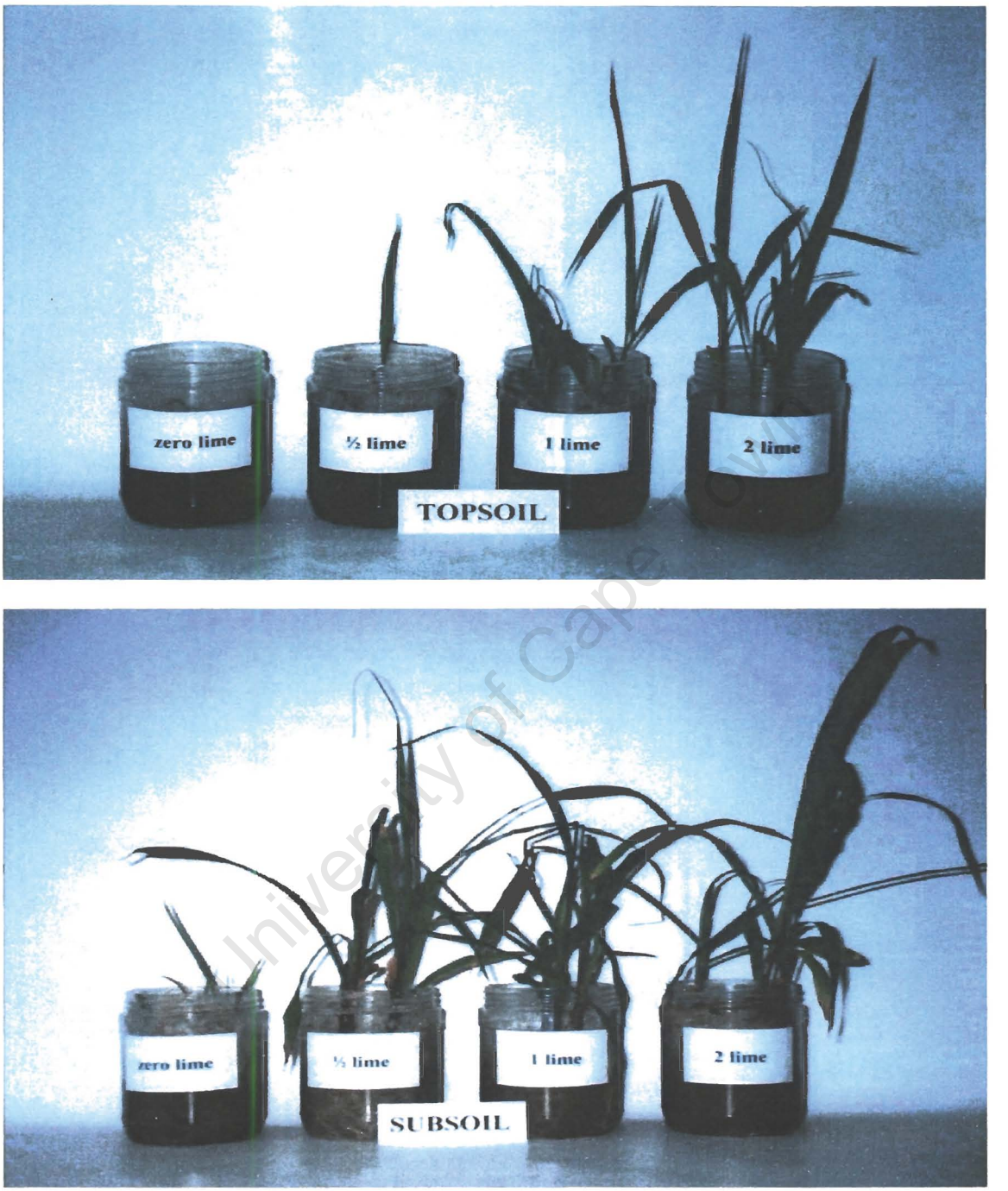

Figure 54. Plant growth experiments using maize (*Zea mays*) in residual saturated pastes from the limed incubation soil samples.

The plants in the topsoils reached a relatively healthy state only after the full quota of lime was added and the pH was close to neutral, whereas the plants in the subsoil samples appeared to be healthy, even at half the theoretical lime requirement. It is surprising that the plants have responded so well since the soils have an exceptionally high EC_e, even after liming. According to Ayers and Westcot (1985), the yield potential of maize as influenced by soil salinity is as follows:

EC_e (mS/cm):	**Yield potential:**
1.7	100%
2.5	90%
3.8	75%
5.9	50%
10	0%

This suggests that the maximum EC_e in which maize will survive is 10 mS/cm. The plants from this study are thus not likely to survive for long in these soils. At the termination of the growth trial, the plants were showing distinct signs of physiological stress with some dying back of leaf tissue. Restoring these soils to a fertile state for general plant growth or agricultural activity would thus require that substantial quantities of salts are leached from the soil subsequent to the neutralisation of its acidity.

4.4 Water quality

The quality of the water at this site is, understandably, very poor as can be seen in Table 7. In this table, various water quality guidelines are compared with selected samples from this study. Samples LWE and SDP1 are acidic surface and groundwater samples from the site, the locations of which can be found in Figure 9B (sites LE and SDP1, respectively). Two saturated paste extracts are also presented in Table 7, the first one, TS0, being from the short-term incubation topsoil sample and the second, SL3, representing the least contaminated limed soil sample. The relatively uncontaminated wetland sample (AWH) from the vicinity (site AH in Figure 9A) has also been included. It can be seen from Table 7 that, although liming has greatly reduced the concentration of potentially toxic elements such as Al, Fe, As, Cd, Cr and Se, the water quality remains unacceptable for most purposes in terms of water quality guidelines. It is also interesting to note that even the wetland sample is unsuitable in quality, especially with respect to its salinity. It is therefore evident that the water at the site and vicinity is of a poor quality in spite of the environmental implications associated with the S fire. The soil solution samples, TS0 and SL3 were included in Table 7 to provide some indication of the likely composition of leachate emanating from the site.

Liming was successful in neutralising the soil acidity and consequently bringing the pH to within acceptable limits. There was also a significant reduction in the EC of the soil with liming, although the salinity remains over an order of magnitude higher than the acceptable limits of the World Health Organisation (1984) and the Department of Water Affairs and Forestry (1996). The resultant pH increase from liming has also led to an important reduction in most trace elements as can be seen in sample SL3 (Table 7) in which the concentration of most trace elements has decreased to below the limits of detection.

Because the waters at this site are highly saline, it is unlikely that any degree of liming will improve water quality to acceptable levels. Considerable quantities of solutes will need to be leached from the site before this environment can be restored to a state in which the surface and groundwater are safe for use. In the context of this discussion, it is important to note that due to the topographic and climatic conditions of the site, and its close proximity to the ocean, this site may have been naturally saline, even before the inception of the industrial complex in the area. The quality of the water at this site may thus have never been acceptable in terms of water quality guidelines. It is therefore important to decide on the expected land-use of the site before attempting to restore the environment to an unrealistically pristine state.

Table 7. Water quality regulation data compared with data from this study.

	Domestic (WHO)	**Domestic** (DWAF)	**Industrial** (DWAF)	**Irrigation** (DWAF)	**Livestock** (DWAF)	**LWE** surface water	**SDP1** ground-water	**TS0** acid topsoil	**SL3** limed subsoil	**AWH** wetland water
EC (µS/cm)		<450	1000			66750	45550	107000	16000	2400
pH	6.5 - 8.5	6 – 9	6 - 9	6.5 - 8.4		1.5	3.0	1.8	6.6	7.3
TDS	1000	<300			1000					
Alkalinity (mg/L $CaCO_3$)			150			nd	nd	nd	28.9	na
Solutes (mg/L):										
DOC		5				180	61	250	25	na
Na^+	200			<70	2000	110	160	690	968	176
Cl^-	250		20	<100	1500	79	210	452	234	236
F^-	1.5	1		2	2	24.5	45.5	184	2.2	0.2
NO_3^-	44	27			100	nd	nd	nd	nd	nd
SO_4^{2-}	400		400		1000	45800	25260	47500	6704	522
Al	0.2	0.15		5	5	1369	413	4800	2.9	1.3
Fe	0.3	0.1	0.5	5	10	1905	212	1887	nd	0.7
Mn	0.1	0.05	0.2	0.02	10	14.6	33	29.9	14.4	0.06
As	0.05			0.1	1	0.903	0.014	1	nd	0.003
Cd	0.005			0.01	0.01	0.017	0.05	0.12	nd	0.0006
Cr	0.05			0.1	1	2.46	0.166	5.28	nd	nd
Pb	0.05			0.2	0.1	0.358	0.046	0.51	0.2	0.06
Se	0.01			0.02	0.05	0.016	0.016	0.32	nd	0.01

nd = not detected; na = not analysed; all data in mg/L unless otherwise stated
WHO = World Health Organisation
DWAF = Department of Water Affairs and Forestry

4.5 Summary and conclusions

The results from the incubation study showed that the pH increased to neutrality with liming and was accompanied by an associated decrease in acidity. The EC_e and SO_4^{2-} concentration of the soil solutions also decreased considerably with liming. The topsoil samples show an increase in soluble Mg^{2+} and a slight decrease in Ca^{2+}. The relationship between soluble Ca^{2+} and Mg^{2+} in the subsoil is more complicated, with Mg^{2+} decreasing slightly with liming and Ca^{2+} remaining relatively stable. Levels of trace elements in solution expectedly decrease as the pH increases to neutral values. The concentration of DOC is exceptional high at low pH, decreases considerably at intermediate acid pH values (~4) and, once again, increases at neutral pH. At low pH, DOC is expected to complex strongly with Al, Fe and other metal cations in solution, and once these metals are removed from solution, the DOC is likely to co-precipitate with them. Further increases in pH may promote the dissolution of organic matter as is evident in the DOC concentrations of the topsoils of this study. The alkalinity of the solutions was found to increase linearly with pH as would be expected.

The activities of selected ions and saturation indices of selected minerals were considered, with special reference to Al and Fe. These data show that the solutions are supersaturated with respect to alunite and jurbanite above pH 3 with the trend of data points suggesting equilibrium with jurbanite. At pH values below 4, the solutions are undersaturated with respect to gibbsite but not to jurbanite, which suggests that the Al^{3+} activities are controlled by the latter.

A *pe* window of between 10 and 12 was used for discussion of Fe activities in solution, since this represents a reasonable estimation of redox for this system. Solubility windows for goethite and amorphous $Fe(OH)_3$ were thus developed showing that the solutions are supersaturated with respect to goethite and approximately in equilibrium with amorphous $Fe(OH)_3$. The saturation indices of goethite, $Fe(OH)_3$ and jarosite have been compared with pH under various *pe* conditions and show that the solutions become supersaturated with respect to goethite and jarosite at *pe* 12.

Saturation index data for other phases show that the system is close to being in equilibrium with quartz and gypsum over the full acidic pH range, and comes into equilibrium with dolomite and sepiolite at neutral pH. The precipitation of gypsum from solution may partly explain the reduction of SO_4^{2-} in solution with liming.

Plant growth experiments conducted using maize verified that liming was successful in reducing the Al toxicity to levels that supported growth. However, the salinity of the soils remained excessively high, even after liming, and all plants began to show signs of physiological stress after ~14 days of incubation.

Liming the soils did little to improve the overall quality of the water in the area, although it was successful in bringing the pH to neutral and reducing the concentrations of potentially toxic trace metals to acceptable levels.

5 General discussion and conclusions

The initial objectives of this work were to comprehensively assess the geochemistry of the highly contaminated environment at the sulphur site, as well as to devise practical means for ameliorating the soil in terms of its acidity. The extent to which these objectives have been met will be examined in this chapter.

The aqueous and pedogenic environment of the area associated with the S stockpile has become severely acidified, partly due to the slow, bacterially mediated oxidation of S, and partly as a result of the catastrophic fire of 1995 that aided in oxidising S to H_2SO_3. The residual S associated with the soil, as well as the existing acidity within the soil, is likely to maintain a substantial level of acidity in this environment well into the future, unless significant quantities of lime are applied to neutralise the soil. The site will need to be constantly monitored to ensure that re-acidification does not occur as a result of the substantial reserve acidity associated with this soil.

The water in this environment is mostly highly acidic, with pH < 3 being common. The dominant ion in solution is SO_4^{2-} and this is balanced by acidity with Al^{3+}, Fe^{2+}, Fe^{3+} and Mn^{2+}, comprising the bulk of the acid cation suite. The most significant basic cation is Mg^{2+}, with smaller amounts of Ca^{2+} and Na^{+}. The salinity of the water is also extreme with EC values reaching 67 mS/cm for the surface waters and as high as 179 mS/cm for the groundwater (sample SDP2). However, this sample represents a locally developed brine and the overall salinity of the groundwater is more likely to be considerably lower. The low pH of the water has also led to elevated concentrations of other trace elements in solution such as Cr, Ni, Cu, Zn, Sr, Ba and Pb.

The Al^{3+} activity of the water samples suggests that the waters may be in equilibrium with mineral phases typical of acid sulphate environments such as jurbanite and alunite. This is supported by the saturation indices for these minerals which show that the solutions become supersaturated with respect to both jurbanite and alunite at pH > 3. The saturation indices for quartz and gypsum indicate that the solutions are also close to being in equilibrium with both these phases, especially at pH < 4.

Ferrous Fe data were used to predict a *pe* window for this environment based on the modelling program, PHREEQC. According to the Fe^{2+} constraints, the *pe* of the water from this site was estimated to fall between 10 and 12. Lower *pe* values were also considered for modelling purposes since it is important to consider a wider range of *pe* to accommodate more reducing conditions that may prevail over time or at greater soil depths. At a *pe* of 12, the Fe^{2+} activity data for all the water samples plotted against pH follow the solubility lines for soil Fe and goethite in an almost linear fashion suggesting equilibrium with a phase of their basicity. The data also fit discretely between the assumed minima and maxima for (*pe* + pH). At a *pe* of 12, the waters are supersaturated with respect to goethite and jarosite above pH 1 and 2, respectively. The Fe and Al activity data, as well as the data pertaining to the saturation indices of relevant mineral phases are consistent with the work of Lindsay (1979).

The composition of the soil is variable with the topsoil being capped by an ash-rich layer affecting its composition. The subsoil contains less SiO_2 and more Al_2O_3, Fe_2O_3 and MgO due to a higher clay content as opposed to the more sandy topsoil. The most notable component of these soils occurring in anomalous concentrations is SO_3, originating from the S stockpile.

In terms of the chemistry of the soil solution, the topsoil horizon is expectedly more contaminated than the subsoil in terms of both acidity and salinity, with pH values as low as 1.2 and EC values as high as 107mS/cm being recorded. The pH of the subsoil has increased to values between 3 and 4 while the EC has dropped to a quarter of that of the topsoil. The ionic suite is again dominated by SO_4^{2-} with the balance of cations being made up of acidity. The base cation suite of the topsoil is dominated by Ca^{2+} with slightly lower concentrations of Mg^{2+} while the subsoil bases are dominated by Na^+ and Mg^{2+}. Apart from the excessive concentrations of Al, Fe and Mn in solution, trace metals in solution occurring in significant concentrations include Zn, Cu, Ni, Cr, Sr and Pb in the topsoil and Sr, Ni and Zn in the subsoil.

Soil exchangeable acidity data show a logarithmic trend of acid saturation with respect to pH as would be expected. The ash-rich topsoil horizons plot slightly away from the general trend, possibly as a result of the lack of ion exchange soil surfaces in these horizons to allow for more exchangeable Al^{3+} to move into solution, elevating the acid saturation. However, compared with the soil acidity data of Thomas and Hargrove (1984) for natural soils, the data from this study do not show as dramatic an increase in acid saturation, with most of the low pH samples having a lower acid saturation than expected. However, it is important to note that pH values in natural environments are highly unlikely to reach the extremes encountered in this study. The acidity

data from this study may, thus, not be comparable with natural soils, although the general logarithmic trend in the data is evident.

A study of the clay mineralogy revealed that the dominant clay in the soil profile is smectite, which imparts distinctive swelling and shrinking properties to the soil. The mineralogy of both the topsoil and the subsoil comprises kaolinite, quartz and smectite as the dominant phases. The hardened horizons have a similar mineralogy but with minor occurrences of jarosite also being evident. An analysis of a pale yellow precipitate from the site confirmed the presence of jarosite.

In a SEM-EDS inspection of some of the precipitates which had formed on soil surfaces, crystals of gypsum were clearly evident together with Fe sulphate phases (probably jarosite) in addition to various silicate minerals. The EDS capability was also used to verify the nature of a brittle duricrust-type sample taken from the hardened horizon. The brittle material is composed of Si and O, probably representing amorphous silica.

A comparison between the soil and water from the site shows that the SO_4^{2-} concentrations of all the samples are linearly correlated with their total acidity as would be expected for this acidic environment. The major ion composition of the surface water appears to be similar to that of the topsoil suggesting that this water is in equilibrium with the surrounding soil. The composition of the groundwater is variable but is confined to only two samples. More groundwater data would be needed to make this comparison more meaningful. However, since most of the surface water samples taken from the site represented standing water at or close to the soil surface, this water may, in fact, closely reflect the composition of the groundwater in the region. The trace element concentration of the topsoil is generally higher than that of the water samples. Since the topsoil samples were incubated for a lengthy period and the pH of the soil was extremely low, it is likely that trace elements would be released into the solution filling the pore spaces of the soil. The waters pooling at the surface may not have undergone such intense contact with the topsoil, possibly explaining their slightly lower concentrations of most trace elements.

The site was ameliorated using a readily available dolomitic limestone product, which was also used in all liming experiments conducted in this study. Before any liming experiments were attempted, the limestone was crushed to a fine powder with 87% being in the mud fraction. This was done to maximise the reactivity of the limestone and ensure that the results between experiments were consistent.

A incubation experiment was set up using composite topsoil and subsoil samples and applying varying increments of limestone to separate subsamples of soil, based on the acidity of the soils and the CCE of the limestone. Each sample was made in duplicate to accommodate short and long-term incubation periods. The samples were thus incubated in a controlled environment for periods of two and four weeks, respectively. Saturated paste extracts were taken from each incubated sample subsequent to the termination of each experiment and the soil solutions were analysed for major ions, trace elements, DOC, acidity and alkalinity.

The pH was found to increase to neutrality with liming and was accompanied by an associated decrease in acidity. The EC_e of the samples decreased considerably with liming, mainly as a result of the removal of H^+ from solution, but also as a result of the removal of SO_4^{2-} ions from solution and the likely precipitation of certain mineral phases such as gypsum, jarosite, and jurbanite. The topsoil samples show an increase in soluble Mg^{2+} and a slight decrease in Ca^{2+} as a result of the application of dolomitic limestone and the precipitation of gypsum. The relationship between soluble Ca^{2+} and Mg^{2+} in the subsoil is more complicated, probably as a result of the higher concentration of 2:1 layer silicates in the subsoil horizon and the consequent importance of ion exchange on the clay surfaces. The formation of Mg-Al double hydroxides may provide a further explanation for the decrease of soluble Mg^{2+} in the subsoil. Levels of trace elements in solution expectedly decrease as the pH increases to neutral values.

An interesting trend was exhibited by the concentration of organic matter in solution with DOC values being very high at low pH, dramatically decreasing at intermediate acid pH values (~4) and, once again, increasing at neutral pH. At low pH, DOC is expected to complex strongly with Al and Fe in solution and once these metals are removed from solution, the DOC is likely to co-precipitate with them. Further increases in pH promote the dissolution of organic matter which may explain the increase in DOC at pH > 6 in the topsoils of this study.

The alkalinity of the solutions was found to increase linearly with pH as would be expected. The variation in alkalinity for the short and long-term incubation is minimal, suggesting that the limestone has reached its maximum efficiency in two weeks under optimum conditions.

The activities of selected ions and saturation indices of selected minerals were, once again, considered for the limed soil solutions to determine the chemical processes associated with liming. The important acid cations, Al and Fe, were again considered, since the mobility of these elements is of major significance in ameliorating acid sulphate environments. Aluminium

data show that the solutions are supersaturated with respect to alunite and jurbanite above pH 3 and since the data points plot parallel to the jurbanite field, the solutions may be in equilibrium with this phase. At pH values below 4, the solutions are undersaturated with respect to gibbsite but not to jurbanite which suggests that the Al^{3+} activities are controlled by the latter which is consistent with other data from other acid sulphate environments (Reddy *et al.*, 1995).

The potential redox conditions of the soil were estimated using the redox data determined for the water samples, since the saturated paste extraction process oxidised all Fe to Fe^{3+} and it was thus not possible to use the Fe speciation results from the soil solutions to predict p*e* values. A likely p*e* window of between 10 and 12 was thus used for discussion of Fe speciation, although it is possible that the horizons lower down in the soil profile may experience more reducing conditions over time. Solubility windows for goethite and $Fe(OH)_3$ were thus developed showing that the solutions are supersaturated with respect to goethite and approximately in equilibrium with $Fe(OH)_3$. The saturated indices of goethite, $Fe(OH)_3$ and jarosite have been compared with pH under various p*e* conditions and show that the solutions become supersaturated with respect to goethite and jarosite at p*e* 12, which is consistent with the fact that jarosite precipitates have been identified at this site.

Saturation index data for other phases show that the system is close to being in equilibrium with quartz and gypsum over the full acidic pH range, and comes into equilibrium with dolomite and sepiolite at neutral pH.

It is important to note that the saturation index data for both the topsoil and subsoil composites follow the same trend for most acid sulphate minerals when compared with pH. This suggests that the solid phases that control the concentrations of dissolved Al and Fe in these soils appear to dominate the soil solution of the entire soil profile.

Plant growth experiments conducted using maize verified that liming was successful in reducing the Al toxicity to levels that supported plant growth. However, the salinity of the soils remained excessively high, even after liming, and all plants began to show physiological signs of stress after approximately 14 days growth.

Liming the soils did little to improve the overall quality of the water in the area, although it was successful in bringing the pH to neutral and reducing the concentrations of potentially toxic trace metals to acceptable levels.

The main findings of this study thus reveal that the geochemical environment is highly acidic and saline, dominated by SO_4^{2-}, Al^{3+}, Fe^{3+} and Fe^{2+}. The findings of this study are consistent with work conducted in other acid sulphate environments, particularly with respect to AMD. Acidity values in AMD environments were found to be equally extreme and the systems were also dominated by SO_4^{2-}, Al^{3+}, Fe^{3+} and Fe^{2+} in solution. In addition to this, there was evidence of common acid sulphate precipitates such as jarosite and jurbanite (Bigham *et al.*, 1992; Bigham *et al.*, 1996a,b; Reddy *et al.*, 1995), as was the case in this study.

Although with careful management it may be possible to ameliorate this site in terms of acidity using limestone, the main concern is the extreme salinity of the environment, and its implications. It is possible that this environment was saline even before the onset of industrial activity and it is thus unlikely that the salinity will be restored to a level that is safe in terms of water quality regulations. It is thus important to consider this land in the context for which it may be used before attempting to place unrealistic objectives on its amelioration. Considerable amounts of solutes will need to be leached from the site before it can be restored to a habitable state, should this be the objective.

There was insufficient time in this study to carry out leaching experiments on the soils. In a brief leaching experiment conducted by Fey and Abanda (1998) on soils from this site limed with cement waste, a unique swelling property of the soil was noted with leaching. To further understand the chemical and physical processes involved in these soils, it may thus be necessary to conduct further leaching experiments and analyses of the leachate.

A time-consuming exercise that may provide instructive results with respect to the acidity of this environment is to conduct a series of liming experiments using a variety of neutralising agents. The experiments may be conducted in a similar fashion to the incubation work of this study, but using reagent grade $CaCO_3$ or NaOH, for example, to produce accurate and repeatable results, and also to provide a maximum benchmark level of treatment against which other neutralising agents can be compared. Since these bases are more soluble than dolomite, the reaction rates are likely to differ considerably. Although the cost of using commercial limestone makes it a more practical proposition, it may be important to determine whether or not the chemical processes controlling this system would differ with the use of other basic neutralising agents. The geochemical benefits of using $CaCO_3$, for example, may out-weigh its cost. It might thus be possible to achieve an optimum state in which the cost of the material used could be weighed up

against its geochemical effect on the environment. In this way, a compromise could be reached in which the best available product could be obtained to ameliorate the site.

An understanding of the chemical and physical processes governing the soil and water at this site must be related to a management strategy for the area to provide efficient and practical means of amelioration allowing for the long-term sustainability of this environment.

6 References

Allison, J.D., Brown, D.S. and Novo-Gradac, K.J. (1990). *MINTEQA2/PRODEFA2, A Geochemical Assessment Model for Environmental Systems: Version 3.0 User's Manual.* Athens, GA: Environmental Research Laboratory, Office of Research and Development, U.S. Environmental Protection Agency. Report No. EPA/600/3-91/021.

Alloway, B.J. (1995). Soil Processes and the Behaviour of Metals. *In B.J. Alloway (ed.) Heavy Metals in Soils.* 2nd edition. Blackie Academic & Professional, Glasgow, UK. p. 11-37.

Ayers, R.S. and Westcot, D.W. (1985). *Water Quality for Agriculture.* Food and Agriculture Organization of the United Nations.

Baas Becking, L.G.M., Kaplan, I.R. and Moore, D. (1960). Limits of the Natural Environment in Terms of pH and Oxidation-Reduction Potential. *J. Geol.* **68**: 243-284.

Ball, J.W. and Nordstrom, D.K. (1991). *User's Manual for WATEQ4F, with Revised Thermodynamic Data Base and Test Cases for Calculating Speciation of Major, Trace and Redox Elements in Natural Waters.* U.S. Geological Survey Open-File Report 91-183.

Bigham, J.M., Schwertmann, U. and Carlson, L. (1992). Mineralogy of Precipitates Formed by the Biogeochemical Oxidation of Fe(II) in Mine Drainage. *In H.C.W. Skinner and R.W. Fitzpatrick (eds.). Biomineralization Processes of Iron and Manganese.* Catena Verlag, Germany. p. 219-232.

Bigham, J.M., Schwertmann, U. and Pfab, G. (1996a). Influence of pH on Mineral Speciation in a Bioreactor Simulating Acid Mine Drainage. *Appl. Geochem.* **11**: 845-849.

Bigham, J.M., Schwertmann, U, Traina, S.J., Winland, R.L. and Wolf, M. (1996b). Schwertmannite and the Chemical Modeling of Iron in Acid Sulfate Waters. *Geochim. Cosmochim. Acta.* **60**: 2111-2121.

Bloomfield, C. (1972). The Oxidation of Iron Sulphides in Soils in Relation to the Formation of Acid Sulphate Soils, and of Ochre Deposits in Field Drains. *Journal of Soil Science* **23**: 1-16.

Blowes, D.W., Reardon, E.J., Jambor, J.L. and Cherry, J.A. (1991). The Formation and Potential Importance of Cemented Layers in Inactive Sulfide Mine Tailings. *Geochim. Cosmochim. Acta.* **55**: 965-978.

Buol, S.W., Hole, F.D., Mc Cracken, R.J. and Southard, R.J. (1997). *Soil Genesis and Classification.* 4th edition. Iowa State University Press, Iowa, USA. pp. 527.

Calmbach, L. (1998). *AQUACHEM v3.7 for Windows 95 98 NT: Aqueous Geochemical Analysis, Plotting and Modelling.* Waterloo Hydrogeologic Inc., Ontario, Canada. pp. 184.

Department of Water Affairs and Forestry. (1996). *Draft of South African Water Quality Guidelines.* 2nd edition. Vol. 1, 3, 4 & 5: Domestic Use, Industrial Use, Agricultural Use, Irrigation.

Dinelli, E., Morandi, N. and Tateo, F. (1998). Fine-Grained Weathering Products in Waste Disposal from two Sulphide Mines in the Northern Apennines, Italy. *Clay Minerals* **33**: 423-433.

Doel, S. (1997). *Effects of Waste Disposal on Soil and Water Chemistry at an Industrial Complex near Somerset West, South Africa.* Unpublished MSc Thesis, University of Cape Town.

Doolittle, J.J. and Hossner, L.R. (1997). Acid-Base Properties of a Limed Pyritic Overburden During Simulated Weathering. *J. Environ. Qual.* **26**: 1655-1662.

Drever, J.I. (1997). *The Geochemistry of Natural Waters: Surface and Groundwater Environments.* 3rd edition. Prentice-Hall, Inc., New Jersey, USA. pp. 436.

Eastell, J. (1986). *A Low Dilution Fusion Technique for the Determination of Major, Minor and Trace Elements in Lamproite and Kimberlite Samples by X-ray Fluorescence Spectrometry.* Unpublished MSc Thesis, University of Cape Town.

Ebbing, D.D. (1987). General Chemistry. 2nd edition. Houghton Mifflin Company, Boston, USA. pp. 979.

Engelbrecht, P.J. (1983). *An Assessment of the Efficiency of Liming Materials in the Amelioration of Acid Soils.* Unpublished MSc Thesis. University of Natal.

Fey, M.V. *Personal Communication.* University of Cape Town.

Fey, M.V. and Abanda, P. (1998). *Determining the Potential of Cement Waste for Remediating the Acidity of a Sulphur-Contaminated Soil.* Unpublished Report, Department of Geological Sciences, University of Cape Town.

Frimmel, H.E.E. *Personal Communication.* University of Cape Town.

Gee, G.W. and Bauder, J.W. (1986). Particle-Size Analysis. *In A. Klute (Ed.). Methods of Soil Analysis: Part 1 - Physical and Mineralogical Methods.* 2nd edition. Am. Soc. Agron., Madison, Wis., USA. p. 383-411.

Goldstein, J.I., Newbury, D.E., Echlin, P., Joy, C.F. and Lifshin, E. (1981). *Scanning Electron Microscopy and X-ray Microanalysis.* Plenum Press, New York, USA. pp. 673.

Hedin, R.S., Watzlaf, G.R. and Nairn, R.W. (1994). Passive Treatment of Acid Mine Drainage with Limestone. *J. Environ. Qual.* **23**: 1338-1345.

Horwitz, W. (Ed.) (1975). *Official Methods of Analysis of the Association of Official Analytical Chemists.* Association of Official Analytical Chemists, Washington DC, USA. pp. 1094.

Kelly, M. (1988). *Mining and the Freshwater Environment.* Elsevier Science Publishers Ltd., Essex, UK. pp. 231.

Leenheer, J.A., McKnight, D.M., Thurman, E.M. and MacCarthy, P. (1994). Structural Components and Proposed Structural Models of Fulvic Acid from the Suwannee River. *In R.C. Averett, J.A. Leenheer, D.M. McKnight and K.A. Thorn (Eds.). Humic*

Substances in the Suwannee River, Georgia: Interactions, Properties, and Proposed Structures. U.S. Geological Survey Water Supply Paper 2373. p. 195-211.

Lindsay, W.L. (1979). *Chemical Equilibria in Soils.* Wiley, New York, USA. pp. 449.

McBride, M.B. (1994). *Environmental Chemistry of Soils.* Oxford University Press, Inc. New York, USA. pp. 406.

McLean, E.O. (1982). Soil pH and Lime Requirement. *In A.L. Page, R.H. Miller and D.R. Keeney (Eds.). Methods of Soil Analysis. Part 2 – Chemical and Microbiological Properties.* 2nd edition. Am. Soc. Agron., Madison, Wis., USA. p. 199-224.

Munsell Soil Color Charts. (1992). Macbeth Color, New York, USA.

Murray, K. and Wade, P. (1996). Checking Anion and Cation Charge Balance of Water Quality Analyses: Limitations of the Traditional Method for Non-Potable Waters. *Water SA* **22**: 27-32.

Nordstrom, D.K. (1982). The Effect of Sulphate on Aluminium Concentrations in Natural Waters: Some Stability Relations in the System Al_2O_3-SO_3-H_2O at 298 K. *Geochim. Cosmochim. Acta.* **46**: 681-692.

Novich, B.E. and Martin, R.T. (1983). Solvation Methods for Expandable Layers. *Clays and Clay Minerals* **31**: 235-238.

Nowicki, T.E. (1997). *The Impact of Plantations of 'Pinus spp' on the Chemical Properties of Soils and Stream Waters in South African Upland Catchments.* Unpublished PhD Thesis. University of Cape Town.

Oades, J.M. (1989). An Introduction to Organic Matter in Mineral Soils. *In J.B. Dixon and S.B. Weed (Eds.). Minerals in Soil Environments.* 2nd edition. SSSA, Madison, Wis., USA. p. 89-159.

Parkhurst, D.L. (1995). *User's Guide to PHREEQC – A Computer Program for Speciation, Reaction Path, Advective-Transport, and Inverse Geochemical Calculations.* Water-Resources Investigations Report 95-4227. U.S. Geological Survey, Lakewood, Colorado, USA.

Pierzynski, G.M., Sims, J.T. and Vance, G.F. (1994). *Soils and Environmental Quality.* Lewis Publishers, Florida, USA. pp. 313.

Plummer, L.N., Parkhurst, D.L., Fleming, G.W. and Dunkle, S.A. (1988). *A Computer Program Incorporating Pitzer's Equations for Calculation of Geochemical Reactions in Brines.* Water-Resources Investigations Report 88-4153. U.S. Geological Survey, Virginia, USA.

Reddy, K.J., Wang, L. and Gloss, S.P. (1995). Potential Solid Phases Controlling Dissolved Aluminium and Iron Concentrations in Acidic Soils. *In R.A. Date, N.J. Grundon, G.E. Rayment and M.E. Probert (Eds.). Plant Soil Interactions at Low pH.* Kluwer Academic Publishers, Netherlands. p. 35-40.

Rhoades, J.D. (1982). Soluble Salts. *In A.L. Page, R.H. Miller and D.R. Keeney (Eds.). Methods of Soil Analysis. Part 2 – Chemical and Microbiological Properties.* Am. Soc. Agron. Madison, Wis., USA. p. 167-171.

Rose, S. and Elliot, W.C. (2000). The Effects of pH Regulation Upon the Release of Sulphate from Ferric Precipitates Formed in Acid Mine Drainage. *Appl. Geochem.* **15**: 27-34.

Rowell, D.L. (1994). *Soil Science: Methods and Applications.* Longman Group Ltd., UK. pp. 350.

Schwertmann, U. and Taylor, R.M. (1989). Iron Oxides. *In J.B. Dixon and S.B. Weed (Eds.). Minerals in Soil Environments.* 2nd edition. SSSA, Madison, Wis., USA. p. 379-438.

Shelp, G.S., Chesworth, W. and Spiers, G. (1995). The Amelioration of Acid Mine Drainage by an *in situ* Electrochemical Method; Part 1: Employing Scrap Iron as the Sacrificial Anode. *Appl. Geochem.* **10**: 705-713.

Shelp, G.S., Chesworth, W. and Spiers, G. (1996). The Amelioration of Acid Mine Drainage by an *in situ* Electrochemical Method; Part 2: Employing Aluminium and Zinc as Sacrificial Anodes. *Appl. Geochem.* **11**: 425-432.

Simpson, A.C. and Morris, R.D. (1996). Soil and Water Quality Investigation at the AECI Sulphur Stockpile, Somerset West. *In Environmental Evaluation Unit. Environmental Study on the Effects of the Sulphur Stockpile Fire at AECI, Somerset West on 16 17 December 1995. Report 159.* University of Cape Town.

Singer, P.C. and Stumm, W. (1970). Acidic Mine Drainage: The Rate-Determining Step. *Science.* **167**: 1121-1123.

Sloan, J.J. and Basta, N.T. (1995). Remediation of Acid Soils by Using Alkaline Biosolids. *J. Environ. Qual.* **24**: 1097-1103.

Standard Methods. (1995). *Standard Methods for the Examination of Water and Wastewater. A.D. Eaton, L.S. Clesceri and A.E. Greenberg (Eds.).* 19th edition. Am. Public Health Assoc., Washington D.C., USA.

Terelak, H., Motowicka-Terelak, T. and Stuczynski, T. (1996). Direct and Residual Effects of Sulphur Pollution on the Acidity of a Loamy Soil. *Appl. Geochem.* **11**: 371-373.

Thomas, G.W. and Hargrove, W.L. (1984). The Chemistry of Soil Acidity. *In F. Adams (Ed.). Soil Acidity and Liming.* 2nd edition. Agronomy No. 12, SSSA, Madison, Wisconsin, USA. p. 3-56.

Tisdale, S.L., Nelson, W.L. and Beaton, J.D. (1985). *Soil Fertility and Fertilizers.* 4th edition. Collier Macmillan International, New York, USA. pp. 754.

Trusler, G.E., Edwards, R.I. and Buckley, C.A. (1991). Sulphate, Calcium and Heavy Metal Removal from Industrial Effluents Using Barium Carbonate. *Water SA.* **17**: 167-172.

Weast, R.C. (Ed.). (1969). *Handbook of Chemistry and Physics.* 50th edition. Chemical Rubber Company, Ohio, USA.

Willis, J.P. (1999). *Instrumental Parameters and Data Quality for Routine Major and Trace Element Determinations by WDXRFS.* Information Circular, Department of Geological Sciences, University of Cape Town.

World Health Organisation. (1984). *Guidelines for Drinking Water Quality.* Vol. 1. Recommendations. pp. 130.

Ziemkiewicz, P.F., Skousen, J.G., Brant, D.L., Sterner, P.L. and Lovett, R.J. (1997). Acid Mine Drainage Treatment with Armoured Limestone in Open Limestone Channels. *J. Environ. Qual.* **26**: 1017-1024.

Appendix A: Soil profile and water descriptions

A.1 Soil profile descriptions

The locations of all the soil profiles described below can be found in Figure 9A. The soil colour in each case is based on dry soil (<2 mm fraction) using the soil colour charts of Munsell (1992). The colours noted under the description of each horizon relate to the *in situ* colour of the soil at the site. Soil profiles have been described 'downprofile' in each case. The underlying bedrock at the site is Malmesbury shale and the depth to the water table is often less than 1m in the rainy season. This was evident in soil profiles C, E and F, in which the pits contained water.

Soil profile A (location AA):

Sample ID	Depth (mm)	Description	Soil colour
A1	0-70	Ash-rich; dark brown to grey; sandy loam; porous; friable	5Y 6/1 (grey)
A2	70-300	Pale brown; blocky; loamy sand; firm but not cemented	2.5Y 6/2 (light brownish grey)
A3	300-400	Yellowish with orange precipitate; sand; cemented; granular	5Y 7/3 (pale yellow)
A4	400-700	Olive greenish brown; sand; slickensides; firm	5Y 7/4 (pale yellow)

Soil profile B (location AB):

Sample ID	Depth (mm)	Description	Soil Colour
B1	0-60	Ash-rich; brownish grey; sandy loam; porous; friable	5Y 5/1 (grey)
B2	60-300	Dark brown (top), light brown (bottom); loamy sand; streaky; poorly sorted;	5Y 4/1 (dark grey)
B3	300-440	Olive grey; sandy loam; friable; gravel-rich	5Y 5/2 (olive grey)
B4	440-550	Light greenish yellow; sand; cemented	5Y 7/2 (light grey)
B5	550-750	Pale yellow; loamy sand; friable	5Y 7/3 (pale yellow)

Soil profile C (location AC):

Sample ID	Depth (mm)	Description	Soil colour
C1	0-130	Reddish brown; loamy sand; firm; gravel and pebble-rich; visible sulphur	10YR 6/3 (pale brown)
C2	130-470	Dark greyish brown; loamy sand; firm; structured; Fe grains	5Y 5/3 (olive)
C3	470-800	Greenish grey; sand; granular; cemented	5Y 7/4 (pale yellow)
C4	800-1200	Greenish grey; sandy clay loam; occ. grit; slightly mottled	5Y 7/2 (light grey)

Soil profile E (location AE):

Sample ID	Depth (mm)	Description	Soil colour
E1	0-160	Dark brown; loamy sand; coarse; structured; hard	10YR 4/1 (dark grey)
E2	160-420	Pale greenish yellow; sand; cemented	5Y 7/2 (light grey)
E3	420-650	Pale creamy yellow; sandy clay loam; black mottles	5Y 7/4 (pale yellow)

Soil profile F (location AF):

Sample ID	Depth (mm)	Description	Soil colour
F1	0-100	Brownish grey; sand; slightly friable	5Y 5/1 (grey)
F2	10-310	Pale grey; sand; cemented	5Y 7/2 (light grey)
F3	310-450	Pale yellow; loamy sand; below water table	5Y 7/2 (light grey)

Composite and test pit sample descriptions

Sample ID	Description	Soil texture	Soil colour
TSC	Topsoil composite (made up of soil horizons A2, B2, B3, C1, C2, E1, F1)	Sand	2.5Y 5/3 (light olive brown)
SSC	Subsoil composite (made up of soil horizons A4, B5, C4, E3, F3)	Sandy loam	5Y 7/3 (pale yellow)
TPT	Test pit topsoil	Sand	2.5Y 4/1 (dark grey)
TPS	Test pit subsoil	Sandy clay	5Y 6/2 (light olive grey)

A2. Water descriptions

Table A1. Character of all surface and groundwater samples.

Sample location	Sample ID	pH	EC (mS/cm)	Colour	Clarity	Aquatic character
AC	AWC	3.4	22.0	clear	clear	no sign of life
AD	AWD	2.2	23.0	red-brown	clear	no sign of life
AF	AWF	1.8	40.0	red-brown	clear	no sign of life
AG	AWG	2.3	24.4	red-brown	clear	no sign of life
AH	AWH	7.3	2.4	clear	clear	abundant aquatic flora and invertibrate fauna
LA	LWA	6.5	2.6	clear	clear	no sign of life
LB	LWB	3.9	33.0	red-brown	clear	no sign of life
LC	LWC	3.0	33.4	red-brown	clear	no sign of life
LD	LWD	6.9	2.4	clear	clear	signs of algae
LE	LWE	1.7	66.8	red-brown	clear	no sign of life
LF	LWF	3.1	na	pale yellow	clear	signs of algae
LG	LWG	2.3	na	red-brown	murky	no sign of life
LH	LWH	2.0	na	red-brown	murky	no sign of life
LI	LWI	2.2	na	red-brown	murky	no sign of life
SDP1	SDP1	3.6	45.6	pale yellow	murky	no sign of life
SDP2	SDP2	3.9	179	yellow	murky	no sign of life

na = not analysed

Appendix B. Analytical methods

B.1 Water and soil solution methods

B.1.1 pH measurement

The pH of all water samples and soil solutions was measured with a *Metrohm 691* pH meter comprising a 3 M KCl combined indicator and reference electrode. The pH meter was calibrated before use with pH 4 and 7 buffer solutions. Duplicate measurements were taken at room temperature to evaluate the accuracy of the instrument. The analytical precision of the instrument can be seen from the results in Table A1.

Table B1. Duplicate pH measurements for the soil horizon samples.

Sample	pH (1)	pH (2)	Mean	Std. Dev.	Std. Error (%)
A1	1.57	1.55	1.56	0.014	0.9
A2	2.20	2.18	2.19	0.014	0.7
A3	3.64	3.62	3.63	0.014	0.4
A4	3.08	3.04	3.06	0.028	0.9
B1	1.26	1.23	1.25	0.021	1.7
B2	1.80	1.78	1.79	0.014	0.8
B3	2.84	2.83	2.84	0.007	0.3
B4	2.77	2.71	2.74	0.042	1.6
B5	2.38	2.29	2.34	0.064	2.7
C1	1.52	1.46	1.49	0.042	2.9
C2	2.55	2.53	2.54	0.014	0.6
C3	3.00	2.98	2.99	0.014	0.5
C4	3.30	3.16	3.23	0.099	3.1
E1	2.62	2.53	2.58	0.064	2.5
E2	3.30	3.20	3.25	0.071	2.2
E3	3.60	3.59	3.60	0.007	0.2
F1	1.72	1.72	1.72	0.000	0.0
F2	2.17	2.15	2.16	0.014	0.7
F3	3.13	3.05	3.09	0.057	1.8

B.1.2 Electrical conductivity (EC)

The electrical conductivity of all the water and soil solution samples was measured with a *Crison microCM 2201* conductivity meter. The meter is fitted with a conductivity cell and a temperature probe to provide automatic temperature compensation. A 0.01 M KCl solution was used as an EC standard for calibration. The expected EC of this standard is 1412 µS/cm at 25°C. Before any measurements were made, the conductivity probe was tested in the standard solution and it was found to have an EC of 1414 µS/cm at 28°C. Duplicate analyses for selected water samples are presented in Table A2 below, demonstrating the accuracy of the instrument.

Table B2. Duplicate EC analyses for selected water samples.

Sample	EC (1)	EC (2)	Mean	Std. Dev.	Std. Error (%)
AWC	21.3	23.0	22.2	1.20	5.4
AWD	23.0	28.2	25.6	3.68	14.4
AWF	40.0	41.3	40.7	0.92	2.3
AWG	24.4	24.3	24.4	0.07	0.3

NOTE. EC values in mS/cm

B.1.3 Alkalinity

Alkalinity was measured by potentiometric titration to a preselected pH of 4.5, using a *Radiometer ABU 80* Autoburette and a *TTT 85* titrator fitted with a *PHG201* glass electrode and a *REF401* calomel reference electrode. A known aliquot (5 ml) of each sample was titrated against 0.01 M HCl to an endpoint of pH 4.5 and the alkalinity was then calculated in mg/L $CaCO_3$ using the following equation from Standard Methods (1995):

Alkalinity = (vol. HCl added x normality of acid x 50000) / vol. of sample

Since the samples from this study on which alkalinity was determined, were between pH 6 and 8, the alkalinity was in the form of HCO_3^- (Drever, 1997), using the following conversion:

HCO_3^- (mg/L) = $CaCO_3$ (mg/L) x 0.61

where mol. weight HCO_3^- / mol. weight $CaCO_3$
= 61.02 / 100.01
= 0.61

B.1.4 Exchangeable acidity

Exchangeable acidity was determined on all soil samples using the KCl extractable acidity method. This method employs a simple extraction with unbuffered salt solution (M KCl in this case) and is followed by titration of an aliquot of the extract with a base (0.01 M NaOH) to estimate the amount of exchangeable acid cations in solution.

Method:

2.5 g of air-dried, sieved soil (<2 mm) was placed in a centrifuge tube with 25 ml M KCl and the mixture was shaken for 4 minutes on a reciprocal shaker. The solution was then centrifuged to settle out the soil and a 10 ml aliquot was extracted for titration with 0.01M NaOH to an end point of pH 8.3. Exchangeable acidity is then calculated as follows:

$$c_A v_A = c_B v_B$$

where c_A = concentration of acid (mol/L)
v_A = volume of acid (ml)
c_B = concentration of base (mol/L)
v_B = volume of base (ml)

Eg. Soil sample A1:

$c_B = 0.01$ M
$v_B = 75.74$ ml (amount of base titrated into sample to pH 8.3)
$v_A = 10$ ml (amount of sample used)

$\therefore c_A = 0.076$ M

Converting to mol/kg:

2.5 g of soil in 25 ml M KCl solution

i.e. Acidity = 0.076 M x 0.025 L / 0.0025 kg
= 0.757 mol/kg
= 757 mmol/kg

A further 10 ml aliquot of the extract is then taken for determination of exchangeable Ca and Mg, which are generally representative of the exchangeable basicity of the solution at low and intermediate pH values. The acid saturation of the sample can then be determined by the following formula:

Acid saturation (%) = 100 x Acidity / (Acidity + Ca + Mg)

where Acidity, Ca and Mg are expressed as $mmol_c/kg$

B.1.5 Ion analysis by High Performance Ion Chromatography (HPIC)

The major ions in solution (Na^+, K^+, NH_4^+, Ca^{2+}, Mg^{2+}, Cl^-, F^-, NO_3^-, NO_2^-, PO_4^{3-} and SO_4^{2-}) were determined for all water samples and soil saturated paste extracts by High Performance Ion Chromatography (HPIC). Solutions were first filtered through a 0.45 µm membrane filter and diluted to within the operating range of the instrument (<100 µS/cm) before being filtered again with *Dionex On-Guard P* filters to remove organics. Analyses were carried out using a *Dionex DX300* series suppressed IC system with a conductivity detector. The system is operated by AI-450 chromatography software and the analytical parameters of the instruments are given in Table B3 below.

Table B3. Analytical parameters of the *Dionex* HPIC system.

	Anions	**Cations**
Guard column	HPIC-AG4A	CG12A
Separator column	HPIC-AS4A	CS12A
Eluent	1.8 mM Na_2CO_3; 1.7 mM $NaHCO_3$	11 mM H_2SO_4
Flow rate	2 ml / minute	1 ml / minute
Suppressor	AMMS	CSRS-I
Run time	8 minutes	15 minutes

The precision of the HPIC was tested by randomly running duplicate samples through the equipment in addition to running a series of standards at the beginning of each session with the instrument. Duplicate analyses are presented in Table B4 below to provide a rough indication of the precision of this analytical technique. Only the ions with detectable concentrations are presented in Table B4.

Table B4. Duplicate HPIC analyses for selected soil solution samples.

	Na^+	K^+	NH_4^+	Ca^{2+}	Mg^{2+}	F^-	Cl^-	SO_4^{2-}
SS1 (1)	1046	22	0	570	938	2.8	284	7762
SS1 (2)	1048	20	0	602	940	2.6	286	7711
Mean	**1047**	**21**	**0**	**586**	**939**	**2.7**	**285**	**7737**
Std. Dev.	**1.41**	**1.41**	**0.0**	**22.63**	**1.41**	**0.14**	**1.41**	**36.06**
Std. Error (%)	**0.1**	**6.7**	**0.0**	**3.9**	**0.2**	**5.2**	**0.5**	**0.5**
TS3 (1)	356	14	14	506	3002	0.0	123	18701
TS3 (2)	352	12	12	522	3000	0.6	128	18668
Mean	**354**	**13**	**13**	**514**	**3001**	**0.3**	**126**	**18685**
Std. Dev.	**2.83**	**1.41**	**1.41**	**11.31**	**1.41**	**0.42**	**3.54**	**23.33**
Std. Error (%)	**0.8**	**10.8**	**10.8**	**2.2**	**0.05**	**140**	**2.8**	**0.1**
TL0 (1)	744	144	48	1976	1744	80.0	154	51784
TL0 (2)	560	32	56	816	2600	81.6	154	55017
Mean	**652**	**88**	**52**	**1396**	**2172**	**80.8**	**154**	**53401**
Std. Dev.	**130.11**	**79.20**	**5.66**	**820.24**	**605.28**	**1.13**	**0.0**	**2286.08**
Std. Error (%)	**20.0**	**90.0**	**10.9**	**58.8**	**27.9**	**1.4**	**0.0**	**4.3**
SL1 (1)	990	22	14	476	860	4.0	254	8272
SL1 (2)	1084	26	12	610	1004	0.8	199	7204
Mean	**1037**	**24**	**13**	**543**	**932**	**2.4**	**227**	**7738**
Std. Dev.	**66.47**	**2.83**	**1.41**	**94.75**	**101.82**	**2.26**	**38.89**	**755.19**
Std. Error (%)	**6.4**	**11.8**	**10.8**	**17.4**	**10.9**	**94.2**	**17.1**	**9.8**

NOTE: all ion concentrations in mg/L

Another means of testing the accuracy of the measurement of ions in solution is to plot anions and cations as a function of EC. A plot of this nature is presented in Figure B1 showing linear trend in the data suggesting accuracy of measurement.

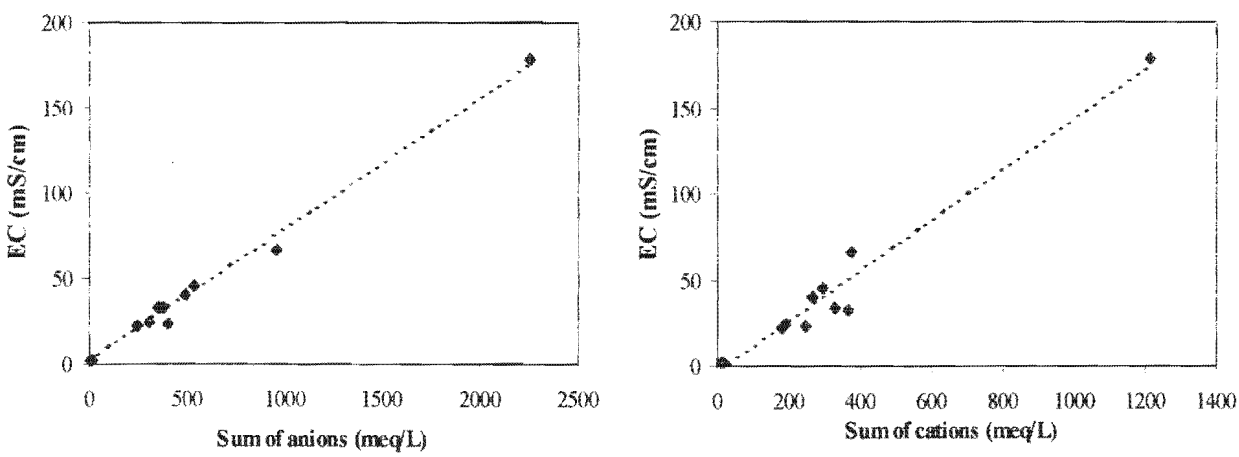

Figure B1. EC of all water samples as a function of the sum of anions and cations, respectively.

B.1.6 Trace metal analysis by Inductively Coupled Plasma Mass Spectrometry (ICP-MS)

An *Elan 6000* ICP-MS was used for multi-element analysis of all water and soil solution samples, with particular emphasis on the heavier elements on the periodic table. All samples analysed by ICP-MS were first filtered through a 0.45 µm membrane filter and acidified with 50% HNO_3 to prevent metals precipitating from solution. All samples were then diluted appropriately to within the range of the ICP-MS (~1% TDS) using 2% HNO_3 before being run. Each sample was also treated with 50 µL of an internal standard Rh solution (3 mg/L Rh) before being analysed. The main function of this is in the calibration of the instrument and to correct for drift.

Two NIST water standards were analysed at the start of the session to test the accuracy of the technique, the results of which are presented in Table B5. Duplicate analyses were also performed on selected soil solutions and water samples and these results are presented in Table B6 showing relatively measurements for most elements.

Table B5. ICP-MS analyses of NIST water standards compared with published results.

	NIST-1640	Published	+/-	NIST-1643d	Published	+/-
Al		52	1.5	140.0	127.6	3.5
Si		4730	120	2644	2700	
Cr	34.7	38.6	1.6	18.4	18.53	0.2
Fe	63.9	34.3	1.6	174	91.2	3.9
Mn	121	121.5	1.1	39.0	37.66	0.83
Ni	29.2	27.4	0.8	59.9	58.1	2.7
Cu	89.7	85.2	1.2	27.2	20.5	3.8
Zn	66.4	53.2	1.1	78.7	72.48	0.65
As	26.4	26.7	0.41	56.5	56.02	0.73
Se	21.3	22.0	0.51	11.4	11.43	0.17
Cd	23	22.8	0.96	6.59	6.47	0.37
Tl	0.06			6.34	7.28	0.25
Pb		27.9	0.14	16.8	18.15	0.64

NOTE: all results in µg/L

Table B6. ICP-MS duplicate results for soil solution (TS0) and water samples (LWE).

	TS0 (1)	TS0 (2)	Mean	Std. Dev.	Std. Err. (%)	LWE (1)	LWE (2)	Mean	Std. Dev.	Std. Err. (%)
Li	5.7	5.9	5.8	0.18	3.1	1.5	1.4	1.4	0.05	3.6
Al	4799	4800	4799	0.09	0.0	1364	1374	1369	7.26	0.5
Si	31.8	28.8	30.3	2.13	7.0	32.2	33.0	32.6	0.54	1.7
Cr	4.8	5.7	5.3	0.62	11.7	2.4	2.5	2.5	0.05	2.0
Mn	29.7	30.0	29.9	0.25	0.8	14.6	14.6	14.6	0.01	0.0
Fe	1819	1856	1837	25.56	1.4	1166	1249	1208	58.98	4.9
Ni	3.9	4.0	3.9	0.13	3.3	1.0	1.0	1.0	0.01	0.0
Cu	7.2	7.5	7.3	0.18	2.5	3.2	3.4	3.3	0.12	3.6
Zn	21.0	21.1	21.0	0.10	0.5	5.7	5.9	5.8	0.09	1.6
As	1.0	1.0	1.0	0.07	7.0	0.9	0.9	0.9	0.02	0.0
Se	0.0	0.6	0.3	0.45	150	0.0	0.0	0.0	0.00	0.0
Rb	0.2	0.3	0.3	0.02	6.7	0.3	0.3	0.3	0.01	0.0
Sr	6.8	6.9	6.8	0.06	0.9	2.1	2.1	2.1	0.06	2.9
Mo	0.1	0.1	0.1	0.02	0.2	0.0	0.0	0.0	0.00	0.0
Cd	0.1	0.1	0.1	0.00	0.0	0.0	0.0	0.0	0.00	0.0
Cs	0.0	0.0	0.0	0.01	0.0	0.0	0.0	0.0	0.00	0.0
Ba	0.7	0.9	0.8	0.10	12.5	0.0	0.0	0.0	0.00	0.0
Pb	0.4	0.6	0.5	0.10	20.0	0.4	0.4	0.4	0.01	0.0
U	0.3	0.3	0.3	0.00	0.0	0.1	0.1	0.1	0.00	0.0

NOTE: all results in mg/L

B.1.7 Iron colorimetry

The concentration of total and ferrous Fe in solution was measured for selected water samples using the Phenanthroline method as documented in method 3500-Fe D of Standard Methods (1995). A Sequoia-Turner model 340 spectrophotometer was used to measure the light absorbance with the wavelength set at 510 nm. The reagents and the method for the experiment precisely follows method 3500-Fe D mentioned above. Samples selected for Fe determination were filtered in the field through a 0.45 µm membrane filter before being preserved using concentrated HCl to prevent oxidation of Fe^{2+} in solution. A ratio of 2 ml HCl / 100 ml sample was used for preservation.

It is important to note that the method is only valid for Fe ~~concentrations up~~ to ~~200 µg due~~ to limits in the range of colour that can be determined by the spectrophotometer. The concentration of Fe in solution must thus be estimated before the method can be used. This can be done by trial and error or by analysing the samples with another analytical first and then adjusting the

concentrations of Fe by dilution if necessary. Certain samples from this study were thus analysed by FAAS before attempting Fe colorimetry. This also serves as a comparison of the relative accuracy of each technique, as can be seen in Table B7. A set of samples with known concentrations of Fe were analysed to obtain a calibration curve, which was then used to determine the concentration of Fe in all other samples. The calibration curve is presented in Figure B2 together with the equation of the trend line, which was used to estimate the Fe concentration of the samples.

Table B7. A comparison of the total soluble Fe concentrations of selected samples.

Sample	Fe (mg/L) Colorimetry	Fe (mg/L) FAAS	Mean	Std. Dev.	Std. Error (%)
TL0	1564	1485	1525	55.86	3.7
LWF	121.2	130.3	125.8	6.43	5.1
LWH	573.8	628.1	601.0	38.40	6.4

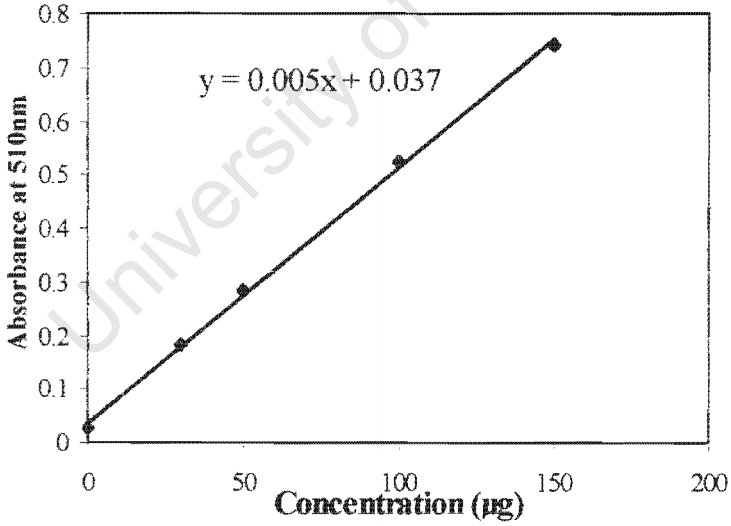

Figure B2. Fe calibration curve used for calculating the concentration of ferrous and total Fe in solution.

B.2 Soil analysis

B.2.1 Soil composition by X-ray Fluorescence Spectrometry (XRFS)

The major elements, Fe, Mn, Ti, Ca, K, S, P, Si, Al, Mg and Na were determined using fusion discs prepared with LiT-LiM flux in the proportion 57:43 ($igma Chemicals) and LiBr as a releasing agent. The discs are analysed on a Philips PW1480 wavelength dispersive XRF spectrometer with a dual target Mo/Sc X-ray tube. All measurements are made with the tube at 50kV and 50mA (Willis, 1999). The analytical conditions are given in Table B8.

Fusion discs made up with 100% Johnson Matthey Specpure SiO_2 are used as blanks for all elements except Si. Fusion discs made up from mixtures of Johnson Matthey Specpure Fe_2O_3 and $CaCO_3$ are used as blanks for Si. Intensity data are collected using the Philips X40 software. The software corrects peaks for background as well as performing spectral overlap and matrix corrections.

Table B8. Analytical conditions for determination of major elements using a Philips PW1480 WDXRF spectrometer (after Willis, 1999).

Element /line	Collimator	Crystal	Detector	PHS LWL	PHS UPL	Counting time (s)	Concentration range **	RMS	Lower limits of determination*	No. of standards
NiKα	F	LiF(220)	FS	22	70	100	0 - 0.48	0.003	0.004	11
FeKα	F	LiF(220)	FL	16	68	100	0 - 17	0.069	0.019	20
MnKα	F	LiF(220)	FL	15	66	100	0 - 0.27	0.004	0.014	22
CrKα	F	LiF(220)	FL	14	70	100	0 - 3.5	0.011	0.008	11
TiKα	F	LiF(200)	FL	32	68	100	0 - 3.9	0.022	0.023	22
CaKα	F	LiF(200)	FL	30	76	50	0 - 77	0.102	0.004	21
KKα	F	LiF(200)	FL	32	74	100	0 - 15.5	0.037	0.003	21
SKα	C	GE(111)	FL	32	74	100	0 - 53.5	0.112	0.100	11
PKα	C	GE(111)	FL	34	74	100	0 - 3.4	0.011	0.008	16
SiKα	C	PE(002)	FL	26	80	100	0 - 100	0.215	0.052	20
AlKα	C	PE(002)	FL	26	80	100	0 - 100	0.084	0.074	21
MgKα	F	PX-1	FL	36	68	100	0 - 85	0.141	0.102	20
NaKα	F	PX-1	FL	30	78	100	0 - 9.1	0.065	0.17	12

** all concentrations expressed as wt% oxide; S as SO_3

* = 10 × lower limit of detection, expressed as wt% oxide

$$RMS = \sqrt{\frac{1}{n-k}\sum\left(Conc_{given} - Conc_{calc}\right)}$$

where

n = no. of standards

k = no. of calibration coefficients, *i.e.* 2, the slope and intercept of the calibration line.

$Conc_{given}$ = recommended concentration for an element in a standard

$Conc_{calc}$ = concentration of an element calculated from the best-fit calibration line

Because the samples from this study contained S, it was necessary to convert all the S to SO_4 before roasting, since S can damage the platinum crucibles that are used in the roasting process. The samples are thus treated with $LiNO_3$ to oxidise the S (Eastell, 1986).

Procedure:

- make up a 20% $LiNO_3$ solution (i.e. 0.2g $LiNO_3$/ml)
- add 2ml of the $LiNO_3$ solution to 2.00g of untreated sample in a porcelain crucible
- heat the crucible to 110°C for 2 hours to evaporate all the H_2O
- transfer to furnace and heat at 450°C for 16 hours
- weight material into platinum crucible and roast at 950°C as for other XRF samples
- retain a separate portion of the sample, weigh accurately and dry at 110°C to determine the H_2O content

Calculations:

$LiNO_3$ oxidises to Li_2O by the reaction (Eastell, 1986):

$$2LiNO_3 = Li_2O + 2NO + {}^3/_2O_2$$

The final oxidised sample thus needs to be corrected for dilution by Li_2O. The amount of Li_2O added is calculated as:

$$29.887 gmol^{-1}\ Li_2O / 137.886 gmol^{-1}\ 2LiNO_3 = 0.21668 \text{ of } 0.4g\ LiNO_3 = 0.08667g\ Li_2O$$

i.e. a dilution of

$$(0.08667g / x\ g) \times 100\ (\%)$$

of the original sample, where x is the original sample mass. The final concentrations of the major elements in the oxidised samples (including LOI) therefore need to be corrected for dilution by multiplying each value by a correction factor of:

$$x\ g / (x\ g - 0.08667g)$$

In order to estimate the proportions of S to SO_4 in the samples from this study, a calibration curve was set up using various proportions of elemental S and $CaSO_4 \cdot 2H_2O$. The S1 and S2 peak heights (corrected for background) of these calibration samples were measured to obtain ratios of S1 to S2. The proportions of S to SO_4 in the calibration samples were then plotted as a function of the S1/S2 ratios to obtain the calibration curve shown in Figure B3.

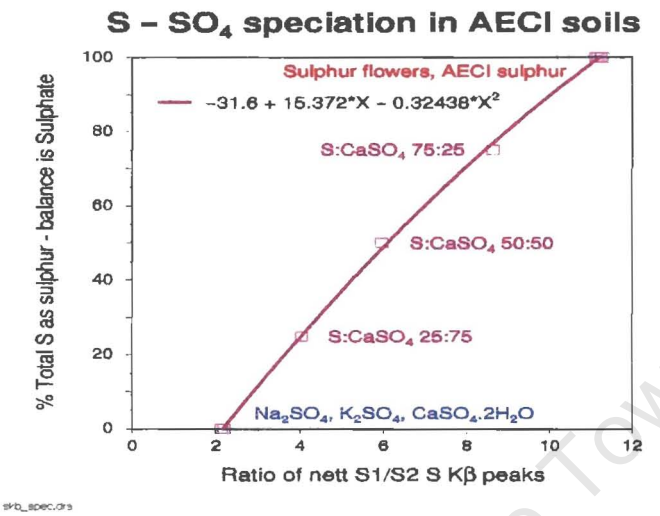

Figure B3. Calibration curve for S speciation using various proportions of S to SO_4.

Powder briquettes of the samples from this study were then made, and the K_β peak heights for S and SO_4 were determined to obtain a S1/S2 ratio for each sample (Figure B4). Using the calibration curve, the percentage of S can then be obtained. The results of these analyses are presented in Table B9.

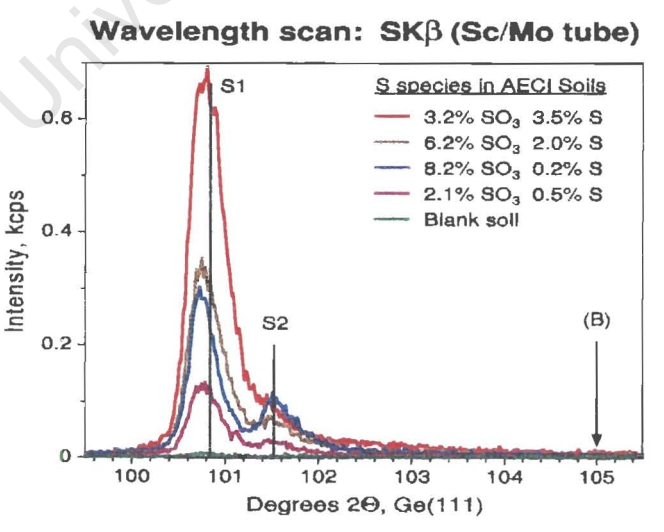

Figure B4. Sulphur K_β peaks for WDXRFS powder briquette soil samples from this study.

Table B9. Sulphur speciation determined by WDXRFS for selected soil samples.

Sample	Actual % SO_3	Actual % S	S1	S2	S1/S2	% S *	% SO_4 **	% SO_3 #	S (as SO_3)
A1	8.2	0.2	0.2140	0.0821	2.607	6.3	93.7	8.72	0.5
B1	6.2	2.0	0.3143	0.0554	5.673	45.2	54.8	11.31	5.1
C1	3.2	3.5	0.6080	0.0737	8.250	73.2	26.8	11.96	8.8
TSC	2.1	0.5	0.1108	0.0223	4.969	36.8	63.2	3.33	1.2
Sulphur	-0.7	100.3	8.8819	0.7907	11.233	100.3	-0.3	250	250.7
$CaSO_4 \cdot 2H_2O$	99.6	0.1	1.2858	0.5899	2.180	0.4	99.6	100	0.4

* read off calibration curve
** calculated as (100 - S%)
\# as determined on fusion discs

B.2.2 Mineralogical characterisation by X-ray Diffractometry (XRD)

An abbreviated clay dispersion technique was used to separate out the clay fraction for determination by XRD. The procedure is as follows:

- place 50-100g of air-dried sub-2mm soil in a 250ml plastic bottle and add distilled water to form a slurry
- add 1M NaOH drop-wise, shaking intermittently, until the pH is stabilised at ~9
- place the bottle on a shaker for 3-4 hours
- transfer the contents to a 3L jar and fill with pH 10 Na_2CO_3 solution
- stir, cover and allow to stand for 16 hours at 22°C
- siphon off supernatant suspension to a depth of 18cm (following Stokes Law of sedimentation)
- repeat this procedure with pH 10 Na_2CO_3, accumulating the decantate in a bucket
- add 1M HCl to the bucket to restore the pH to between 5 and 7
- add NaCl, if necessary, to promote flocculation
- siphon off and discard the clear supernatant
- transfer the clay concentrate from the bucket to a number of centrifuge tubes and finally to a single centrifuge tube concentrating the clay by centrifugation
- transfer the concentrated clay to a section of dialysis tubing and dialyse overnight in running tap water and then in de-ionised water for two days
- check that the bathing water is free of Cl^- by adding a few drops of silver nitrate indicator (a white precipitate indicates Cl^-) to a small aliquot of the water
- discontinue washing when the clay is free from Cl^-
- transfer the clay suspension to a storage bottle and pipette 5ml of the suspension into a weighed porcelain crucible
- dry the sample at 110°C and determine the amount of clay in suspension (i.e. mg clay/ml)
- adjust the suspension concentration to ~20mg/ml, withdraw a 2ml aliquot, transfer it onto a glass slide and allow to dry for XRD analysis

B.2.3 Soil solution analysis by saturated paste extraction

To determine the chemistry of the soil solution, the standard procedure is to make up a saturated paste of soil, allow it to equilibrate and suck out a portion of the solution for further analysis. The procedure is as follows:

Preparation of saturated paste:

- measure out a sample of air-dried sub-2mm soil (~300-400g)
- moisten with de-ionised water and mix with a spatula
- consolidate the mixture by tapping on a work bench
- continue adding de-ionised water until the sample has the properties of a saturated paste
- after an hour, check that the sample still has the properties of a saturated paste
- cover and leave overnight to equilibrate

Properties of saturated paste:

- all the soil pores are filled with water
- the surface is shiny; the paste flows slightly when the container is tilted; free water does not collect when a small trench is drawn on the surface with a spatula; the soil does not cling to the spatula (clayey soils are an exception)

Saturated paste extraction:

- place a sheet of Whatman No. 50 filter paper in a Buchner funnel
- fit the Buchner funnel with an Erlenmeyer flask containing a centrifuge tube to collect the extract
- spoon out the equilibrated saturated paste sample onto the filter paper ensuring that there are no gaps at the sides of the funnel
- switch on the apparatus to begin the extraction process
- the extraction may take some time (~1-2 hours) depending on the soil type. To speed up the process, make sure that any cracks that may develop on the surface of the soil and at the sides of the funnel are closed
- remove the extract in the centrifuge tube and proceed with further chemical analyses

NOTE: If the extract is not clear then filter again using standard membrane filters.

B.2.4 Precipitate analysis by Scanning Electron Microscopy with Energy Dispersive X-ray Spectrometer (SEM-EDS)

Precipitate samples are firstly mounted on specially designed stubs using a organic carbon-based glue for adhesion. Samples are then coated with carbon, as opposed to Au or Pd, since carbon allows for EDS determination of elements, which was required in this study. A *Leica Stereoscan 440i* scanning electron microscope (SEM) was used for analysis, and was operated at an accelerating voltage of 20kV with samples maintained under a vacuum of between 10^{-4} and 10^{-6} torr. The SEM is fitted with an energy dispersive X-ray spectrometer (EDS) which was used to obtain spot semi-quantitative chemical analyses of selected specimens. The SEM is housed in the Electron Microscope Unit of the Physics Department at the University of Cape Town.

B3. Limestone analysis

B3.1. Limestone neutralising value

Reagents:

NaOH	0.25 M
HCl	0.5 M

Method:

1 g of finely ground limestone (< 63 μm) was placed in a 250 ml erlenmeyer flask with 50 ml HCl std soln and the mixture was boiled gently for 5 minutes. This was then cooled and the excess acid was titrated with NaOH std soln to an end point of pH 8.3.

Equation:

% $CaCO_3$ equivalence = 2.5(HCl – NaOH/2)

Calculations:

Standardising the HCl:

10 ml HCl was titrated with 8.7 ml NaOH (std)

i.e. 1 M HCl → 0.87 M

Standardising the NaOH:

10 ml HCl was titrated with 9.4 ml NaOH

i.e. $c_A v_A = c_B v_B$
$0.87 \times 10 = c_B \times 9.4$
$c_B = 0.93$

Amount of NaOH titrated into sample and HCl = 43.5 ml

∴ % $CaCO_3$ equivalent $= 2.5\ [\ (50 \times 0.87) - (43.5 \times 0.93)/2\ ]$
$= 58.2\%$

B3.2. Lime requirement of soil

From the equation

$$CaCO_3 + 2H^+ = Ca^{2+} + H_2O + CO_2$$

it can be seen that 1 mole of $CaCO_3$ neutralises 2 moles of acidity

The neutralising capacity of $CaCO_3$ is thus as follows:

1 g of $CaCO_3$ / 100 $gmol^{-1}$ = 0.01 moles of $CaCO_3$

which neutralises 0.01 x 2 moles of acidity

i.e. 0.02 moles = 20 mmol

and since the limestone is only 58.2% as effective, the neutralising capacity of the limestone is

0.58 x 20 = 11.64 mmol

The lime requirement of the soil is then as follows:

Topsoil: 342 $mmol_c kg^{-1}$ / 11.64 mmol = 29.4 g / kg
Subsoil: 136 $mmol_c kg^{-1}$ / 11.64 mmol = 11.7 g / kg

B3.3. Description of limed incubation samples

Topsoil lime requirement: 29.3 g/kg soil
Subsoil lime requirement: 11.6 g/kg soil

300 g of soil used in each case

i.e. topsoil = 29.3 x 0.3 = 8.7 g lime
subsoil = 11.6 x 0.3 = 3.5 g lime

Table B10. Description of limed incubation samples.

Sample ID	Sample description	Lime added (g)
TS0	topsoil short-term – 0 lime	0
TS1	topsoil short-term – ½ lime req.	4.4
TS2	topsoil short-term – 1x lime req.	8.8
TS3	topsoil short-term – 2x lime req.	17.6
TL0	topsoil long-term – 0 lime	0
TL1	topsoil long-term – ½ lime req.	4.4
TL2	topsoil long-term – 1x lime req.	8.8
TL3	topsoil long-term – 2x lime req.	17.6
SS0	subsoil short-term – 0 lime	0
SS1	subsoil short-term – ½ lime req.	4.4
SS2	subsoil short-term – 1x lime req.	8.8
SS3	subsoil short-term – 2x lime req.	17.6
SL0	subsoil long-term – 0 lime	0
SL1	subsoil long-term – ½ lime req.	4.4
SL2	subsoil long-term – 1x lime req.	8.8
SL3	subsoil long-term – 2x lime req.	17.6

Appendix C: Geochemical data

C1. Water data

Table C1. Geochemical data for all surface and groundwater samples.

	AWC	AWD	AWF	AWG	AWH
pH	3.4	2.2	1.8	2.3	7.3
EC (mS/cm)	22.0	23.0	40.0	24.4	2.4
Solutes (mg/L):					
Na	1458	643	591	520	176
K	18.0	15.0	24.0	16.0	10.2
Mg	908	593	759	592	55.2
Ca	386	198	261	344	173
NH_4	nd	10.0	9.0	12.0	nd
F	4.6	30.3	49.2	24.8	0.2
Cl	501	67.8	304	299	236
NO_3	nd	nd	nd	nd	nd
NO_2	nd	nd	nd	nd	nd
SO_4	11100	19400	23000	14500	522
PO_4	nd	nd	nd	nd	nd
Al	146	1363	1389	846	1.3
Fe	124.0	94.3	141.3	91.2	0.7
Mn	5.1	42.5	20.1	37.6	0.1
Si	24.0	nd	22.1	21.6	6.4
Li	0.7	1.7	2.0	1.4	0.01
B	nd	nd	nd	nd	0.1
Cr	nd	nd	1.2	0.4	nd
Ni	0.5	1.9	1.7	1.6	0.01
Cu	1.5	3.5	2.3	2.4	0.2
Zn	2.3	5.3	3.6	2.6	0.2
As	0.01	0.02	0.1	0.03	0.003
Se	0.1	0.1	0.2	nd	0.01
Rb	0.02	0.1	0.1	0.1	0.02
Sr	5.9	1.8	4.0	3.4	1.0
Mo	0.2	0.1	0.1	0.01	0.004
Cd	0.02	0.07	0.05	0.03	0.001
Cs	nd	0.005	0.005	0.01	nd
Ba	0.4	3.0	0.1	0.1	0.1
Pb	0.5	0.6	1.1	0.3	0.1
U	0.01	0.1	0.05	0.04	0.01

Table C1. (cont.)

	LWA	LWB	LWC	LWD	LWE	SDP1	SDP2
pH	6.5	3.3	3.0	6.2	1.7	3.6	3.9
EC (mS/cm)	2.6	33.0	33.4	2.4	66.8	45.6	178.8
Solutes (mg/L):							
Na	90.0	1640	185	251	110	160	3350
K	9.5	60.0	35.0	4.2	40.0	40.0	100
Mg	34.5	1530	2005	28.6	1485	2460	8075
Ca	107	1205	945	55.4	550	450	850
NH_4	nd	nd	20.0	nd	65.0	40.0	175
F	nd	82.0	105	3.2	24.5	45.5	173
Cl	132	625	437	360	79.0	211	443
NO_3	nd	684	nd	nd	nd	nd	nd
NO_2	nd	nd	nd	nd	nd	nd	nd
SO_4	272	16700	16000	219	45800	25300	107000
PO_4	nd	nd	nd	nd	nd	nd	nd
Al	nd	864	905	1.0	1369	413	3107
Fe	0.2	86.5	81.0	0.6	1208	212	9.5
Mn	3.9	141.0	83.5	0.1	14.6	33.4	36.9
Si	na	na	na	na	32.6	12.6	0.9
Li	0.04	4.6	1.6	0.02	1.4	0.8	1.0
B	na	na	na	na	na	na	na
Cr	nd	nd	0.9	nd	2.5	0.2	0.1
Ni	0.04	4.7	1.7	0.01	1.0	1.4	1.2
Cu	0.2	6.1	1.7	0.03	3.3	6.6	0.1
Zn	0.1	5.6	10.6	0.1	5.8	6.5	0.8
As	0.01	0.1	0.03	0.01	0.9	0.01	0.02
Se	nd	nd	nd	nd	0.02	0.02	0.01
Rb	0.01	0.1	0.2	0.004	0.3	0.03	0.01
Sr	0.5	5.9	4.1	0.5	2.1	1.0	0.3
Mo	na	na	na	na	0.01	0.002	0.004
Cd	0.01	0.1	0.1	0.001	0.02	0.05	0.04
Cs	nd	nd	0.005	0.0002	0.04	0.003	0.02
Ba	0.1	2.0	1.5	0.0	0.04	0.03	0.2
Pb	nd	0.2	0.1	0.2	0.4	0.05	0.1
U	nd	0.03	0.02	0.0002	0.1	0.03	0.2

Notes: na = not analysed; nd = not detected

C1.1. Water activities and saturation indices

Table C2. Activities of selected species at p*e* = 4.

	pH	log(Al^{3+})	log (H_4SiO_4)	log (Fe^{2+})	log(K^+)	log(SO_4^{2-})
AWC	3.36	-4.53	-3.49	-3.5	-3.54	-1.64
AWD	2.23	-3.63		-3.66	-3.64	-1.59
AWF	1.82	-3.62	-3.51	-3.5	-3.44	-1.6
AWG	2.31	-3.75	-3.53	-3.63	-3.59	-1.66
AWH	7.32		-4.08	-5.65	-3.65	-2.64
LWA	6.48			-5.6	-3.67	-2.86
LWB	3.33	-3.76		-3.64	-3.03	-1.68
LWC	3.01	-3.68		-3.64	-3.25	-1.74
LWD	6.2			-5.23	-4.02	-2.92
LWE	1.7	-3.93	-3.293	-1.61	-3.27	-1.37
SDP1	3.56	-4.41	-3.74	-3.38	-3.25	-1.44
SDP2	3.89	-3.96	-4.734	-4.8	-2.92	-1.06

Table C3. Saturation indices of selected minerals at p*e* = 4.

	pH	alunite	jurbanite	gypsum	quartz	goethite	jarosite
AWC	3.36	1.13	0.41	0.05	0.5	-1.44	-15.03
AWD	2.23	-2.95	0.23	-0.24		-4.99	-22.29
AWF	1.82	-5.19	-0.17	-0.14	0.48	-6.06	-24.08
AWG	2.31	-2.91	0.13	-0.02	0.46	-4.73	-21.82
AWH	7.32			-0.77	-0.1	8.29	0.17
LWA	6.48			-1.12		5.79	-5.24
LWB	3.33	3.7	1.12	0.52		-1.68	-15.2
LWC	3.01	1.68	0.82	0.38		-2.64	-17.46
LWD	6.2			-1.45		5.35	-6.19
LWE	1.7	-6.21	-0.37	0.26	0.7	-5.42	-21.16
SDP1	3.56	3.38	0.94	0.19	0.25	-0.73	-12.78
SDP2	3.89	7.76	2.09	0.69	-0.73	-1.16	-13.98

Table C4. Saturation indices of goethite and jarosite at p*e* = 12.

	pH	goethite	jarosite
AWC	3.4	5.62	6.15
AWD	2.2	2.07	-1.08
AWF	1.8	1.02	-2.85
AWG	2.3	2.39	-0.48
AWH	7.3		
LWA	6.5		
LWB	3.3	5.40	6.03
LWC	3.0	4.51	3.95
LWD	6.2		
LWE	1.7	1.52	-0.37
SDP1	3.6	6.18	7.93
SDP2	3.9	5.41	5.74

C1.2. Equilibrium reactions and log K values of selected minerals at 25°C (after Drever, 1997).

Reaction:	**log K_{25}**
Al phases:	
$Al(OH)_{3\ gibbsite} + 3H^+ = Al^{3+} + 3H_2O$	7.74
$KAl_3(SO_4)_2(OH)_{6\ alunite} + 6H^+ = K^+ + 3Al^{3+} + 2SO_4^{2-} + 6H_2O$	–1.4
$AlOHSO_{4\ jurbanite} + H^+ = Al^{3+} + SO_4^{2-} + H_2O$	–3.23
Fe^{3+} phases:	
$FeOOH_{\ goethite} + 3H^+ = Fe^{3+} + 2H_2O$	–1.0
$KFe_3(SO_4)_2(OH)_{6\ jarosite} + 6H^+ = K^+ + 3Fe^{3+} + 2SO_4^{2-} + 6H_2O$	–14.8
$Fe(OH)_{3\ soil} + 3H^+ = Fe^{3+} + 3H_2O$	2.70
Silicate phases:	
$SiO_{2\ quartz} + 2H_2O = H_4SiO_4^0$	–3.98
$Al_2Si_2O_5(OH)_{4\ kaolinite} + 6H^+ = 2Al^{3+} + 2\ H_4SiO_4^0 + H_2O$	7.44

The following derivations can be made from the reactions above, which allow for linear solubility lines or zones to be plotted on diagrams of log M_a versus pH (M_a = activity of metal ion):

Gibbsite: $\log Al^{3+} = -3pH + 7.74$

Alunite: $\log Al^{3+} = -2pH - ({}^1/_3\log K^+ + {}^2/_3\log SO_4^{2-}) - {}^{1.4}/_3$

Jurbanite: $\log Al^{3+} = -pH - \log SO_4^{2-} - 3.23$

Goethite: $\log Fe^{3+} = -3pH - 1$

Jarosite: $\log Fe^{3+} = -2pH - ({}^1/_3\log K^+ + {}^2/_3\log SO_4^{2-}) - {}^{14.8}/_3$

$Fe(OH)_3$: $\log Fe^{3+} = -3pH + 2.7$

Quartz: $\log H_4SiO_4 = -3.98$

Kaolinite: $\log Al^{3+} = -3pH - \log H_4SiO_4 + {}^{7.44}/_2$

C2. Soil data

C2.1. Soil texture and organic carbon.

Table C5. Texture and organic carbon content of all soil profile and composite samples.

Sample ID	Description	Organic C	Sand	Silt	Clay
A1	Soil profile - site A	1.0	67.6	18.8	13.6
A2	Soil profile - site A	0.2	80.4	13.0	6.6
A3	Soil profile - site A	0.1	92.6	2.2	5.2
A4	Soil profile - site A	0.2	91.2	3.2	5.6
B1	Soil profile - site B	2.3	79.2	10.8	10.0
B2	Soil profile - site B	1.3	85.8	7.0	7.2
B3	Soil profile - site B	0.6	75.2	16.0	8.8
B4	Soil profile - site B	0.1	90.6	3.6	5.8
B5	Soil profile - site B	0.2	85.2	7.6	7.2
C1	Soil profile - site C	0.8	84.8	7.6	7.6
C2	Soil profile - site C	0.1	84.4	10.0	5.6
C3	Soil profile - site C	1.4	88.0	4.8	7.2
C4	Soil profile - site C	0.2	59.2	8.8	32.0
E1	Soil profile - site E	1.8	83.8	7.4	8.8
E2	Soil profile - site E	0.1	88.6	5.2	6.2
E3	Soil profile - site E	0.2	71.6	5.2	23.2
F1	Soil profile - site F	0.4	86.4	7.2	6.4
F2	Soil profile - site F	0.7	88.8	3.8	7.4
F3	Soil profile - site F	0.1	79.2	9.0	11.8
ATSC	Topsoil composite	0.8	85.6	7.8	6.6
ASSC	Subsoil composite	0.1	78.6	6.2	15.2
TPT	Test pit topsoil	1.5	87.6	5.6	6.8
TPS	Test pit subsoil	0.1	58.8	5.8	35.4
LCN	Limed composite - north	0.8	87.0	7.2	5.8
LCC	Limed composite - central	2.6	85.2	7.6	7.2
LCS	Limed composite - south	0.1	84.6	8.6	6.8

Note: all values as %

C2.2. Extractable acidity

C2.2.1. KCl extractable acidity of all soil samples

Table C6. KCl extractable acidity of all soil profile, composite and limed incubation samples.

Sample ID	pH (KCl)	pH (H_2O)	Acidity ($mmol_c/kg$)	Ca ($mmol_c/kg$)	Mg ($mmol_c/kg$)	Acid sat. (%)	ECEC ($mmol_c/kg$)
A1	1.6	1.8	756.4	789.6	145.3	44.7	1691.3
A2	2.2	2.5	416.7	171.1	196.7	53.1	784.5
A3	3.6	4.1	62.5	93.2	290.5	14.0	446.2
A4	3.1	3.5	155.1	50.6	166.2	41.7	371.9
B1	1.3	1.4	552.4	771.7	28.7	40.8	1352.8
B2	1.8	2.0	305.8	275.1	23.4	50.6	604.3
B3	2.8	3.2	294.0	98.7	107.0	58.8	499.7
B4	2.7	3.2	314.9	140.4	117.2	55.0	572.5
B5	2.3	2.6	320.7	58.2	61.9	72.8	440.8
C1	1.5	1.7	744.1	42.6	33.7	90.7	820.4
C2	2.5	2.7	377.4	58.8	35.7	80.0	471.9
C3	3.0	3.4	238.0	30.4	115.2	62.0	383.6
C4	3.2	3.9	45.0	36.6	206.5	15.6	288.1
E1	2.6	3.1	33.3	14.8	23.8	46.3	71.9
E2	3.3	4.2	69.0	27.4	80.4	39.0	176.8
E3	3.6	4.8	11.5	40.7	130.0	6.3	182.2
F1	1.7	1.9	434.6	34.2	82.4	78.8	551.2
F2	2.2	2.5	271.8	22.9	80.0	72.5	374.7
F3	3.1	3.8	112.3	30.6	206.9	32.1	349.8
TSC	2.5	2.7	341.0	93.5	62.6	68.6	497.1
SSC	3.3	3.8	134.5	43.4	146.5	41.5	324.4
LCN	3.5	3.6	66.1	258.4	60.7	17.2	385.2
LCC	4.7	5.2	15.7	368.1	122.7	3.1	506.5
LCS	5.7	6.0	1.1	376.9	144.5	0.2	522.5
TPT	5.6	6.4	0.9	34.0	12.8	1.9	47.7
TPS	7.0	8.3	0.4	29.9	105.6	0.3	136.0
TS0	2.5	na	499.0	68.6	110.2	73.6	677.8
TS1	4.4	na	49.6	188.9	184.9	11.7	423.3
TS2	6.6	na	0.6	264.4	271.9	0.1	536.9
TS3	6.9	na	0.2	262.7	248.3	0.0	511.2
SS0	3.5	na	147.7	53.7	164.3	40.4	365.7
SS1	4.8	na	14.2	90.3	201.5	4.6	306.0
SS2	6.9	na	0.4	125.0	232.4	0.1	357.8
SS3	6.9	na	0.0	102.5	218.1	0.0	320.6
TL0	2.4	na	343.8	78.1	77.0	68.9	498.9
TL1	4.0	na	57.5	177.9	250.8	11.8	486.3
TL2	6.6	na	0.6	241.1	281.5	0.1	523.2
TL3	6.6	na	0.4	242.0	267.2	0.1	509.6
SL0	3.2	na	127.4	34.2	254.1	30.6	415.8
SL1	4.1	na	15.4	65.8	202.9	5.4	284.1
SL2	6.2	na	1.2	103.2	238.3	0.3	342.6
SL3	6.6	na	0.0	102.3	215.7	0.0	318.0

na = not analysed

C2.2.2 KCl extractable acidity of sulphur melting experiments

Table C7. KCl extractable acidity of soil/sulphur melting experiments.

Sample	S (g)	pH	Acidity	Ca	Mg	Acid saturation (%)	ECEC
				($mmol_c/kg$)			
S0	0.0	7.1	0	36.1	9.4	0	45.5
S1	0.1	4.7	6.7	37.2	11.0	12	54.9
S2	0.2	4.6	7.2	33.5	10.5	14	51.3
S3	0.5	4.2	17.3	36.1	10.4	27	63.8
S4	0.75	4.4	10.6	27.0	9.4	23	47.0
S5	1.0	5.0	4.0	21.5	8.1	12	33.7
Repeat experiment:							
S1	0.1	4.3	4.1				
S2	0.2	4.1	4.3				
S3	0.5	3.7	12.1				
S4	0.75	3.6	8.6				
S5	1.0	4.1	3.1				
S4 (R)	0.75	4.8	3.1				
S5 (R)	1.0	4.8	3.0				

Table C8. pH_{KCl} of soil/sulphur melting experiments.

Sample	S (g)	pH_{KCl}
S0	0.0	6.5
S1	0.1	4.4
S2	0.2	4.4
S3	0.5	4.2
S4	0.75	4.0
S5	1.0	3.8
Repeats:		
S1	0.1	4.3
S2	0.2	4.1
S3	0.5	3.7
S4	0.75	3.6
S5	1.0	4.0
S4 (R)	0.75	4.7
S5 (R)	1.0	4.8

C2.3. Incubation results - major ions in solution

(all values in meq/L)

Table C9. Major ions in solution for limed incubation samples.

A. Short-term incubation:

	TS0	TS1	TS2	TS3	SS0	SS1	SS2	SS3
F	9.7	1.5	0.0	0.0	2.8	0.1	0.0	0.1
Cl	12.8	5.4	5.7	3.5	8.4	8.0	10.0	11.3
NO_3	nd	nd	nd	nd	nd	nd	nd	nd
PO_4	nd	nd	nd	nd	nd	nd	nd	nd
SO_4	989.8	440.5	480.9	389.3	289.1	161.6	189.5	152.4
Alkalinity	nd	nd	0.7	0.8	nd	nd	0.2	0.3
Anions:	**1012.3**	**447.5**	**487.3**	**393.5**	**300.3**	**169.7**	**199.7**	**164.1**
Na	30.0	20.9	19.3	15.5	61.6	45.5	52.5	49.3
NH_4	2.8	1.4	0.9	0.8	0.6	0.0	0.0	0.0
K	0.5	0.3	0.7	0.4	0.6	0.6	0.5	0.6
Mg	137.4	276.4	328.1	247.0	113.9	77.2	92.1	73.7
Ca	106.8	29.9	27.1	25.2	24.7	28.4	30.3	37.9
Acidity	954.5	116.1	nd	nd	163.1	14.1	nd	nd
Cations:	**1232.0**	**444.9**	**376.2**	**288.8**	**364.4**	**165.8**	**175.5**	**161.5**

B. Long-term incubation:

	TL0	TL1	TL2	TL3	SL0	SL1	SL2	SL3
F	4.2	2.3	0.0	0.0	2.5	0.2	0.0	0.1
Cl	4.3	4.7	3.6	2.9	5.9	7.2	6.6	6.6
NO_3	nd	nd	nd	nd	nd	nd	nd	nd
PO_4	nd	nd	nd	nd	nd	nd	nd	nd
SO_4	1078.0	507.8	409.7	346.0	254.7	172.2	146.1	139.6
Alkalinity	nd	nd	0.6	1.2	nd	nd	0.2	0.3
Anions:	**1086.6**	**514.8**	**413.9**	**350.1**	**263.1**	**179.6**	**153.0**	**146.6**
Na	32.4	18.6	15.3	15.7	54.7	43.1	42.5	42.1
NH_4	2.7	1.6	0.9	1.1	0.8	0.8	0.4	0.4
K	3.7	0.2	0.5	0.6	0.7	0.6	0.6	0.5
Mg	143.5	276.1	250.4	247.5	91.3	70.8	69.3	67.8
Ca	98.6	30.5	26.9	26.7	25.2	23.8	25.3	26.6
Acidity	1000.0	148.8	nd	nd	130.4	19.0	nd	nd
Cations:	**1280.8**	**475.8**	**294.1**	**291.6**	**303.2**	**157.9**	**138.1**	**137.4**

nd = not detected

C2.4. Incubation results - trace elements in solution

(all values in mg/L)

Table C10. Trace elements in solution for limed incubation samples.

A. Short-term incubation:

	TS0	TS1	TS2	TS3	SS0	SS1	SS2	SS3
Li	5.8	0.6	0.1	0.1	6.5	0.8	0.2	0.3
Al	4799.5	245.2	nd	nd	396.8	12.2	1.5	0.3
Si	30.3	37.4	nd	0.7	57.4	39.5	8.2	16.9
Cr	5.3	nd	nd	nd	nd	nd	nd	0.3
Mn	29.9	38.7	16.0	11.3	59.6	27.5	13.3	5.7
Fe	1837.5	3.4	9.4	10.6	0.2	9.4	10.6	10.9
Ni	3.9	1.9	0.1	0.1	3.5	1.2	0.1	0.1
Cu	7.3	nd	nd	0.2	0.8	nd	nd	nd
Zn	21.0	7.2	1.2	1.8	3.9	2.4	0.3	0.3
Sr	6.8	2.0	1.3	1.2	6.9	3.4	2.4	2.4
Ba	0.8	0.1	0.1	3.7	1.6	0.1	1.0	0.1
Pb	0.5	0.1	0.3	0.4	1.4	0.3	0.2	0.2

B. Long-term incubation:

	TL0	TL1	TL2	TL3	SL0	SL1	SL2	SL3
Li	6.6	0.8	0.4	nd	5.6	1.4	0.5	0.3
Al	5239.4	276.8	nd	nd	427.0	24.4	0.5	2.9
Si	49.7	1.3	11.1	nd	60.1	19.4	15.5	7.0
Cr	6.5	0.3	0.3	nd	0.6	0.1	0.2	nd
Mn	32.0	39.1	9.0	7.8	60.4	30.1	7.2	14.4
Fe	1424.2	nd	nd	nd	139.2	112.1	2.6	nd
Ni	4.3	1.9	0.1	0.1	3.1	1.4	0.1	nd
Cu	9.0	nd	nd	0.1	nd	nd	0.0	nd
Zn	28.7	7.8	0.4	0.3	2.9	1.5	0.5	1.2
Sr	7.7	2.4	1.0	1.0	6.4	3.4	1.7	1.6
Ba	0.7	0.1	nd	nd	nd	0.4	nd	1.2
Pb	1.6	0.1	0.1	0.3	0.1	0.2	0.3	0.2

nd = not detected

elements with concentrations less than 1mg/L have been omitted

C2.5. Incubation results - activities and saturation indices

Table C11. Selected activities of limed soil solutions below pH 5.

	pH	log(Al^{3+})	log(Fe^{2+})	log(SO_4^{2-})	log(K^+)
TL0	1.9	-3.07	-3.41	-1.58	-2.68
TL1	4.1	-4.51	-7.53	-1.50	-3.94
TS0	1.8	-3.06	-3.25	-1.60	-3.53
TS1	4.2	-4.44	-7.59	-1.57	-3.83
SL0	3.9	-4.01	-7.65	-1.68	-3.35
SL1	4.9	-5.21	-9.60	-1.74	-3.43
SS0	3.5	-4.11	-6.20	-1.64	-3.42
SS1	5.0	-5.50	-9.64	-1.79	-3.43

Saturation indices of selected minerals:

Table C12. Saturation indices of selected Al phases of limed soil solutions.

Sample ID	pH	alunite	jurbanite	kaolinite	gibbsite	basaluminite
TL0	1.9	-2.15	0.51	-8.32	-5.46	-17.51
TL1	4.1	5.39	1.28	-1.45	-0.39	-1.55
TL2	6.9					
TL3	7.3					
TS0	1.8	-3.72	0.36	-9.39	-5.78	-18.61
TS1	4.2	6.35	1.40	2.41	0.08	-0.04
TS2	7.2					
TS3	7.2					
SL0	3.9	6.16	1.41	1.95	-0.34	-1.38
SL1	4.9	8.35	1.15	4.55	1.46	3.78
SL2	6.9	6.26	-1.48	6.98	2.78	5.26
SL3	7.1	7.81	-1.16	7.79	3.53	7.82
SS0	3.5	3.41	0.94	-0.73	-1.66	-5.84
SS1	5.0	7.53	0.84	4.72	1.24	2.80
SS2	6.9	7.50	-1.03	7.28	3.20	6.98
SS3	6.8	5.54	-1.64	6.41	2.45	4.08

Table C13. Saturation indices of selected silicate and carbonate phases of limed soil solutions.

Sample ID	pH	gypsum	quartz	SiO_2 (a)	dolomite	sepiolite
TL0	1.9	0.80	0.89	-0.38		-21.59
TL1	4.1	0.30	-0.75	-2.02		-17.36
TL2	6.9	0.22	0.18	-1.09	-1.40	-3.46
TL3	7.3	0.18			0.06	
TS0	1.8	0.81	0.67	-0.60		-22.67
TS1	4.2	0.26	0.71	-0.56		-12.35
TS2	7.2	0.23			-0.56	
TS3	7.2	0.18	-1.01	-2.28	-0.48	-5.59
SL0	3.9	0.13	0.90	-0.37		-13.73
SL1	4.9	0.09	0.40	-0.87		-11.36
SL2	6.9	0.09	0.30	-0.97	-2.76	-3.71
SL3	7.1	0.18	-0.05	-1.32		-3.77
SS0	3.5	0.13	0.89	-0.38		-15.28
SS1	5.0	0.14	0.71	-0.56		-10.23
SS2	6.9	0.19	0.03	-1.24	-3.84	-4.30
SS3	6.8	0.25	0.34	-0.93	-2.11	-3.93

Table C14. Saturation indices of selected Fe (III) phases of limed soil solutions.

Sample ID	pH	jarosite	$Fe(OH)_3$ (a)	goethite
p*e* = 4:				
TL0	1.9	-19.57	-10.65	-4.76
TL1	4.1	-19.14	-7.95	-2.06
TS0	1.8	-20.82	-10.86	-4.97
TS1	4.2	-18.28	-7.52	-1.63
SL0	3.9	-20.58	-8.66	-2.77
SL1	4.9	-16.36	-6.18	-0.29
SS0	3.5	-19.12	-8.58	-2.69
SS1	5.0	-16.25	-6.10	-0.20
p*e* = 8:				
TL0	1.9	-7.57	-6.65	-0.76
TL1	4.1	-7.14	-3.95	1.94
SL0	3.9	-8.59	-4.66	1.23
SL1	4.9	-4.40	-2.20	3.70
p*e* = 12:				
TL0	1.9	1.54	-3.60	2.29
TL1	4.1	1.11	-1.20	4.69
SL0	3.9	0.08	-1.77	4.12
SL1	4.9	0.01	-0.72	5.17